ANALYTICAL SOLUTIONS FOR TEMPERATURE PROFILE PREDICTION IN MULTI-LAYERED PAVEMENT SYSTEMS

BY

DONG WANG

DISSERTATION

Submitted in partial fulfillment of the requirements
for the degree of Doctor of Philosophy in Civil Engineering
in the Graduate College of the
University of Illinois at Urbana-Champaign, 2010

Urbana, Illinois

Doctoral Committee:

Associate Professor Jeffery R. Roesler, Chair and Director of Research
Professor Imad L. Al-Qadi
Professor William G. Buttlar
Associate Professor Lev Khazanovich, University of Minnesota

Abstract

Accurate prediction of pavement temperature profile is essential to better characterize the mechanistic properties of paving materials and predict pavement responses under traffic and environmental loadings. In practice, characterizing the field temperature profiles are desired in order to calculate the moduli of various pavement layers, analyze Falling Weight Deflectometer (FWD) testing data, as well as assess the load transfer efficiency across joints in concrete pavements.

To facilitate estimation of pavement temperature profiles, one-dimensional (1-D) analytical solutions for temperature profiles in multi-layered pavements have been derived using the method of separation of variables and the Laplace transforms. The derived theoretical solutions consider the pavement geometries, material thermal properties, solar radiation, and air temperature. Field validation justified that these analytical solutions generate reasonable temperature profiles in the concrete slab of a four-layered continuously reinforced concrete pavement (CRCP) test section. The main advantages of these solutions are that they can rapidly predict the pavement temperature profile for short time durations, e.g., a few days, with limited input data. Under the assumption of axisymmetric thermal conditions, analytical solution for two-dimensional (2-D) temperature profiles in a multi-layered pavement system has been derived using the Hankel transform and the method of separation of variables, and validated for predicting the temperature profile in the concrete slab of a four-layered CRCP test section.

Finally, rapidly varying temperature profiles in pavement systems due to transient thermal loadings generated by vertical take-off aircraft engines are systematically studied. 1-D analytical solutions for temperature fields in a two-layered pavement system using Laplace transforms are proposed for two different surface boundary conditions, i.e., specified transient surface temperature and mixed boundary condition involving heat flux emanating from the aircraft engine. Furthermore, 2-D axisymmetric temperature field in a homogeneous half-space subjected to transient thermal loading was solved under the specified surface temperature condition. Two solution methods, one based on the Hankel transforms and the method of separation of variables while another based on the Hankel and Laplace transforms, were introduced. Numerical experiments suggest that the combined results based on those two methods give reasonable approximation

to the rapidly varying temperature profile.

In memory of my father-in-law, Xingcai Huang, my admired civil engineer

Acknowledgments

I express my utmost gratitude to my thesis advisor, Dr. Jeffery R. Roesler, for suggesting the topic, for his many helpful discussions and support in the development of this thesis, for his efforts made in proof-reading this thesis.

I thank all the other members of doctoral committee, Dr. Imad L. Al-Qadi, Dr. William G. Buttlar, and Dr. Lev Khazanovich, for their invaluable comments and corrections to this thesis.

Financial support received from the Illinois Department of Transportation, Eisenhower Graduate Transportation Fellowship Program, and U.S. Air Force Research Laboratory is much obliged and appreciated.

I thank my mother-in-law, Suxian Lin; my parents, Tianzhong Wang and Fengying Sun, for their unselfish efforts made in taking care our kids, Firmiana and Max. Finally, I thank my wife, Huihua Huang, for her patience, love, support, encouragement, and countless efforts made in raising and educating our kids during my studies at the University of Illinois at Urbana-Champaign, graduate program.

Table of Contents

List of Tables

List of Figures

Chapter 1

Introduction

It is well known that temperature variation in pavement layers plays an important role in the performance of both flexible and rigid pavement systems [19]. In flexible pavement systems, the surface layer is usually made of hot-mix asphalt (HMA), which is a viscoelastic material and its behavior is highly related to its temperature, i.e., HMA responds nearly like an elastic solid under low temperature and strain conditions; on the other hand, it also acts as a viscous material at high temperature in the sense that the deformation due to traffic loadings cannot be fully recovered within a finite time period under the unloading condition [13, 50]. Thus, an accurate prediction of the temperature profile in the HMA layer is desired when selecting the asphalt binder and predicting asphalt pavement responses under traffic and environmental loadings. For rigid pavement design, the thermal curling stress in the concrete slab cannot be ignored [55] and by some manner must be added to the traffic loading stresses [1, 12]. In order to accurately capture the critical thermal stresses in the Portland cement concrete (PCC) slab, the temperature profile throughout the day must be known. In practice, pavement temperature distribution serves as a pre-requisite condition in order to calculate strains, stresses, deflection in a forward analysis, back-calculate the moduli of various pavement layers, evaluate the load transfer efficiency across joints in concrete pavements using nondestructive testing (NDT) data, etc. For example, in order to accurately assess the in situ structural capacity of flexible or rigid pavements from Falling Weight Deflectometer (FWD) test results, knowledge of the temperature profile in the surface layer is essential. One challenge in obtaining accurate temperature profile data during FWD testing is that the profile is continuously changing and testing can last the entire day. Air and surface temperatures are typically collected to correct back-calculated asphalt moduli to a standard temperature using a statistics-based method that introduces some errors [4, 35], but this empirical method is insufficient for accurate temperature curling corrections in concrete pavements.

1.1 Methods of Predicting Pavement Temperature Profile

Many research efforts have been taken on developing different mathematical models to predict temperature profile within a pavement system. There are mainly three types of methods developed so far, namely, statistics-based models, numerical methods, and analytical approaches, as explained next.

1.1.1 Statistics-Based Pavement Temperature Prediction Models

The statistics-based regression formulas are usually developed based on large databases of climatic, meteorological, and geographical factors, such as air temperature, wind speed, solar radiation and latitude, etc., as well as the measured field pavement temperatures. There are many such regression formulas in the pavement research literature. To mention a few here, e.g., Rumney and Jimenez approximated temperature at the surface and at a 2-in. depth based on air temperature and hourly solar radiation [41]; Lukanen et al. predicted the 7-day average high pavement temperature using the 7-day average high air temperature [34]; more recently, Diefenderfer et al. calculated the maximum and minimum temperature at any depth by using air temperature, daily solar radiation, and depth within the pavement [18]. Empirical formulas are usually applied to rapidly predict certain extreme temperatures within a pavement system or a specific temperature at a given pavement depth. However, the disadvantage of these types of formulas is that they only give reasonable prediction for the input data included within the original sample database, but do not guarantee the accuracy of prediction for the input data outside the original sample database.

1.1.2 Numerical Methods

Numerical methods to predict pavement temperature profile typically consist of four steps. First, the governing equation to account for the heat conduction within a pavement system must be set up, which is usually a 1-dimensional (1-D) or 2-dimensional (2-D) heat transfer model represented by a time-dependent partial differential equation (PDE). Second, either a Dirichlet type boundary condition, i.e., transient surface temperature need to be specified or a mixed type boundary condition must be established linking the climatic parameters with the temperature gradient along depth evaluated at surface and the pavement surface temperature. In the latter case, the link is accomplished by analyzing the energy balance at the pavement surface. Third, the spatial domain needs to be discretized using a numerical method, such as finite difference method, finite element method, etc., which results in a large system of ordinary differential equations (ODEs) in time. Lastly, an appropriate time integrator is required to solve these ODEs. For example, this time integrator can be either a linear multistep method or a Runge-Kutta method.

There are also many research work on predicting pavement temperature profile based on numerical methods. A few are listed here for illustrative purposes. Dempsey and Thompson were among the first researchers to develop a numerical simulation approach by using the 1-D heat transfer model and an explicit finite difference method [17]. Hsieh et al. proposed a 3-dimensional (3-D) numerical model to calculate the temperature distribution within concrete pavement [20]. Recently, Rasmussen et al. and Schindler et al. proposed models to predict the temperature distribution in the early-age PCC pavement by incorporating both the climatic factors and the heat of hydration of cementitious materials into the models using a finite element and a 1-D finite difference method, respectively [39, 42]. Yavuzturk et al. also simulated temperature fluctuations in asphalt pavements due to thermal environmental conditions by using a 2-D finite difference method [58].

1.1.3 Analytical Approaches

Regarding analytical solution of temperature profiles through a multi-layered pavement system, very few results are available due to the complexity encountered in deriving the closed-form analytical solution. Barber calculated the maximum pavement temperature from weather reports for a one-layered system [3]. Solaimanian and Kennedy proposed a simple analytical equation to predict the maximum pavement surface temperature based on maximum air temperature and hourly solar radiation [44]. Liang and Niu derived a closed-form analytical solution of temperature distribution in a three-layered system using a simplified boundary condition, which only involved the convection of heat between the atmosphere and pavement surface but not any solar radiation effect [31]. Finally, Liu and Yuan also derived a closed-form solution for 1-D temperature profile generation in a three-layered system by solving the heat conduction equation with the assumption that the time-dependent pavement surface temperatures were known throughout the time period of interest [32].

1.2 Motivation

In this thesis, we are mainly interested in the analytical approaches to calculate pavement temperature profiles. The key purpose of this thesis work is to derive easily implementable closed-form solutions for temperature profile prediction in multi-layered pavement system, which are accessible to a wide range of users including field engineers. The proposed analytical solutions consist of 1-D and axisymmetric 2-D ones, where 1-D results should be of interests to researches conducting FWD testing and the 2-D axisymmetric solutions lay the foundation for further investigating thermal stresses in asphalt pavements based on layered

elastic theory.

The main advantages of these proposed analytical approaches is that they can rapidly predict temperature fields in a multi-layered pavement system with limited input data, such as measured air temperature, solar radiation intensities, pavement layer thicknesses, and the thermal properties of layer materials. Also analytical approach does not require any spatial discretization of physical domain or time integrator to evolve the time-dependent temperature profile, eliminating the computational issues related to numerical methods, such as discretization/truncation errors and computational stabilities, etc.

Another purpose of this thesis work is to develop robust analytical methods to predict temperature profile in a multi-layered PCC pavement subjected to rapid transient thermal loading. New generation military aircraft are being developed to take-off and land vertically resulting in large thermal loads on the pavement surface. Traditional paving materials such as concrete and asphalt concrete will not have the same longevity under this repeated thermal loading condition [21, 22, 23, 26, 27, 40]. Thus, the thermal load induced stresses must be taken into account in the material design for this new type of airfield pavements. As a prerequisite condition of calculating thermal stresses and developing the appropriate material, rapidly varying temperature profile in multi-layered pavement systems due to transient thermal loading have to be known.

Chapter 2

1-Dimensional Pavement Temperature Profile Prediction

In this chapter, 1-dimensional analytical solutions of temperature profile in multi-layered pavement systems, i.e., temperature distribution along pavement depth, are presented. From now on, all materials in the multi-layered pavement systems are assumed to be continuous, homogeneous, and isotropic. In this chapter, we first discuss the mathematical model for predicting 1-D pavement temperature profile, then derive its analytical solution using the separation of variables and the Laplace transforms, respectively.

2.1 Mathematical Temperature Model

The time-dependent temperature distribution in a N-layered pavement system, shown in Fig. 2.1, can be modeled as a boundary value problem (BVP), where h_i = thickness of the ith layer (m) for $1 \leq i \leq n-1$ while the thickness of layer n (subgrade) is assumed to be infinite; λ_i = thermal conductivity of the ith layer (Kcal/m h C); α_i = thermal diffusivity of the ith layer (m^2/h); and $T_i(z,t)$ = temperature function for layer i (C). Based on the Cartesian coordinate system in Fig. 2.1, the 1-D heat transfer problem can be modeled using the following heat equation

$$\frac{\partial T_i}{\partial t} = \alpha_i \frac{\partial^2 T_i}{\partial z^2}, \qquad H_{i-1} \leq z \leq H_i \tag{2.1}$$

where $H_i = \sum_{k=1}^{i} h_k, i = 1, 2, \ldots, n-1; H_0 = 0$ and $H_n = \infty$. The temperature and heat flow are assumed to be continuous along the interface of two consecutive layers, i.e.,

$$T_i(H_i, t) = T_{i+1}(H_i, t) \tag{2.2}$$

$$\lambda_i \frac{\partial T_i}{\partial z}(H_i, t) = \lambda_{i+1} \frac{\partial T_{i+1}}{\partial z}(H_i, t) \tag{2.3}$$

The first of the two boundary conditions assumes the temperature remains bounded as z approaches infinity, i.e.,

$$|T_n(z,t)| \leq M \qquad \text{as} \quad z \to \infty \tag{2.4}$$

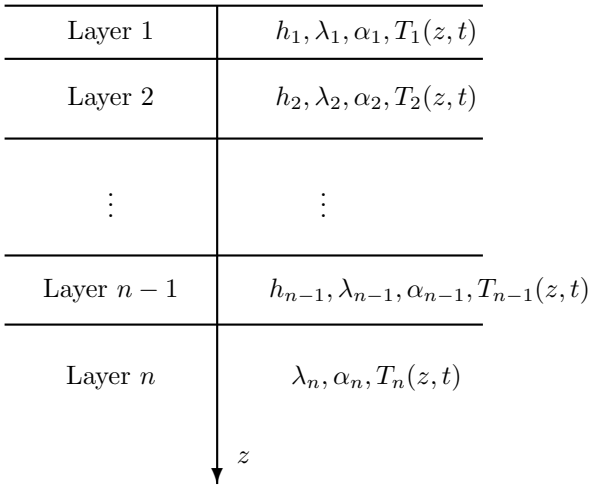

Figure 2.1: 1-D time-dependent temperature profile in a multi-layered pavement system

where M is a constant. The second boundary condition (BC) describes the energy balance at the pavement surface and has been defined previously as [17, 57]:

$$-\lambda_1 \frac{\partial T_1}{\partial z}(0,t) = a_s Q(t) - F(t) + B(T_a(t) - T_1(0,t)) \tag{2.5}$$

where $Q(t)$ = solar radiation flux (Kcal/m^2 h); a_s = surface material absorptivity relative to the total solar radiation (dimensionless); $F(t)$ = irradiation flux emitted by pavement surface (Kcal/m^2 h); B = surface material convection coefficient (Kcal/m^2 h C); $T_a(t)$ and $T_1(0,t)$ are the air and pavement surface temperatures (C), respectively.

In order to derive a closed-form solution of the 1-D pavement temperature field, continuous functions representing $T_a(t)$ and $Q(t)$ are desired. Given time interval $[0, t_e]$ and a positive integer m, suppose that $[0, t_e]$ is divided into $2m$ sub-intervals of equal lengths. Now, assume that the air temperature and solar radiation flux are measured at two end points of each sub-interval except at time t_e, then the interpolatory trigonometric polynomials, based on the discrete least squares approximation, can be constructed for the air temperature and solar radiation as follows [5]:

$$T_a(t) = \frac{a_0}{2} + \frac{a_m}{2}\cos(m\bar{t}) + \sum_{k=1}^{m-1}\left[a_k \cos(k\bar{t}) + b_k \sin(k\bar{t})\right], \qquad 0 \le t \le t_e - \frac{t_e}{2m} \tag{2.6}$$

with

$$\bar{t} = \pi\left(\frac{2t}{t_e} - 1\right) \tag{2.7}$$

$$a_k = \frac{1}{m}\sum_{l=0}^{2m-1} T_l \cos\left[\frac{k\pi}{m}(l-m)\right] \quad \text{for each} \quad k = 0, 1, \ldots, m \tag{2.8}$$

$$b_k = \frac{1}{m}\sum_{l=0}^{2m-1} T_l \sin\left[\frac{k\pi}{m}(l-m)\right] \quad \text{for each} \quad k = 1, 2, \ldots, m-1 \tag{2.9}$$

where T_l = measured air temperature at l^{th} partitioning point of $[0, t_e]$, i.e., at time $t_l = \frac{l}{2m}t_e$ for each $l = 0, 1, 2, \ldots, 2m-1$.

Similarly, $Q(t)$ can be modeled by the interpolatory trignometric polynomial

$$Q(t) = \frac{c_0}{2} + \frac{c_m}{2}\cos(m\bar{t}) + \sum_{k=1}^{m-1}\left[c_k \cos(k\bar{t}) + d_k \sin(k\bar{t})\right], \qquad 0 \le t \le t_e - \frac{t_e}{2m} \tag{2.10}$$

where $\bar{t}$ is given in Eq. (2.7) and

$$c_k = \frac{1}{m}\sum_{l=0}^{2m-1} Q_l \cos\left[\frac{k\pi}{m}(l-m)\right] \quad \text{for each} \quad k = 0, 1, \ldots, m \tag{2.11}$$

$$d_k = \frac{1}{m}\sum_{l=0}^{2m-1} Q_l \sin\left[\frac{k\pi}{m}(l-m)\right] \quad \text{for each} \quad k = 1, 2, \ldots, m-1 \tag{2.12}$$

where Q_l = measured solar radiation flux at time $t_l = \frac{l}{2m}t_e$ for each $l = 0, 1, 2, \ldots, 2m-1$.

The irradiation energy emitted by pavement surface, $F(t)$, is usually expressed by a fourth-order equation as follows [17]:

$$F(t) = (1 - NW)\sigma\left[\epsilon\left(T_1(0,t)\right)^4 - \left(G - 10^{-\rho p}J\right)\left(T_a(t)\right)^4\right] \tag{2.13}$$

where N = cloud-base factor; W = percentage of cloud cover at night; σ = Stefan-Boltzmann constants; ϵ = emissivity of radiation by pavement surface; T_a = Rankine air temperature; and $G, J, \rho,$ and p are model parameters. It is clear that Eq. (2.13) causes difficulty in deriving the closed-form solution of 1-D temperature profile. To remove this hurdle, Barber [3] took irradiation energy into account by reducing the surface absorptivity by a factor of $\frac{1}{3}$, and the same assumption is also applied in this study. Thus Eq. (2.5) becomes

$$-\lambda_1 \frac{\partial T_1}{\partial z}(0,t) = B\left[\frac{\widetilde{a_s}}{B}Q(t) + T_a(t) - T_1(0,t)\right] \tag{2.14}$$

where $\widetilde{a_s}$ = effective surface absorptivity.

Substituting Eqs. (2.6) and (2.10) into Eq. (2.14) and using the trignometric identity $\cos x = \sin(\frac{\pi}{2} + x)$

yields the following BC

$$-\lambda_1 \frac{\partial T_1}{\partial z}(0,t) = B\left\{\frac{a_0}{2} + \frac{\widetilde{a}_s c_0}{2B} + \left(\frac{a_m}{2} + \frac{\widetilde{a}_s c_m}{2B}\right)\sin\left(m\bar{t} + \frac{\pi}{2}\right) + \sum_{k=1}^{m-1}\left[\left(a_k + \frac{\widetilde{a}_s c_k}{B}\right)\sin\left(k\bar{t} + \frac{\pi}{2}\right) + \left(b_k + \frac{\widetilde{a}_s d_k}{B}\right)\sin(k\bar{t})\right] - T_1(0,t)\right\} \tag{2.15}$$

Alternatively, Eq. (2.15) can be written as follows:

$$-\lambda_1 \frac{\partial T_1}{\partial z}(0,t) = B\left[\sum_{i=1}^{2m} A_i \sin(\omega_i t + \phi_i) - T_1(0,t)\right] \tag{2.16}$$

where

$$A_i = \begin{cases} \frac{a_0}{2} + \frac{\widetilde{a}_s c_0}{2B} & \text{if } i = 1 \\ \frac{a_m}{2} + \frac{\widetilde{a}_s c_m}{2B} & \text{if } i = 2 \\ a_{i-2} + \frac{\widetilde{a}_s c_{i-2}}{B} & \text{if } i = 3, 4, \ldots, m+1 \\ b_{i-m-1} + \frac{\widetilde{a}_s d_{i-m-1}}{B} & \text{if } i = m+2, m+3, \ldots, 2m \end{cases}$$

$$\omega_i = \begin{cases} 0 & \text{if } i = 1 \\ \frac{2m\pi}{t_e} & \text{if } i = 2 \\ \frac{2(i-2)\pi}{t_e} & \text{if } i = 3, 4, \ldots, m+1 \\ \frac{2(i-m-1)\pi}{t_e} & \text{if } i = m+2, m+3, \ldots, 2m \end{cases}$$

$$\phi_i = \begin{cases} \frac{\pi}{2} & \text{if } i = 1 \\ \left(\frac{1}{2} - m\right)\pi & \text{if } i = 2 \\ -\left(i + \frac{3}{2}\right)\pi & \text{if } i = 3, 4, \ldots, m+1 \\ -(i - m + 1)\pi & \text{if } i = m+2, m+3, \ldots, 2m \end{cases}$$

Thus, Eqs. (2.1)–(2.4) and (2.16) constitute the mathematical model for predicting 1-D time-dependent temperature profile in a N-layered pavement system based on the measured air temperature and solar radiation intensities.

2.2 Theoretical Solution Based on Separation of Variables

The method of separation of variables is one powerful method to solve BVPs [38]. In view of the sinusoidal terms in Eq. (2.16) and the linearities presented in the governing equation (2.1) and constraint conditions in Eqs. (2.2)–(2.4), the principle of superposition can be applied for this problem. Thus, we only need to

consider the following model BC

$$-\lambda_1 \frac{\partial T_1}{\partial z}(0,t) = B\left[A\sin(\omega t+\phi) - T_1(0,t)\right] \tag{2.17}$$

where A, ω, ϕ are magnitude, frequency, and phase angle of each sine function in Eq. (2.16), respectively. Furthermore, the final solution of $T_i(z,t)$ based on Eq. (2.16) equals the summation of temperature values based on each sinusoidal term in the right hand side of Eq. (2.16). Also, $\sin(\omega t+\phi)$ can be related to the complex number $e^{j(\omega t+\phi)}$ via the Euler formula

$$e^{j(\omega t+\phi)} = \cos(\omega t+\phi) + j\sin(\omega t+\phi) \tag{2.18}$$

where j = imaginary unit number with $j^2 = -1$.

If the unknown variable $T_i(z,t)$ in Eqs. (2.1)–(2.4) and (2.17) are replaced by the complex-valued function $Y_i(z,t)$ and $\sin(\omega t+\phi)$ replaced by $e^{j(\omega t+\phi)}$, then a new BVP can be formulated. Since the derivation of the theoretical solution of $Y_i(z,t)$ is much simpler than that of $T_i(z,t)$, $Y_i(z,t)$ is solved first. The theory of complex-valued functions of real variables implies that the corresponding solution of 1-D temperature profile $T_i(z,t)$ is simply the imaginary part of $Y_i(z,t)$.

To facilitate the derivation of the theoretical solution, the underlying governing equation and constraint conditions for the new BVP in terms of $Y_i(z,t)$ are summarized as follows:

1. Governing differential equation

$$\frac{\partial Y_i}{\partial t} = \alpha_i \frac{\partial^2 Y_i}{\partial z^2}, \qquad H_{i-1} \le z \le H_i \tag{2.19}$$

2. Interlayer contact conditions

$$Y_i(H_i,t) = Y_{i+1}(H_i,t) \tag{2.20}$$

$$\lambda_i \frac{\partial Y_i}{\partial z}(H_i,t) = \lambda_{i+1}\frac{\partial Y_{i+1}}{\partial z}(H_i,t) \tag{2.21}$$

3. Boundary conditions

$$|Y_n(z,t)| \le M \qquad \text{as} \quad z\to\infty \tag{2.22}$$

$$-\lambda_1 \frac{\partial Y_1}{\partial z}(0,t) = B\left[Ae^{j(\omega t+\phi)} - Y_1(0,t)\right] \tag{2.23}$$

where α_i, H_i, λ_i, B, and M are defined in Section 2.1.

The main steps involved in deriving the theoretical solution of $Y_i(z,t)$ are presented next. By the method of separation of variables [38], $Y_i(z,t)$ can be expressed as

$$Y_i(z,t) = u_i(z)e^{j(\omega t+\phi)} \tag{2.24}$$

It follows that

$$\frac{\partial Y_i}{\partial t}(z,t) = j\omega Y_i(z,t) \qquad \text{and} \qquad \frac{\partial^2 Y_i}{\partial z^2} = \frac{d^2 u_i}{dz^2}e^{j(\omega t+\phi)} \tag{2.25}$$

Substituting Eqs. (2.24) and (2.25) into Eq. (2.19) yields

$$\frac{d^2 u_i}{dz^2} - j\frac{\omega}{\alpha_i}u_i = 0 \tag{2.26}$$

The solution of Eq. (2.26) takes the following form

$$u_i(z) = C_i e^{-v_i(1+j)z} + D_i e^{v_i(1+j)z} \tag{2.27}$$

where $v_i = \sqrt{\frac{\omega}{2\alpha_i}}$ and C_i, D_i are constants of integration to be determined using the constraint conditions, thus the complex-valued function for temperature is

$$Y_i(z,t) = \left[C_i e^{-v_i(1+j)z} + D_i e^{v_i(1+j)z}\right] e^{j(\omega t+\phi)} \tag{2.28}$$

Based on Eq. (2.28) and interlayer contact conditions, i.e., Eqs. (2.20) and (2.21), the relationship between C_{i+1}, D_{i+1} and C_i, D_i can be determined as follows:

$$\begin{bmatrix} C_{i+1} \\ D_{i+1} \end{bmatrix} = \begin{bmatrix} e^{-(v_i-v_{i+1})H_i}P_i^{11} & e^{(v_i+v_{i+1})H_i}P_i^{12} \\ e^{-(v_i+v_{i+1})H_i}P_i^{21} & e^{(v_i-v_{i+1})H_i}P_i^{22} \end{bmatrix} \begin{bmatrix} C_i \\ D_i \end{bmatrix} \tag{2.29}$$

where $P_i^{lm}, l, m = 1, 2$ are defined in Appendix A. A recurrence formula linking C_i, D_i for $i = 2, 3, \ldots, n-1$ and C_1, D_1 can be further deduced as follows:

$$C_i = \left[e^{-2H_1 v_1}R_{i-1}^{11}C_1 + R_{i-1}^{12}D_1\right] e^{H_{i-1}(v_i+v_{i-1})} \tag{2.30}$$

$$D_i = \left[e^{-2H_1 v_1}R_{i-1}^{21}C_1 + R_{i-1}^{22}D_1\right] e^{-H_{i-1}(v_i-v_{i-1})} \tag{2.31}$$

where $R_1^{lm} = P_1^{lm}$ for $l, m = 1, 2$ and R_i^{lm} for $i = 2, 3, \ldots, n-1$ and $l, m = 1, 2$ are given in Appendix A. A

bounded solution for $Y_n(z,t)$ as $z \to \infty$ implies that $D_n = 0$ from Eq. (2.28), and the relationship between C_1 and D_1 can be obtained by setting $D_n = 0$ in Eq. (2.31), thus

$$D_1 = -e^{-2H_1 v_1} \frac{R_{n-1}^{21}}{R_{n-1}^{22}} C_1 \tag{2.32}$$

C_1 and D_1 can be determined by using Eqs. (2.23) and (2.32). Furthermore, C_i and D_i for the ith layer can be obtained by using the recurrence equations (2.30) and (2.31). Explicit expressions for C_i and D_i, $i = 1, 2, \ldots, n$ are given in Appendix A. Substituting C_i and D_i into Eq. (2.28) gives $Y_i(z,t)$.

As mentioned previously, the desired solution of the BVP represented by Eqs. (2.1)-(2.4) and (2.17) is the imaginary part of $Y_i(z,t)$. A complete set of solutions of $T_i(z,t)$ are given next.

If $0 \le z \le H_1$, then

$$T_1(z,t) = \Delta_{11} e^{-v_1 z} \sin(\omega t + \phi - v_1 z + \delta_{11}) + \Delta_{12} e^{v_1 z} \sin(\omega t + \phi + v_1 z + \delta_{12}) \tag{2.33}$$

If $H_{i-1} \le z \le H_i$ and $i = 2, 3, \ldots, n-1$, then

$$\begin{aligned} T_i(z,t) \quad = \quad & \Delta_{i1} e^{H_{i-1} v_{i-1} + v_i (H_{i-1} - z)} \sin(\omega t + \phi - v_i z + \delta_{i1}) \\ & + \Delta_{i2} e^{H_{i-1} v_{i-1} - v_i (H_{i-1} - z)} \sin(\omega t + \phi + v_i z + \delta_{i2}) \end{aligned} \tag{2.34}$$

If $z \ge H_{n-1}$, then

$$T_n(z,t) = \Delta_{n1} e^{H_{n-1} v_{n-1} + v_n (H_{n-1} - z)} \sin(\omega t + \phi - v_n z + \delta_{n1}) \tag{2.35}$$

where $\Delta_{i1}, \Delta_{i2}, \delta_{i1}$ for $i = 1, 2 \ldots, n$ and δ_{i2} for $i = 1, 2, \ldots, n-1$ in Eqs. (2.33)-(2.35) are given in Appendix A.

2.2.1 Model Verification with Measured Field Data

A FORTRAN computer program was coded to predict the time-dependent temperature profile in an N-layered pavement system using the above 1-D analytical solution. For the model verification, the calculated temperature profile through the concrete slab in a four-layered continuously reinforced concrete pavement (CRCP) is compared with measured field data from the Advanced Transportation Research and Engineering Laboratory (ATREL) at the University of Illinois [30]. The CRCP cross-section was composed of a reinforced concrete slab (0.254m), asphalt concrete base (0.102m), aggregate subbase (0.152 m), and supported by a silty-clay soil. Temperature at five different slab depth locations, i.e., $z = 0.0254$, 0.0762, 0.127, 0.178, and

0.229 m from the pavement surface, along with the air temperature, solar radiation intensity, and wind speed were measured at a half-hour interval.

In this study, temperature profile at the five slab depth locations were predicted every half-hour for a 61.5 and 71.5 hour period in the winter and summer, respectively. The calculated profiles started at 10:00 on December 21, 2002 until 23:30 on December 23, 2002 and in the summer from 0:00 on July 16, 2003 until 23:30 on July 18, 2003. The measured air temperature and solar radiation intensity at a half-hour interval for those calculation periods along with the fitted interpolatory trigonometric polynomials are shown in Figs. 2.2 and 2.3 and Figs. 2.4 and 2.5 for winter and summer conditions, respectively. Table 2.1 lists the thermal properties assumed for these pavement materials in the model validation [2, 17].

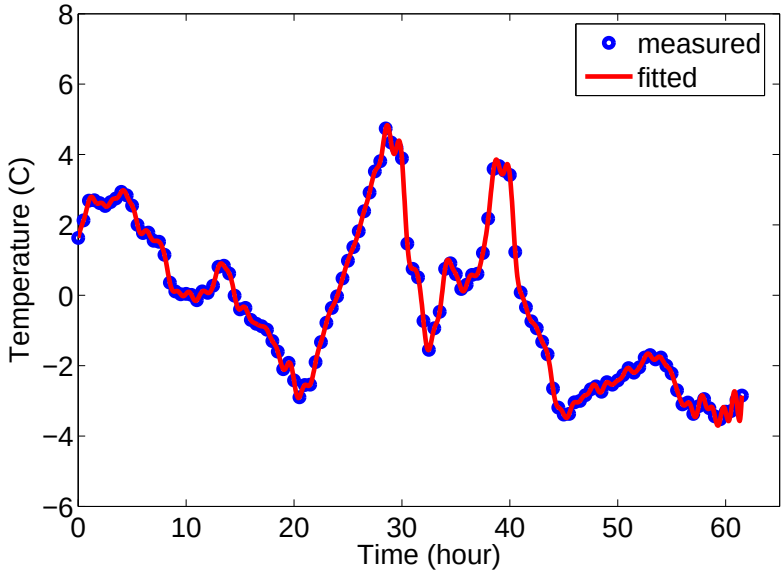

Figure 2.2: Measured and fitted air temperature for 61.5 hours in December 2002

The predicted and measured pavement temperatures at $z = 0.0254$ m, $z = 0.0762$ m, $z = 0.1270$ m, and $z = 0.1778$ m are plotted in Figs. 2.6 and 2.7 for December 2002 and Figs. 2.8 and 2.9 for July 2003, respectively. Table 2.2 summarizes the minimum and maximum values of $T_{\rm p} - T_{\rm m}$ and the average absolute error, i.e., $|T_{\rm p} - T_{\rm m}|$, at five different depth locations for both winter and summer conditions, where $T_{\rm p}$ and $T_{\rm m}$ are predicted and measured pavement temperatures, respectively.

Since temperature differential between the top and bottom of concrete slab plays an important role in calculating the curling stress in concrete slab, Table 2.3 summarizes the minimum and maximum value of $\Delta T_p - \Delta T_m$, and the average absolute errors, i.e., $|\Delta T_p - \Delta T_m|$ during the testing periods, where $\Delta T(t) = T_1(0.0254, t) - T_1(0.2286, t)$, and the subscripts p and m indicate the predicted and measured

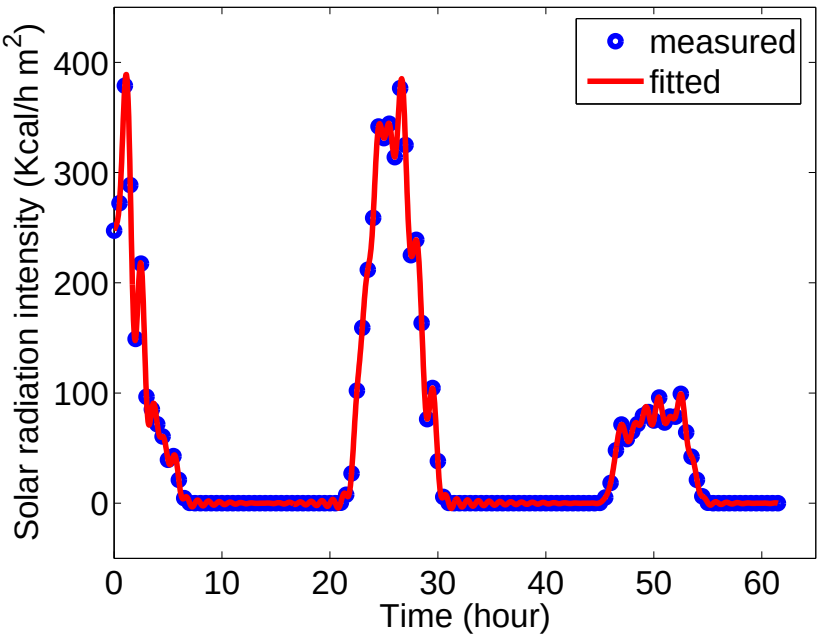

Figure 2.3: Measured and fitted solar radiation intensity for 61.5 hours in December 2002

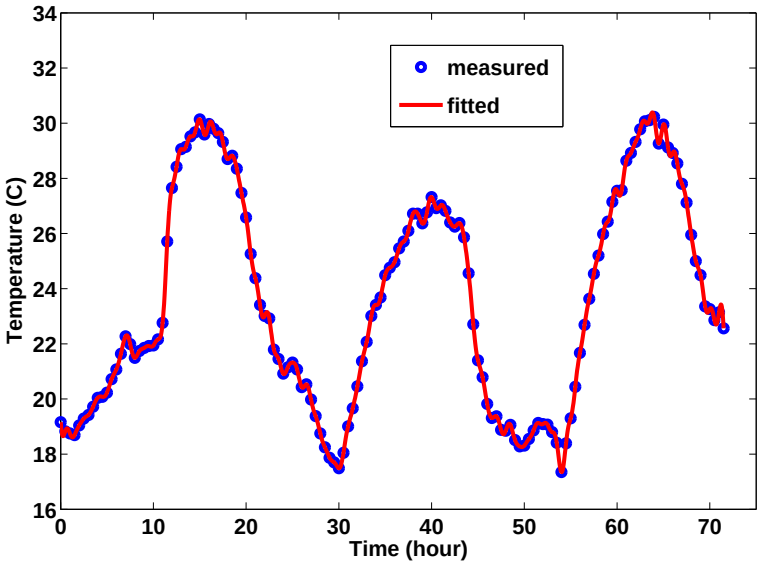

Figure 2.4: Measured and fitted air temperature for 71.5 hours in July 2003

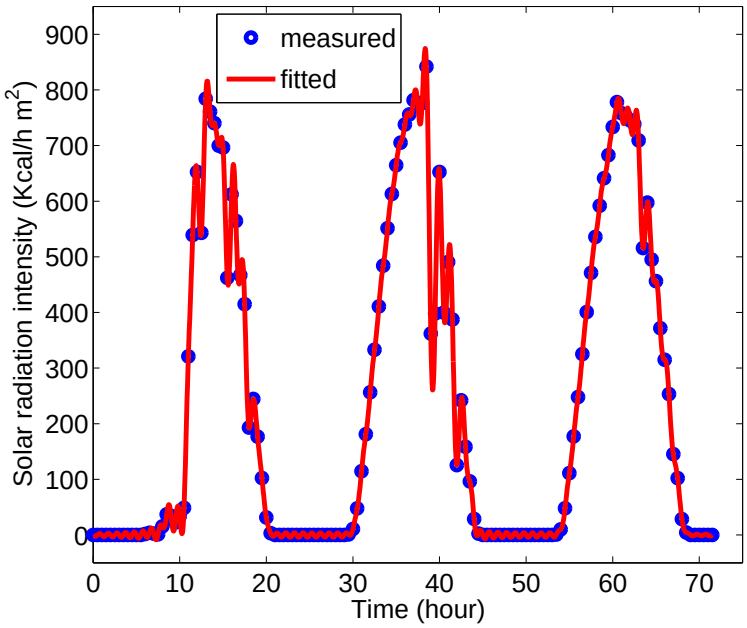

Figure 2.5: Measured and fitted solar radiation intensity for 71.5 hours in July 2003

Table 2.1: Thermal input parameters in model verification

Parameters	Value
Thermal conductivity, λ (Kcal/h m C)	
PCC slab	1.85
Asphalt concrete base	1.38
Aggregate subbase	2.58
Subgrade	1.00
Thermal diffusivity, α (m^2/h)	
PCC slab	0.0035
Asphalt concrete base	0.0021
Aggregate subbase	0.0030
Subgrade	0.0030
Effective absorptivity, $\widetilde{a_s}$	0.6 (summer)
	0.5 (winter)
Pavement surface convection coefficient, B (Kcal/m^2 h C)	16.29

Table 2.2: Minimum, maximum, and average absolute error values between predicted and measured temperature at different slab depths

		Slab depth location z (m)				
Date		0.0254	0.0762	0.127	0.178	0.229
Dec. 21-23, 2002	minimum	-0.68	-1.24	-2.03	-2.75	-3.32
	maximum	1.60	0.84	0.32	-0.15	-0.57
	average	0.62	0.51	0.64	1.04	1.46
July 16-18, 2003	minimum	-2.64	-0.65	0.42	1.15	1.83
	maximum	4.41	3.28	3.10	3.22	3.50
	average	1.16	1.17	1.68	2.27	2.76

values, respectively.

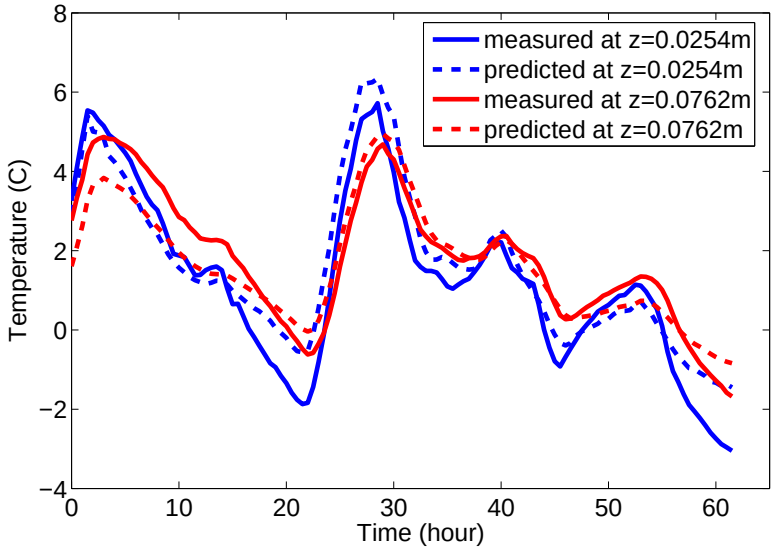

Figure 2.6: Predicted and measured temperature at $z = 0.0254$ m and $z = 0.0762$ m in December 2002

From Figs. 2.6 to 2.9 and Tables 2.2 and 2.3, the 1-D analytical solution gives reasonable time-dependent temperature profile in the concrete surface layer of the four-layer CRCP section but with some limitations. The prediction error can be related to a couple of assumptions in the model and material property inputs. The irradiation heat flux occurring at night is only indirectly accounted for by decreasing the surface absorptivity. This is likely the largest error source in the temperature prediction. There can be errors associated with the assumption of continuous interfacial heat flux. Furthermore, the pavement material thermal properties, e.g., thermal conductivity and thermal diffusivity, were estimated from published values. The pavement surface convection coefficient, B, used in Eq. (2.15) was assumed constant but is known to vary with wind speed and the difference between the air and pavement surface temperature. Finally, the actual pavement temperature

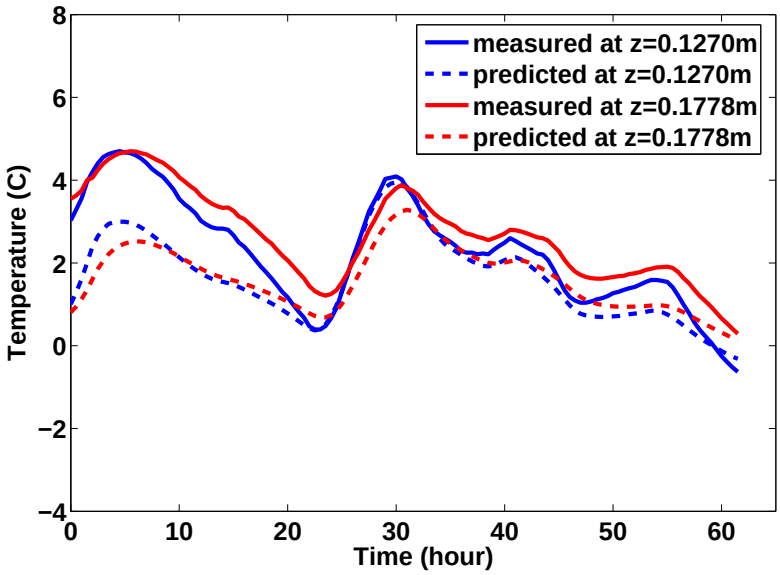

Figure 2.7: Predicted and measured temperature at $z = 0.127$ m and $z = 0.178$ m in December 2002

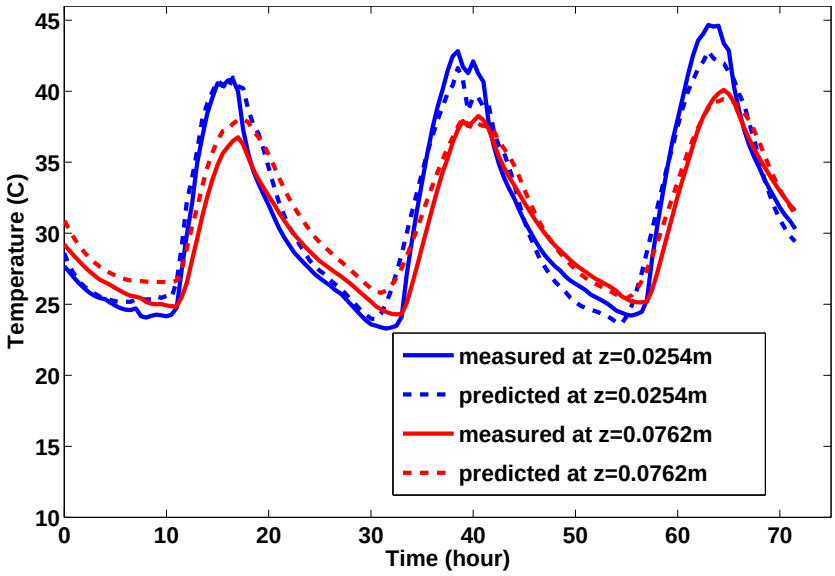

Figure 2.8: Predicted and measured temperature at $z = 0.0254$ m and $z = 0.0762$ m in July 2003

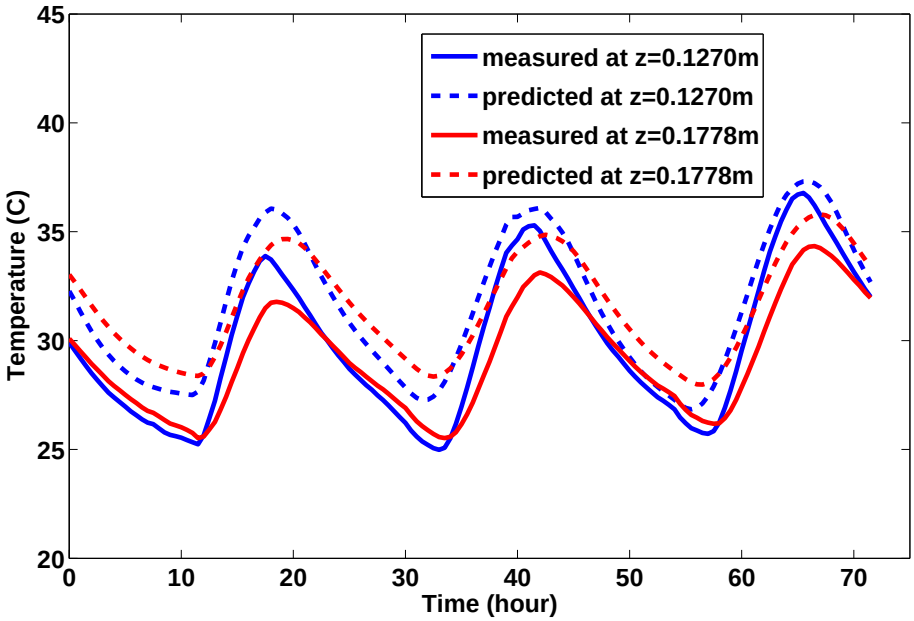

Figure 2.9: Predicted and measured temperature at $z = 0.127$ m and $z = 0.178$ m in July 2003

Table 2.3: Minimum, maximum, and average absolute error values between predicted and measured temperature differentials

		$\Delta T_p - \Delta T_m$
Dec. 21-23, 2002	minimum	0.48
	maximum	3.09
	average	1.79
July 16-18, 2003	minimum	-5.51
	maximum	1.20
	average	2.47

profile at time zero is not considered in this study.

2.2.2 Discussion of the Proposed 1-D Analytical Solution

Figs. 2.6 to 2.9 and Table 2.2 show that the proposed 1-D analytical solution gives more accurate temperature prediction on average when the evalution point is closer to the surface. The main reason for this behavior is that the temperature near the surface is more sensitive to air temperature and solar radiation, which are the main driving forces for the variation in pavement temperature profile. The current model also does not take into account the actual temperature profile at time zero in the pavement system, which can significantly influence the initial temperature predictions. It is worthy mentioning that the derived 1-D analytical solution does provide approximation to the initial pavement temperature profile. To improve the accuracy in predicting the initial temperature values evaluated at the locations near to the surface, extra values of air temperature and solar radiation intensity measured prior to $t = 0$ can be used in generating $T_a(t)$ in Eq. (2.6) and $Q(t)$ in Eq. (2.10), as explained below.

It is noted that the values of air temperature and solar radiation intensity measured every half-hour from 0:00 to 9:30 on December 21, 2002 are also used to calculate $T_a(t)$ in Eq. (2.6) and $Q(t)$ in Eq. (2.10) in generating Figs. (2.6) and (2.7) above, i.e., $t = 0$ and t_e in Eqs. (2.6) and (2.10) correspond to 0:00 on December 21, 2002 and 0:00 on December 24, 2002, respectively. The term "shift 10 hours" is used to indicate this fact. To study the effects of extra data used in calculating $T_a(t)$ and $Q(t)$ on the predicted pavement temperature profile between 10:00 on December 21, 2002 and 23:30 on December 23, 2002, temperature predictions are also carried out under the assumptions that "shift 3 hours" and "shift 6 hours" are made, respectively. The predicted temperature histories at $z = 0.0254$, 0.0762, 0.127, 0.178, and 0.229 m from the pavement surface using these three different "shifts" are plotted in Figs. 2.10 to 2.14, respectively, where Hour 0 corresponds to 10:00 on December 21, 2002 and Hour 61.5 to 23:30 on December 23, 2002. Table 2.4 lists the minimum and maximum values of ΔT_1 and ΔT_2 as well as the average values of $|\Delta T_1|$ and $|\Delta T_2|$, where ΔT_1 = predicted temperature value based on "shift 10 hours" minus that based on "shift 3 hours", ΔT_2 = predicted temperature value based on "shift 10 hours" minus that based on "shift 6 hours". Figs. 2.10 to 2.14 and Table 2.4 show that "shift 6 hours" and "shift 10 hours" do not make too much difference in estimating the temperature profile in the concrete layer for the period of testing, i.e., starting at 10:00 on December 21, 2002 until 23:30 on December 23, 2002. There is no such "shift" made in model verification for summer case, i.e., $t = 0$ corresponds to 0:00 on July 16, 2003 in Eqs. (2.6) and (2.10), and Figs. 2.8 and 2.9.

In order to improve the prediction accuracy, especially when applying to FWD testing, it is preferred to

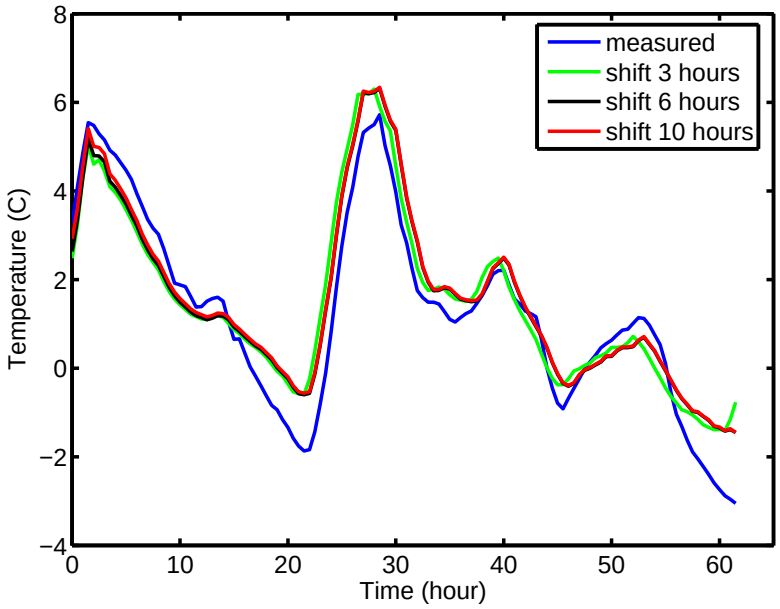

Figure 2.10: Predicted temperature histories at $z = 0.0254$ m based on three different "shifts" along with the measured one

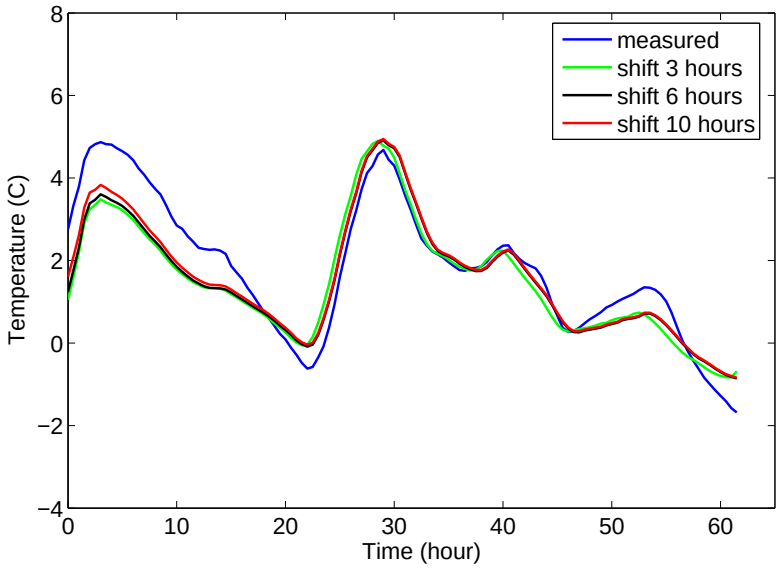

Figure 2.11: Predicted temperature histories at $z = 0.0762$ m based on three different "shifts" along with the measured one

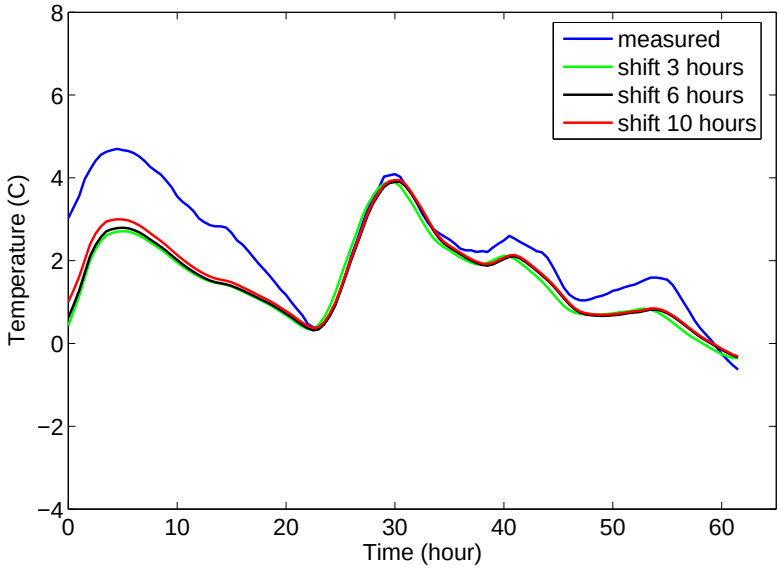

Figure 2.12: Predicted temperature histories at $z = 0.1270$ m based on three different "shifts" along with the measured one

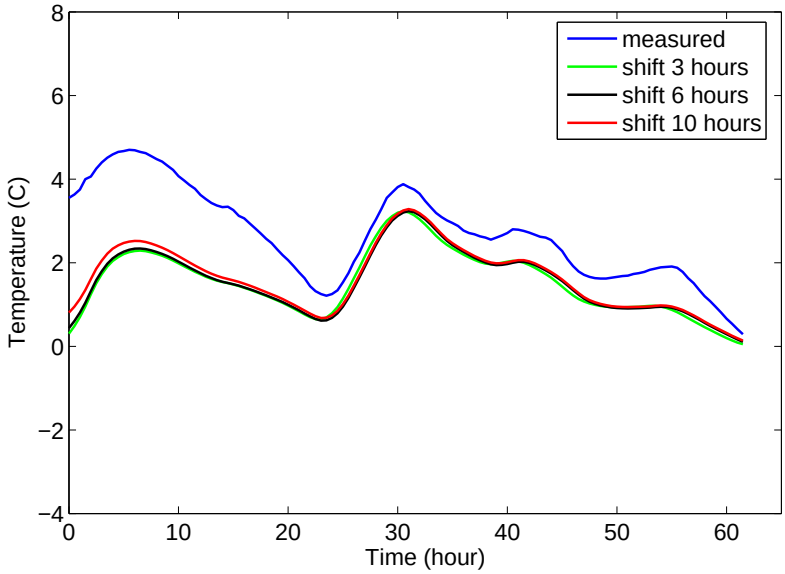

Figure 2.13: Predicted temperature histories at $z = 0.1778$ m based on three different "shifts" along with the measured one

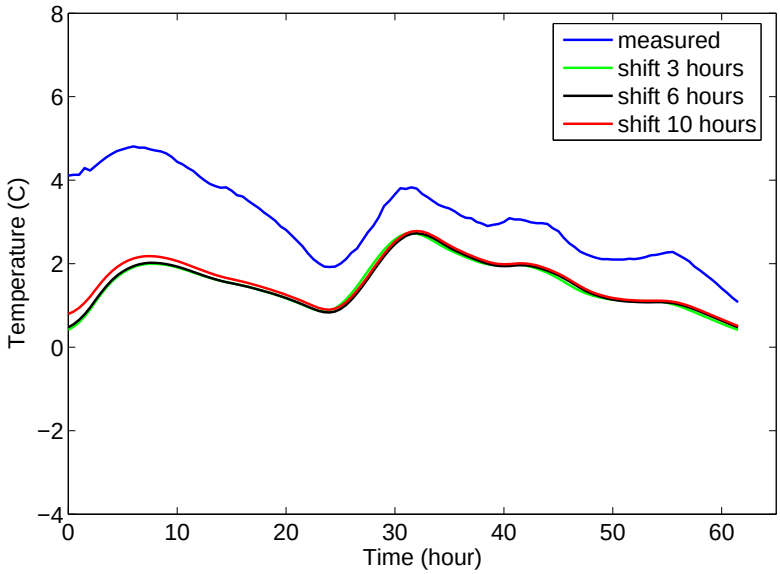

Figure 2.14: Predicted temperature histories at $z = 0.229$ m based on three different "shifts" along with the measured one

Table 2.4: Minimum, maximum, and average absolute error values between predicted temperatures based on adding extra data before time zero (3, 6, and 10 hours shift)

	Minimum (C)		Maximum (C)		Average (C)	
z (m)	ΔT_1	ΔT_2	ΔT_1	ΔT_2	ΔT_1	ΔT_2
0.0254	-0.77	0.002	0.83	0.29	0.24	0.05
0.0762	-0.48	0.02	0.55	0.36	0.19	0.06
0.127	-0.28	0.02	0.57	0.38	0.15	0.08
0.178	-0.19	0.03	0.50	0.37	0.13	0.08
0.229	-0.12	0.03	0.38	0.32	0.11	0.08

use measured air temperature and solar radiation intensities for both the FWD testing day and the previous day when generating the trigonometric interpolatory polynomials presented in Eqs. (2.6) and (2.10). The initial pavement temperature predictions are then shifted back to the day before FWD testing was performed. If no measured air temperature and solar radiation are available, published climatical data, such as daily mean, minimum and maximum air temperatures, and total solar radiation intensity can be used to generate continuous functions in time as long as those functions can be expressed as the summation of trigonometric sine functions. This proposed 1-D analytical solution is limited to estimating pavement temperature profile in a more steady state condition, that is without intermittent periods of rain or snow.

2.2.3 Section Summary

The analytical solution of the time-dependent 1-D temperature profile in a multi-layered pavement system has been successfully derived. Pavement temperature profile can be estimated using this proposed 1-D solution with input data such as pavement layer thicknesses, material thermal properties, air temperature, and solar radiation intensities. The interpolatory trigonometric polynomials, based on the discrete least squares approximation, are used to fit the measured air temperature and solar radiation intensities for a time period which are the essential components in the surface boundary conditions for this heat transfer problem. Field model validation demonstrates that the proposed 1-D analytical solution generates reasonable temperature profiles in a concrete slab that is part of a four-layered CRCP section. The main advantage of this 1-D analytical solution is that it is easy to implement and useful for a range of practical pavement engineering problems such as asphalt concrete temperature correction and temperature differetials in a concrete slab during FWD testing.

2.3 Theoretical Solution Based on the Laplace Transform

In this section, we derive the 1-D analytical solution using the method of Laplace integral transformation. Integral transformations have also been proven to be powerful methods to solve heat conduction problems in solids [9]. Recently, Chong et al. applied Laplace transforms and numerical inverse Laplace transforms to predict temperature profile in a two-layered pavement system based on material thermal properties, measured air temperature data, and calculated solar radiation intensities from meteorological studies [10].

To apply the Laplace transform to solve the temperature profile, the initial pavement temperature has to be known. For simplicity, we assume uniform initial pavement temperature profile in this study, i.e.,

$$T_j(z,0) = c, \;\; j = 1, 2, \ldots, n \tag{2.36}$$

where c is a constant.

To facilitate the derivation of the solution, we introduce the variable $U_j(z,t)$ for $j = 1, 2, \ldots, n$

$$U_j(z,t) = T_j(z,t) - T_j(z,0) \tag{2.37}$$

the BVP can now be written in terms of $U_j(z,t),\ j = 1, 2, \ldots, n$ as follows:

$$\frac{\partial U_j}{\partial t}(z,t) = \alpha_j \frac{\partial^2 U_j}{\partial z^2}(z,t) \quad 0 < t < \infty,\ H_{j-1} < z < H_j,\ j = 1, 2, \ldots, n \tag{2.38}$$

$$U_j(H_j,t) = U_{j+1}(H_j,t) \tag{2.39}$$

$$\lambda_j \frac{\partial U_j}{\partial z}(H_j,t) = \lambda_{j+1} \frac{\partial U_{j+1}}{\partial z}(H_j,t) \tag{2.40}$$

$$|U_j(z,t)| < M \;\text{ for all } j = 1, 2, \ldots, n \tag{2.41}$$

$$-\lambda_1 \frac{\partial U_1}{\partial z}(0,t) = B \left\{ \frac{a_0}{2} + \frac{\widetilde{a}_s c_0}{2B} + \left(\frac{a_m}{2} + \frac{\widetilde{a}_s c_m}{2B} \right) \cos(m\bar{t}) + \sum_{k=1}^{m-1} \left[\left(a_k + \frac{\widetilde{a}_s c_k}{B} \right) \cos(k\bar{t}) + \left(b_k + \frac{\widetilde{a}_s d_k}{B} \right) \sin(k\bar{t}) \right] - c - U_1(0,t) \right\} \tag{2.42}$$

$$U_j(z,0) = 0 \;\text{ for all } j = 1, 2, \ldots, n \tag{2.43}$$

with the symbols defined previously.

Let $\mathcal{L}$ denote the Laplace transform operator, $\hat{U}_j(z,s)$ be the Laplace transform of $U_j(z,t)$ with respect to time t, and s denote the transform variable. Furthermore, the following fundamental operational property

of the Laplace transformation is needed [43, p. 148]

$$\mathcal{L}\left[f'(t)\right] = s\hat{f}(s) - f(0) \tag{2.44}$$

where $\hat{f}(s)$ is assumed to exist.

Applying Laplace transform with respect to t to Eq. (2.38) in conjunction with Eqs. (2.43) and (2.44) produces

$$\frac{\partial^2 \hat{U}_j(z,s)}{\partial z^2} - \frac{s}{\alpha_j}\hat{U}_j(z,s) = 0, \;\; H_{j-1} < z < H_j, \; j = 1, 2, \ldots, n \tag{2.45}$$

Let $r_j(s) = \sqrt{\frac{s}{\alpha_j}}$, then the solution of Eq. (2.45) is

$$\hat{U}_j(z,s) = C_j(s)e^{-r_j z} + D_j(s)e^{r_j z}, \; j = 1, 2, \ldots, n \tag{2.46}$$

where $C_j(s), \; D_j(s), \; j = 1, 2, \ldots, n$ are to be determined using the Laplace transforms of the boundary and interface conditions. It follows from Eq. (2.46) that

$$\frac{\partial \hat{U}_j}{\partial z}(z,s) = -r_j\left[C_j e^{-r_j z} - D_j e^{r_j z}\right], \; j = 1, 2, \ldots, n \tag{2.47}$$

Applying Laplace transform with respect to t to the interface conditions in Eqs. (2.39) and (2.40) in conjunction with Eqs. (2.46) and (2.47) yields Eqs. (2.48) and (2.49), respectively.

$$C_j e^{-r_j H_j} + D_j e^{r_j H_j} = C_{j+1}e^{-r_{j+1}H_j} + D_{j+1}e^{r_{j+1}H_j} \tag{2.48}$$

$$\lambda_j r_j\left(C_j e^{-r_j H_j} - D_j e^{r_j H_j}\right) = \lambda_{j+1} r_{j+1}\left(C_{j+1}e^{-r_{j+1}H_j} - D_{j+1}e^{r_{j+1}H_j}\right) \tag{2.49}$$

Defining for $j = 1, 2, \ldots, n-1$,

$$\begin{aligned} \xi_j &= e^{(r_j - r_{j+1})H_j} \\ \eta_j &= e^{(r_j + r_{j+1})H_j} \end{aligned}$$

then the relationship between C_{j+1}, D_{j+1} and C_j, D_j for $j = 1, 2, \ldots, n-1$ can be established using Eqs. (2.48) and (2.49) as follows:

$$C_{j+1} = \frac{1}{\xi_j}P_j^{11}C_j + \eta_j P_j^{12}D_j \tag{2.50}$$

$$D_{j+1} = \frac{1}{\eta_j}P_j^{21}C_j + \xi_j P_j^{22}D_j \tag{2.51}$$

where

$$\begin{aligned} P_j^{11} &= \frac{1}{2}\left[1+\frac{\lambda_j}{\lambda_{j+1}}\sqrt{\frac{\alpha_{j+1}}{\alpha_j}}\right] \\ P_j^{12} &= \frac{1}{2}\left[1-\frac{\lambda_j}{\lambda_{j+1}}\sqrt{\frac{\alpha_{j+1}}{\alpha_j}}\right] \\ P_j^{21} &= P_j^{12} \\ P_j^{22} &= P_j^{11} \end{aligned} \tag{2.52}$$

Furthermore, relationship between $C_j, D_j,\ j = 2, 3, \ldots, n$ and C_1, D_1 can be deduced from Eqs. (2.50) and (2.51)

$$C_j = \left(e^{-2r_1h_1}R_{j-1}^{11}C_1 + R_{j-1}^{12}D_1\right)\eta_{j-1} \tag{2.53}$$

$$D_j = \left(e^{-2r_1h_1}R_{j-1}^{21}C_1 + R_{j-1}^{22}D_1\right)\xi_{j-1} \tag{2.54}$$

where

$$R_1^{kl} = P_1^{kl},\ k, l = 1, 2 \tag{2.55}$$

and for $j = 2, 3, \ldots, n-1$

$$\begin{aligned} R_j^{11} &= e^{-2r_jH_j}\eta_{j-1}P_j^{11}R_{j-1}^{11} + \xi_{j-1}P_j^{12}R_{j-1}^{21} \\ R_j^{12} &= e^{-2r_jH_j}\eta_{j-1}P_j^{11}R_{j-1}^{12} + \xi_{j-1}P_j^{12}R_{j-1}^{22} \\ R_j^{21} &= e^{-2r_jH_j}\eta_{j-1}P_j^{21}R_{j-1}^{11} + \xi_{j-1}P_j^{22}R_{j-1}^{21} \\ R_j^{22} &= e^{-2r_jH_j}\eta_{j-1}P_j^{21}R_{j-1}^{12} + \xi_{j-1}P_j^{22}R_{j-1}^{22} \end{aligned} \tag{2.56}$$

As shown in Eq. (2.46), there are $2N$ unknown constants of integration, $C_j,\ D_j, j = 1, 2, \ldots, N$ in an N-layer pavement system, which are determined using the Laplace transforms of the boundary and interface conditions. With the help of Eqs. (2.53) and (2.54), a linear system of two rather than $2N$ equations needs to be solved.

In view of the bounded temperature assumption, i.e., Eq. (2.4), it follows that $U_n(z,t)$ is also bounded for all $z > H_{n-1}$ and $t > 0$. Using this fact and the sufficient condition for existence of the Laplace transforms [11, pp. 6-7], we can easily prove that for fixed complex number s with $\mathrm{Re}(s) > 0$, $\hat{U_n}(z,s)$ is bounded for all $z > H_{n-1}$, where $\mathrm{Re}(s)$ denotes the real part of complex number s. Thus, for this reason $D_n(s) = 0$ from

which the following equation can be obtained using Eq. (2.54)

$$D_1 = -\frac{R_{n-1}^{21}}{R_{n-1}^{22}} e^{-2r_1 h_1} C_1 \tag{2.57}$$

Let

$$\begin{aligned} f(t) &= \frac{a_0}{2} + \frac{\widetilde{a}_s c_0}{2B} + \left(\frac{a_m}{2} + \frac{\widetilde{a}_s c_m}{2B}\right)\cos(m\bar{t}) + \sum_{k=1}^{m-1}\left[\left(a_k + \frac{\widetilde{a}_s c_k}{B}\right)\cos(k\bar{t})\right. \\ &\quad \left. + \left(b_k + \frac{\widetilde{a}_s d_k}{B}\right)\sin(k\bar{t})\right] - c \end{aligned} \tag{2.58}$$

then Eq. (2.42) becomes

$$-\lambda_1 \frac{\partial U_1}{\partial z}(0,t) = B[f(t) - U_1(0,t)] \tag{2.59}$$

Applying Laplace transform on t to the both sides of Eq. (2.59) yields

$$-\lambda_1 \frac{\partial \hat{U}_1}{\partial z}(0,s) = B\left[\hat{f}(s) - \hat{U}_1(0,s)\right] \tag{2.60}$$

where

$$\begin{aligned} \hat{f}(s) &= \mathcal{L}[f(t)] \\ &= \left(\frac{a_0}{2} + \frac{\widetilde{a}_s c_0}{2B} - c\right)\frac{1}{s} + \left(\frac{a_m}{2} + \frac{\widetilde{a}_s c_m}{2B}\right)\frac{(-1)^m s}{s^2 + \beta_m^2} \\ &\quad + \sum_{k=1}^{m-1} \frac{(-1)^k}{s^2 + \beta_k^2}\left[\left(a_k + \frac{\widetilde{a}_s c_k}{B}\right)s + \left(b_k + \frac{\widetilde{a}_s d_k}{B}\right)\beta_k\right] \end{aligned} \tag{2.61}$$

where $\beta_k = \frac{2k\pi}{t_{\text{end}}},\ k = 1, 2, \ldots, m$.

From Eq. (2.47), we know

$$\frac{\partial \hat{U}_1}{\partial z}(0,s) = -r_1 (C_1 - D_1) \tag{2.62}$$

Also, setting $j = 1$ and $z = 0$ in Eq. (2.46) gives

$$\hat{U}_1(0,s) = C_1 + D_1 \tag{2.63}$$

Inserting Eqs. (2.57), (2.62) and (2.63) into Eq. (2.60) produces

$$C_1 = \frac{BR_{n-1}^{22}\hat{f}(s)}{(B+\lambda_1 r_1)R_{n-1}^{22} - (B-\lambda_1 r_1)R_{n-1}^{21}e^{-2r_1h_1}} \tag{2.64}$$

$$D_1 = \frac{BR_{n-1}^{21}\hat{f}(s)e^{-2r_1h_1}}{(B-\lambda_1 r_1)R_{n-1}^{21}e^{-2r_1h_1} - (B+\lambda_1 r_1)R_{n-1}^{22}} \tag{2.65}$$

Furthermore, any $C_j,\ j = 2,3,\ldots,n$ and $D_j,\ j = 2,3,\ldots,n-1$ can be determined using Eqs. (2.53) and (2.54), respectively. Finally, $U_j(z,t)$ can be obtained by inverse Laplace transform [15, p. 265] as follows:

$$U_j(z,t) = \frac{1}{2\pi i}\int_{\nu-i\infty}^{\nu+i\infty}\hat{U}_j(z,s)e^{st}ds, \quad H_{j-1} < z < H_j \tag{2.66}$$

where ν is some real number such that $\hat{U}_j(z,s)$ converges absolutely along the line $\mathrm{Re}(s) = \nu$, i = pure imaginary number with $i^2 = -1$, and $\hat{U}_j(z,s)$ is given in Eq. (2.46).

2.3.1 Numerical Inversion of the Laplace Transform

Due to the complexities of $\hat{U}_j(z,s),\ j = 1,2,\ldots,n$, the closed-form solution of Eq. (2.66) is difficult to obtain. In this study, a 10-point Gaussian quadrature formula for numerically evaluating the inverse Laplace transformation is employed [48]

$$\frac{1}{2\pi i}\int_{\nu-i\infty}^{\nu+i\infty}\frac{e^p}{p}F(p)\,dp \approx \sum_{j=1}^{10} w_j F(p_j) \tag{2.67}$$

where $w_j, p_j,\ j = 1,2,\ldots,10$ are weights and abscissae, respectively.

For fixed z with $H_{j-1} \le z \le H_j$ and t, let $st = p$, then the complex integral in Eq. (2.66) can be written in the form of the integrals in Eq. (2.67) as follows:

$$U_j(z,t) = \frac{1}{2\pi i}\int_{\gamma-i\infty}^{\gamma+i\infty}\frac{e^p}{p}F_j(p)\,dp \tag{2.68}$$

where $F_j(p) = \hat{U}_j(z,\frac{p}{t})\frac{p}{t}$, then Eq. (2.68) is ready to be approximated using Eq. (2.67). For the sake of completeness, $p_j, w_j,\ j = 1,3,\ldots,9$ are listed in Table 2.5, and $p_j,\ w_j$ are equal to the conjugate of p_{j-1}, w_{j-1} for $j = 2,4,\ldots,10$, respectively [48, pp. 308-309].

Table 2.5: Ascissae and weights used in the 10-point Gaussian quadrature formula

i	p_i	w_i
1	0.1283767707781087E2+i0.1666062584162301E1	-0.8684606112670226E3+i0.1545742053305275E5
3	0.1222613148416215E2+i0.5012719263676864E1	0.1551634444257753E4-i0.8439832902983925E4
5	0.1093430343060001E2+i0.8409672996003092E1	-0.8586520055271992E3+i0.2322065401339348E4
7	0.8776434640082609E1+i0.1192185389830121E2	0.1863271916070924E3-i0.2533223820180114E3
9	0.5225453367344361E1+i0.1572952904563926E2	-0.1034901907062327E2+i0.4110935881231860E1

2.3.2 Model Verification with Measured Field Data

A FORTRAN computer program was developed to predict the time-dependent temperature distribution in an N-layered pavement system using the above numerical inversion of the Laplace transform. For the model justification, the computed temperature profile through the same concrete slab in a four-layered CRCP system is compared with the measured field data from ATREL, as mentioned in Section 2.2.1.

In this study, the temperature at the five slab depth locations, i.e., z = 0.0254, 0.0762, 0.127, 0.178, and 0.229 m from the pavement surface, were computed every half an hour for a 32-hour period in the winter and summer. The calculated profiles started in the winter from 10:00 on December 21, 2002 until 18:00 on December 22, 2002 and in the summer from 0:00 on July 16, 2003 until 08:00 on July 17, 2003. The measured air temperature and solar radiation intensity for those calculation periods along with the fitted interpolatory trigonometric polynomials are presented in Figs. 2.15 and 2.16 and Figs. 2.17 and 2.18 for winter and summer conditions, respectively. Table 2.6 lists the thermal properties assumed for these pavement materials in the model validation [2, 17].

The predicted and measured pavement temperatures at z =0.0254 m, z =0.0762 m, z =0.1270 m, and z =0.1778 m are plotted in Figs. 2.19 and 2.20 for December 2002 and Figs. 2.21 and 2.22 for July 2003, respectively. Table 2.7 presents the minimum and maximum values of $T_{\rm p} - T_{\rm m}$ and the average absolute error, i.e., $|T_{\rm p} - T_{\rm m}|$, at five different depth locations for both winter and summer conditions, where $T_{\rm p}$ and $T_{\rm m}$ are predicted and measured pavement temperatures, respectively. Also, Table 2.8 summarizes the minimum and maximum value of $\Delta T_p - \Delta T_m$, and the average absolute errors, i.e., $|\Delta T_p - \Delta T_m|$ during the testing periods, where $\Delta T(t) = T_1(0.0254, t) - T_1(0.2286, t)$, and ΔT_p and ΔT_m are predicted and measured temperature differentials, respectively.

From Figs. 2.19 to 2.22 and Tables 2.7 and 2.8, the 1-D analytical solution based on the Laplace transform generated reasonable time-dependent temperature distribution in the concrete slab but with some limitations. The prediction error can be attributed to a couple of assumptions in the model, material property inputs, and the numerical inversion of the Laplace transform. The irradiation heat flux occurring in the pavement

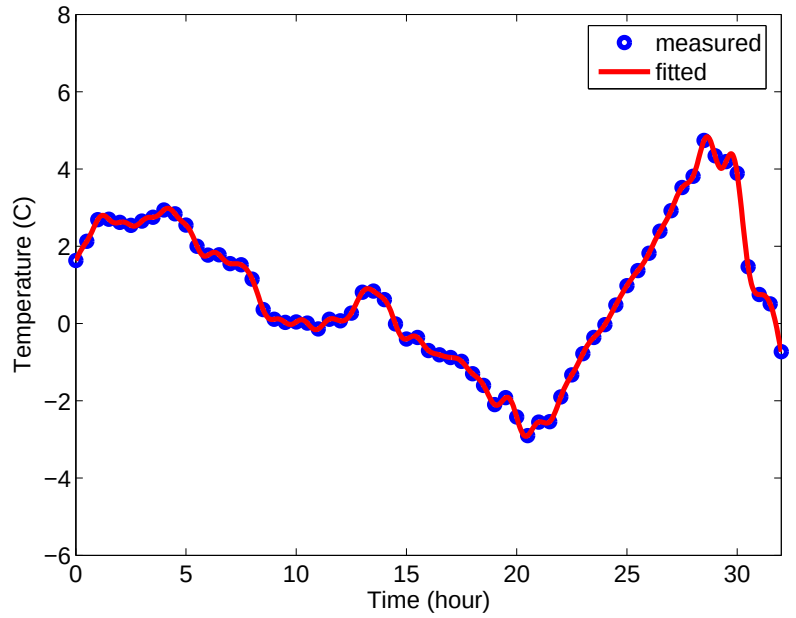

Figure 2.15: Measured and fitted air temperature for 32 hours in December 2002

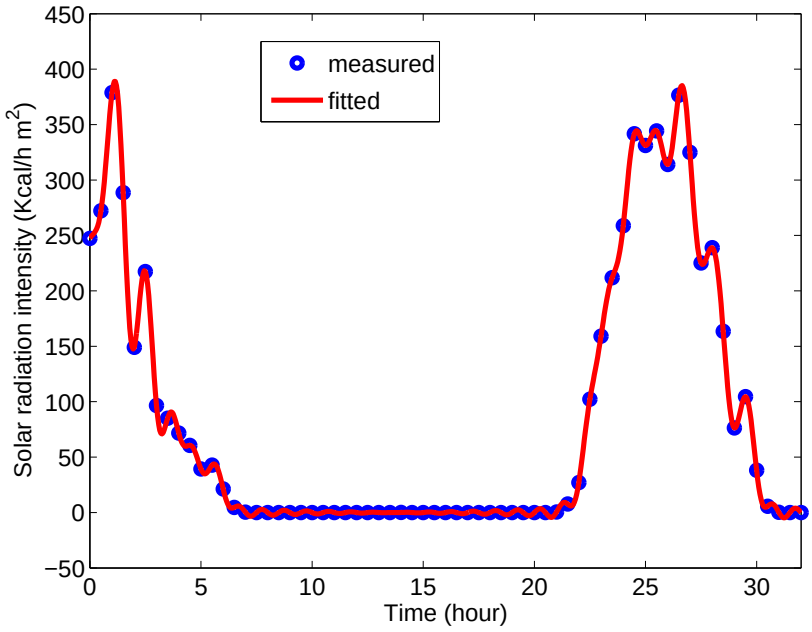

Figure 2.16: Measured and fitted solar radiation intensity for 32 hours in December 2002

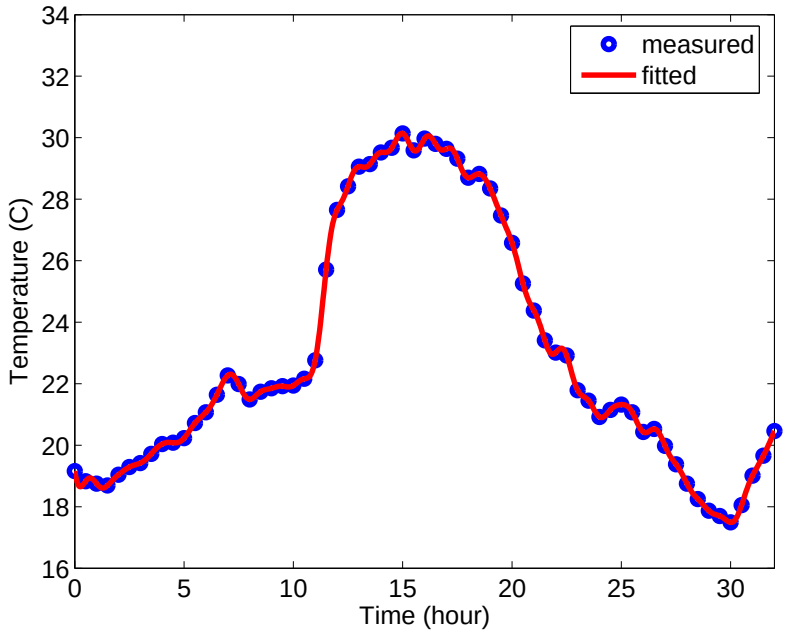

Figure 2.17: Measured and fitted air temperature for 32 hours in July 2003

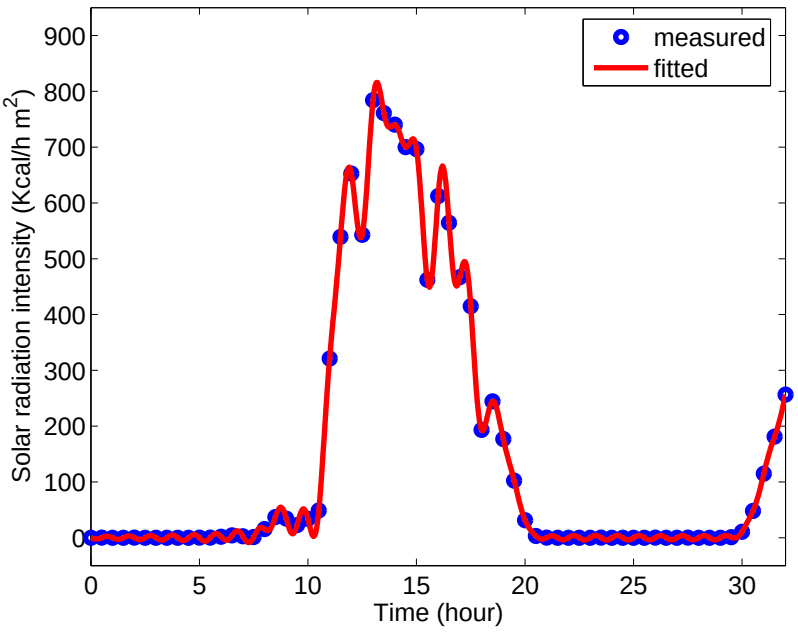

Figure 2.18: Measured and fitted solar radiation intensity for 32 hours in July 2003

Table 2.6: Thermal input parameters in model verification

Parameters	Value
Thermal conductivity, λ (Kcal/h m C)	
PCC slab	1.85
Asphalt concrete base	1.38
Aggregate subbase	2.58
Subgrade	1.00
Thermal diffusivity, α (m^2/h)	
PCC slab	0.0035
Asphalt concrete base	0.0021
Aggregate subbase	0.0030
Subgrade	0.0030
Effective absorptivity, $\widetilde{a_s}$	0.6 (summer)
	0.5 (winter)
Pavement surface convection coefficient, B (Kcal/m^2 h C)	16.29
Initial temperature c (Celsius Degree)	30 (summer)
	2 (winter)

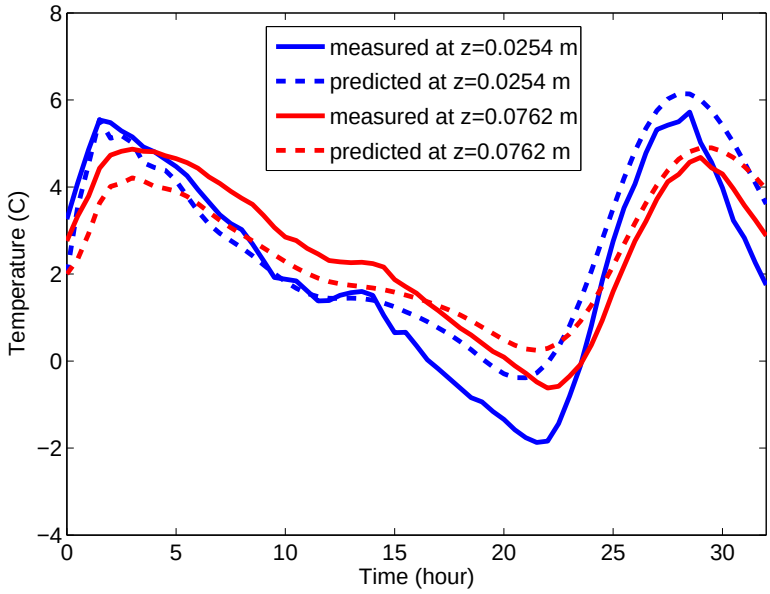

Figure 2.19: Predicted and measured temperature at $z = 0.0254$ m and $z = 0.0762$ m in December 2002

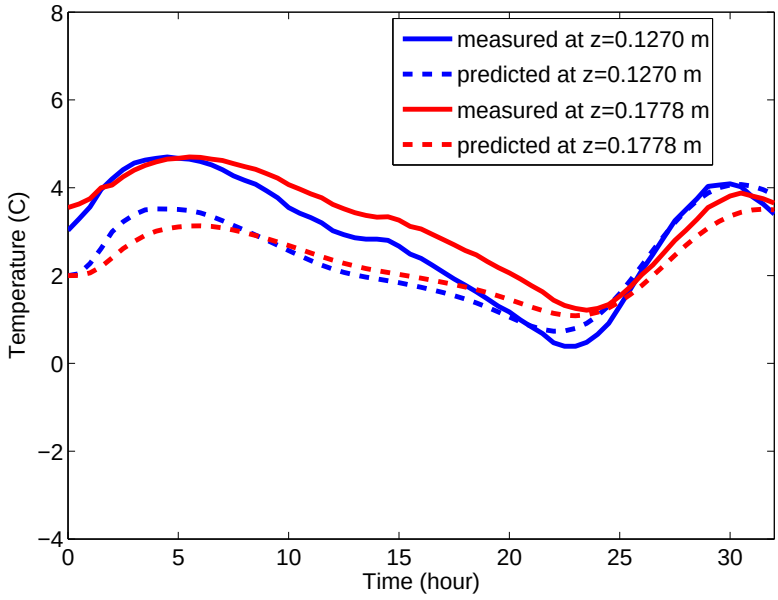

Figure 2.20: Predicted and measured temperature at $z = 0.1270$ m and $z = 0.1778$ m in December 2002

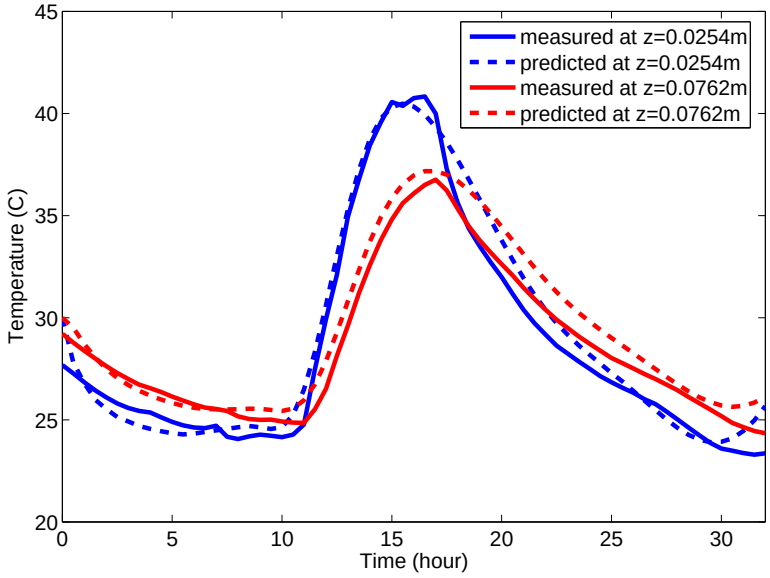

Figure 2.21: Predicted and measured temperature at $z = 0.0254$ m and $z = 0.0762$ m in July 2003

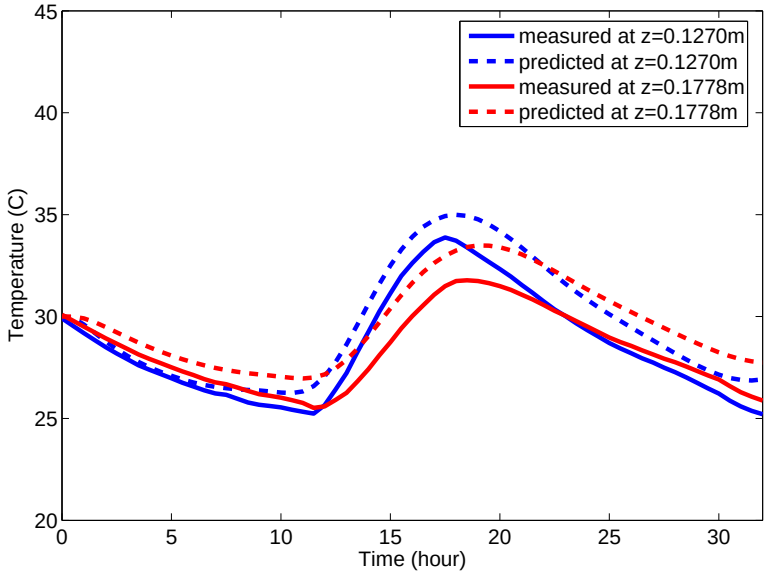

Figure 2.22: Predicted and measured temperature at $z = 0.127$ m and $z = 0.1778$ m in July 2003

Table 2.7: Minimum, maximum, and average absolute error values between predicted and measured temperature at different slab depths

		Slab depth location z (m)				
Date		0.0254	0.0762	0.1270	0.1778	0.2286
Dec. 21-22, 2002	minimum	-1.26	-0.99	-1.34	-1.80	-2.24
	maximum	1.86	1.07	0.44	-0.08	-0.55
	average	0.72	0.60	0.64	0.95	1.37
July 16-17, 2003	minimum	-0.89	-0.37	0.09	-0.09	0.08
	maximum	2.40	1.93	1.86	1.98	2.15
	average	0.79	0.82	1.02	1.31	1.59

Table 2.8: Minimum, maximum, and average absolute error values between predicted and measured temperature differentials

		$\Delta T_p - \Delta T_m$
Dec. 21-22, 2002	minimum	0.85
	maximum	2.70
	average	1.85
July 16-17, 2003	minimum	-2.73
	maximum	2.24
	average	1.26

system, likely the largest error source, is only indirectly accounted for by decreasing the surface absorptivity. There can also be errors associated with the assumptions of continuous temperature and heat flux at the layer interface. Furthermore, the pavement material thermal properties, e.g., thermal conductivity and thermal diffusivity, were estimated from published values. The pavement surface convection coefficient, B, was assumed constant but is known to vary with wind speed and the difference between the air and pavement surface temperature. Finally, the initial pavement temperature profile was uniformly fixed in this study.

Figs. 2.19 to 2.22 and Table 2.7 suggest that the proposed 1-D analytical solution gives more accurate temperature prediction on average than the separation of variables method for shorter time duration especially when the evalution point is near the surface. The current model also assumes uniform initial temperature profile, which can significantly influence the initial temperature profile predictions.

In this study, numerical experiments on the inverse Laplace transform suggest that it is better to have $t_e < 40$ hours in order to obtain more accurate temperature values. If no measured air temperature and solar radiation are available, published climatical data, such as daily mean, minimum, and maximum air temperatures, and total solar radiation intensity may be used to generate air temperature and solar radiation intensity functions with respect to time. In this case, the proposed 1-D analytical solution will still work provided that the Laplace transforms of those functions exist and the numerical inversion of Laplace transform is stable, if the numerical inversion is necessary. Again, this proposed 1-D analytical solution is limited to estimating pavement temperature profile in a more steady state condition, that is, without intermittent periods of rain or snow.

2.3.3 Section Summary

The analytical solution of the time-dependent 1-D temperature profile in an N-layered pavement system has been successfully derived using the Laplace transfomation with the inverse Laplace transform being resolved numerically using Gaussian quadrature formula. The relationship between the constants of integration for the ith layer and the first layer was deduced which expedited the solution process. As the main driving forces for the variation of time-dependent pavement temperature profile, transient air temperature and solar radiation intensities were considered in the boundary condition. Model verification with the measured pavement temperature profiles demonstrates that the proposed 1-D analytical solution predicts reasonable temperature profiles in a concrete slab for a consecutive 32-hour period in both winter and summer conditions. With the aid of Gaussian quadrature formula to solve the inverse Laplace transform, the proposed solution technique is easy to employ, and useful for a range of practical pavement engineering problems such as estimating the temperature in the asphalt concrete layer or temperature differentials in a concrete slab

during FWD testing.

Chapter 3

2-Dimensional Axisymmetric Pavement Temperature Profile Prediction

In this chapter, 2-dimensional axisymmetric analytical solutions of temperature profile in multi-layered pavement systems are presented. The main mathematical tools used are the method of separation of variables and Hankel integral transform. The temperature profile in the layer i, $T_i(r, z, t)$ is assumed to be axisymmetrical. One advantage of this assumption is that the thermal stresses in multi-layered pavement system due to temperature change can be easily incorporated with the traffic loading stresses by using the layered elastic theory, since the latter is also considered to be axisymmetric [6, 7, 8].

3.1 Mathematical Temperature Model

The 2-D axisymmetric temperature distribution in a multi-layered pavement system can be modeled as a heat transfer problem (Fig. 3.1), where h_i = layer thickness (m); λ_i = thermal conductivity (Kcal/m hr C); α_i = thermal diffusivity (m^2/hr); and $T_i(r, z, t)$ = temperature (C) for layer i. The thickness of the last layer (subgrade) h_n is assumed to be infinite along the positive z direction.

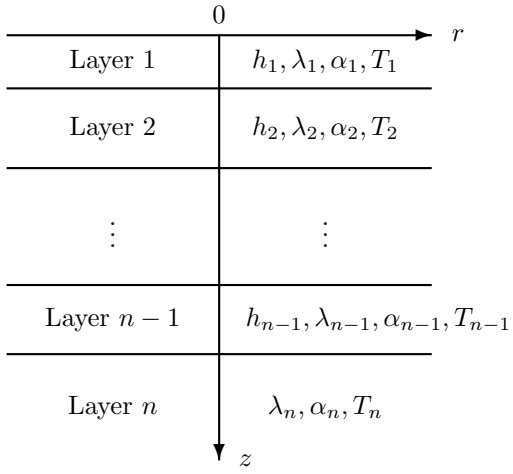

Figure 3.1: 2-D axisymmetric temperature profile in a multi-layered pavement system

The governing time-dependent PDE for the temperature model in each layer is the heat equation

$$\frac{\partial T_i}{\partial t} = \alpha_i \nabla^2 T_i \qquad \text{for} \qquad H_{i-1} \le z \le H_i \tag{3.1}$$

where $H_i = \sum_{k=1}^{i} h_k$ and $\nabla^2 = \frac{\partial^2}{\partial r^2} + \frac{1}{r}\frac{\partial}{\partial r} + \frac{\partial^2}{\partial z^2}$, Laplace operator in cylindrical coordinate for the axisymmetric problem.

It is assumed that the temperature and heat flow are continuous along the interface of two consecutive layers, i.e., the inter-layer contact conditions are

$$T_i(r, H_i, t) = T_{i+1}(r, H_i, t) \tag{3.2}$$

$$\lambda_i \frac{\partial}{\partial z} T_i(r, H_i, t) = \lambda_{i+1} \frac{\partial}{\partial z} T_{i+1}(r, H_i, t) \tag{3.3}$$

Refer to Eq. (2.15) in Section 2.1, the following surface boundary condition for solving 2-D axisymmetric temperature prolem is considered in this thesis

$$\begin{aligned} -\lambda_1 \frac{\partial T_1}{\partial z}(r, 0, t) = B \Bigg\{ e^{-\mu r} \Bigg[\frac{a_0}{2} + \frac{\widetilde{a}_s c_0}{2B} + \left(\frac{a_m}{2} + \frac{\widetilde{a}_s c_m}{2B} \right) \sin\left(m\bar{t} + \frac{\pi}{2} \right) + \sum_{k=1}^{m-1} \Bigg[\left(a_k + \frac{\widetilde{a}_s c_k}{B} \right) \sin\left(k\bar{t} + \frac{\pi}{2} \right) \\ + \left(b_k + \frac{\widetilde{a}_s d_k}{B} \right) \sin(k\bar{t}) \Bigg] \Bigg] - T_1(r, 0, t) \Bigg\} \end{aligned} \tag{3.4}$$

where $e^{-\mu r}$ term is introduced to take account of temperature variation along the radial direction [1], and all the other symbols are defined in Section 2.1.

Another boundary condition is that the temperature at an infinite depth is assumed to be bounded,

$$|T_n(r, z, t)| \le M \qquad \text{as} \qquad z \to \infty \tag{3.5}$$

where M = constant.

Equations (3.1)–(3.5) constitute the underlying 2-D axisymmetric heat transfer problem in multi-layered pavement system.

3.2 Derivation of 2-D Axisymmetric Analytical Solution

As explained in the first paragraph in Section 2.2, it is sufficient to derive 2-D analytical solution satisfying Eqs. (3.1), (3.2), (3.3), (3.5) and the following model surface boundary condition

[1] μ is a parameter with unit 1/m.

$$-\lambda_1 \frac{\partial}{\partial z} T_1(r,0,t) = B\left[e^{-\mu r} A \sin(\omega t + \phi) - T_1(r,0,t)\right] \tag{3.6}$$

, and the desired 2-D analytical solution satisfying Equations (3.1)–(3.5) can be obtained using the principle of superposition.

The underlying solution methods for solving the model heat equation are the approach of separation of variables and Hankel integral transform, with the purpose of the latter is to transform a PDE with respect to r and z into an ODE with respect to z for each layer. The ODE in each layer can be easily solved with two unknown constants of integration. A systematical way to determine those constants is then developed using BCs and inter-layer contact conditions, as explained below.

As in Section 2.2, relating $\sin(\omega t + \phi)$ with $e^{j(\omega t+\phi)}$ can greatly facilitate the derivation of the analytical solution, the temperature distribution is first derived for the complex-valued functions $Y_i(r,z,t)$. The desired solution of temperature profile for the 2-D heat transfer problem $T_i(r,z,t)$ is then simply the imaginary part of $Y_i(r,z,t)$. To easily present the derivation, the field equations expressed in terms of $Y_i(r,z,t)$ are summarized as follows:

- Two-dimensional heat transfer equation

$$\frac{\partial Y_i}{\partial t} = \alpha_i \nabla^2 Y_i \qquad \text{for} \qquad H_{i-1} \le z \le H_i \tag{3.7}$$

  where $H_i = \sum_{k=1}^{i} h_k$.

- Interlayer heat contact conditions

$$Y_i(r,H_i,t) = Y_{i+1}(r,H_i,t) \tag{3.8}$$

$$\lambda_i \frac{\partial}{\partial z} Y_i(r,H_i,t) = \lambda_{i+1} \frac{\partial}{\partial z} Y_{i+1}(r,H_i,t) \tag{3.9}$$

- Bounded temperature value at infinite depth

$$|Y_n(r,z,t)| \le M \qquad \text{as} \qquad z \to \infty \tag{3.10}$$

  where M = constant.

- Boundary condition

$$\lambda_1 \frac{\partial}{\partial z} Y_1(r,0,t) = B\left[e^{-\mu r} A e^{j(\omega t+\phi)} - Y_1(r,0,t)\right] \tag{3.11}$$

The following outlines the main steps involved in deriving the analytical solution of $Y_i(r,z,t)$:

1. By using the approach of separation of variables [38], $Y_i(r,z,t)$ can be expressed as

$$Y_i(r,z,t) = u_i(r,z)e^{j(\omega t+\phi)} \tag{3.12}$$

it follows that

$$\frac{\partial Y_i}{\partial t} = j\omega Y_i \tag{3.13}$$

2. Substituting Eqs. (3.12) and (3.13) into Eq. (3.7) yields

$$j\omega u_i(r,z) = \alpha_i \nabla^2 u_i(r,z) \tag{3.14}$$

3. The Hankel integral transform is used to solve Eq. (3.14). Let $\widetilde{f}(\xi)$ be the Hankel transform of order zero of function $f(r)$ and then from [43]

$$\widetilde{f}(\xi) = \int_0^\infty r f(r) J_0(\xi r) dr \tag{3.15}$$

where $J_0(\xi r)$ = first kind of Bessel function of order zero. The inverse Hankel transform of order zero of $\widetilde{f}(\xi)$ is

$$f(r) = \int_0^\infty \xi \widetilde{f}(\xi) J_0(\xi r) d\xi \tag{3.16}$$

Furthermore, the Hankel transform of order zero of $\left(\frac{d^2}{dr^2} + \frac{1}{r}\frac{d}{dr}\right) f(r)$ is given by Eq. (5-4-7) in [43]

$$\int_0^\infty r \left(\frac{d^2}{dr^2} + \frac{1}{r}\frac{d}{dr}\right) f(r) J_0(\xi r) dr = -\xi^2 \widetilde{f}(\xi) \tag{3.17}$$

4. Let $\widetilde{u}_i(\xi,z)$ be the Hankel transform of order zero of $u_i(r,z)$ with respect to r. Applying the Hankel transform of order zero to both sides of Eq. (3.14) with respect to r in conjunction with Eq. (3.17) yields

$$\frac{\partial^2 \widetilde{u}_i}{\partial z^2}(\xi,z) - \left(\xi^2 + \frac{\omega}{\alpha_i} j\right) \widetilde{u}_i(\xi,z) = 0 \tag{3.18}$$

5. Solving Eq. (3.18) in the Hankel domain gives

$$\widetilde{u}_i(\xi,z) = C_i \exp\left(-\xi z \sqrt{1 + j\frac{\omega}{\alpha_i \xi^2}}\right) + D_i \exp\left(\xi z \sqrt{1 + j\frac{\omega}{\alpha_i \xi^2}}\right) \tag{3.19}$$

where C_i, D_i = constants of integration for layer i, which are determined using the constraint conditions.

6. Taking the inverse Hankel transform of order zero of Eq. (3.19) and considering Eq. (3.12) yields $Y_i(r,z,t)$ as follows:

$$Y_i(r,z,t) = \int_0^\infty \xi \left(C_i e^{-\xi z M_i} e^{-j\xi z N_i} + D_i e^{\xi z M_i} e^{j\xi z N_i} \right) J_0(\xi r) e^{j(\omega t+\phi)} d\xi \tag{3.20}$$

where M_i and N_i are defined in Appendix B.

7. Determining C_i and D_i

- The relationship between C_{i+1}, D_{i+1} and C_i, D_i can be exploited in the following matrix-vector form by using Eq. (3.20) and the interlayer heat contact condition stated in Eqs. (3.8) and (3.9):

$$\begin{bmatrix} C_{i+1} \\ D_{i+1} \end{bmatrix} = \begin{bmatrix} e^{-\xi H_i (M_i - M_{i+1}) P_i^{11}} & e^{\xi H_i (M_i + M_{i+1}) P_i^{12}} \\ e^{-\xi H_i (M_i + M_{i+1}) P_i^{21}} & e^{\xi H_i (M_i - M_{i+1}) P_i^{22}} \end{bmatrix} \begin{bmatrix} C_i \\ D_i \end{bmatrix} \tag{3.21}$$

  where $P_i^{11}, P_i^{12}, P_i^{21}, P_i^{22}$ are defined in Appendix B.

- The recursive formula linking C_i, D_i and C_1, D_1 can be further deduced from Eq. (3.21) as follows:

$$\begin{bmatrix} C_i \\ D_i \end{bmatrix} = \begin{bmatrix} e^{\xi H_{i-1}(M_i + M_{i-1})} & 0 \\ 0 & e^{-\xi H_{i-1}(M_i - M_{i-1})} \end{bmatrix} \begin{bmatrix} e^{-2\xi H_1 M_1} R_{i-1}^{11} & R_{i-1}^{12} \\ e^{-2\xi H_1 M_1} R_{i-1}^{21} & R_{i-1}^{22} \end{bmatrix} \begin{bmatrix} C_1 \\ D_1 \end{bmatrix} \tag{3.22}$$

  where $i = 2, 3, \cdots, n$ and $R_i^{kl} (k, l = 1, 2)$ are defined in Appendix B, and Eq. (3.22) can be easily proved by using the method of mathematical induction.

- A bounded solution for $Y_n(r,z,t)$ as $z \to \infty$ indicates that $D_n = 0$ from Eq. (3.20), and the relationship between C_1 and D_1 can be further derived by setting $D_n = 0$ in Eq. (3.22) as follows:

$$D_1 = -e^{-2\xi H_1 M_1} \frac{R_{n-1}^{21}}{R_{n-1}^{22}} C_1 \tag{3.23}$$

- C_1 and D_1 can be obtained by using Eq. (3.23) in conjunction with the BC in Eq. (3.11). Furthermore, C_i and D_i for the ith layer can be solved by using Eq. (3.22).

- Once C_i and D_i are determined, the desired solution $T_i(r,z,t)$ for the ith layer is simply the imaginary part of $Y_i(r,z,t)$ in Eq. (3.20). The expression for $T_i(r,z,t)$ is given in Eq. (3.24) with all the symbols defined in Appendix B

$$T_i(r,z,t) = \int_0^\infty \xi \Big\{ \Delta_{i1} e^{\xi[H_{i-1}(M_i+M_{i-1})-zM_i]} \sin(\omega t + \phi + \delta_{i1} - \xi z N_i) + \Delta_{i2} e^{\xi[-H_{i-1}(M_i-M_{i-1})+zM_i]} \sin(\omega t + \phi + \delta_{i2} + \xi z N_i) \Big\} J_0(\xi r) d\xi \quad (3.24)$$

3.3 Model Verification with Field Data

A FORTRAN computer program was developed to predict the temperature profile in a multi-layered pavement system by using the derived analytical solution of the temperature field. For the model validation, the computed temperature profile in the same CRCP test section is compared with measured field data from the ATREL, as explained in Section 2.2.1.

In this study, temperatures in CRCP test section at the five slab depth locations, i.e., z = 0.0254, 0.0762, 0.127, 0.178, and 0.229 m from the pavement surface, were continuously predicted using the derived analytical solution for 71.5 hours at a half-hour interval in both winter and summer conditions, i.e., starting from 0:00 a.m. on January 12, 2003 until 11:30 p.m. on January 14, 2003 and from 0:00 a.m. on June 28, 2003 until 11:30 p.m. on June 30, 2003. Half-hour measured air temperature and solar radiation intensity for each three-day period were employed to generate the fitting interpolatory trigonometric polynomials as shown in Figs. 3.2, 3.3, 3.4, and 3.5. The other input parameters including the typical thermal properties for these pavement materials [1, 17] are listed in Table 3.3.

To determine the appropriate upper limit x_u of the integral in Eq. (3.24), numerical convergence tests for the inverse Hankel integral transform are carried out using the above input parameters. The numerical implementation indicated that the improper integral in Eq. (3.24) usually converged faster as the value of z increased, thus, the dimensionless quantity x_u is selected as

$$x_u = \text{int}\left(\frac{H_{n-1}}{3z}\right) \cdot 3I \quad (3.25)$$

where int = integer function converting its argument into the largest integer less than or equal to itself; I = test number; and H_{n-1} = sum of thickness of pavement layers except subgrade layer (m).

Table 3.1 shows different upper integral limits x_u when $I = 1$ in Eq. (3.25) for five slab depth locations. Table 3.2 illustrates the convergence of the inverse Hankel integral transform in predicting temperature values at these five different slab depths at 4:00 a.m. on June 28, 2003. Based on the convergence test, the minimum value for x_u in Table 3.2 (Test No. 1) still gave three significant digits accuracy in the predicted temperature at all depths.

Table 3.1: Values of upper integral limit x_u when $I = 1$ for different depths z

z (m)	x_u (dimensionless)
0.0254	21
0.0762	9
0.1270	6
0.1778	3
0.2286	3

Table 3.2: Numerical convergence test results for the inverse Hankel integral transform (predicted temperatures at five different slab depths, C)

Test No.	Slab depth z (m)				
(I)	0.0254	0.0762	0.1270	0.1778	0.2286
1	20.6228784	23.0413174	24.9482524	26.3758674	27.3348095
2	20.6215549	23.0375610	24.9429443	26.3539092	27.3228534
3	20.6214680	23.0371050	24.9416775	26.3514324	27.3217703
4	20.6214579	23.0370260	24.9416126	26.3510673	27.3217703
5	20.6214557	23.0370067	24.9415936	26.3510028	27.3216457
6	20.6214553	23.0370047	24.9415857	26.3509899	27.3216288
7	20.6214552	23.0370042	24.9415851	26.3509871	27.3216263
8	20.6214551	23.0370040	24.9415848	26.3509865	27.3216263
9	20.6214551	23.0370040	24.9415847	26.3509863	27.3216259
10	20.6214551	23.0370040	24.9415847	26.3509863	27.3216258

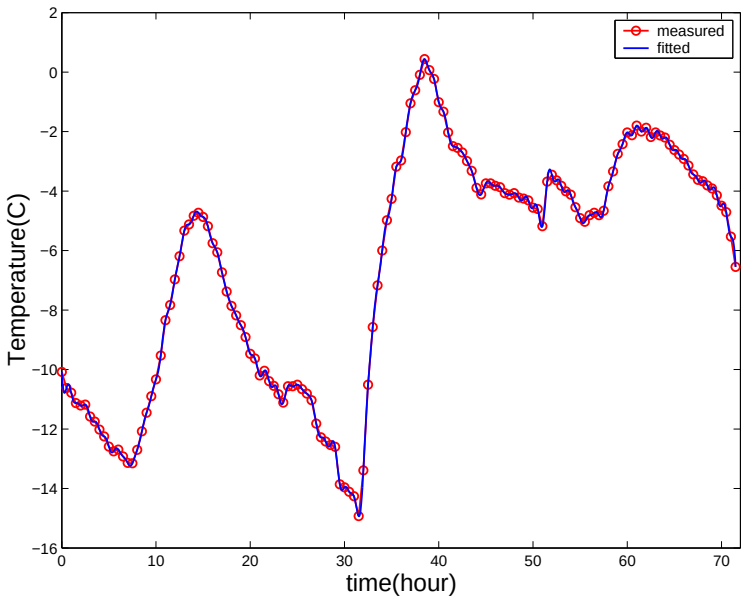

Figure 3.2: Measured and fitted air temperature for three days in Jan. 2003

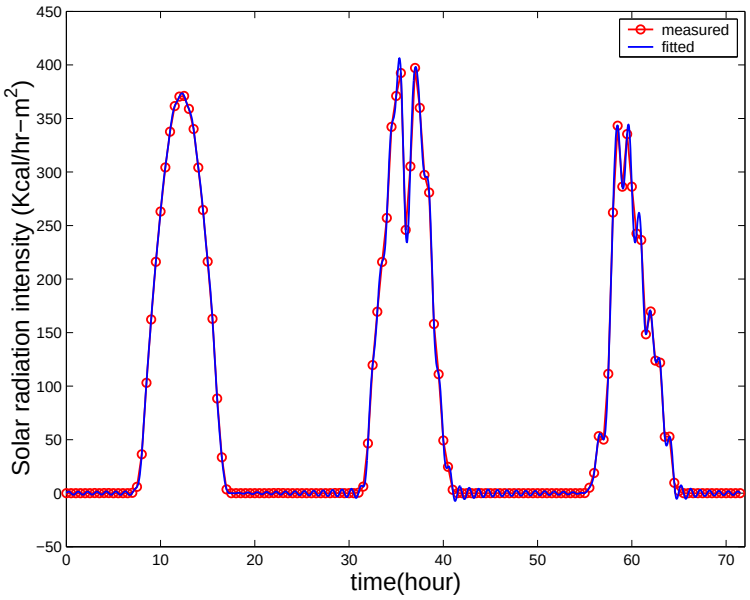

Figure 3.3: Measured and fitted solar radiation intesities for three days in Jan. 2003

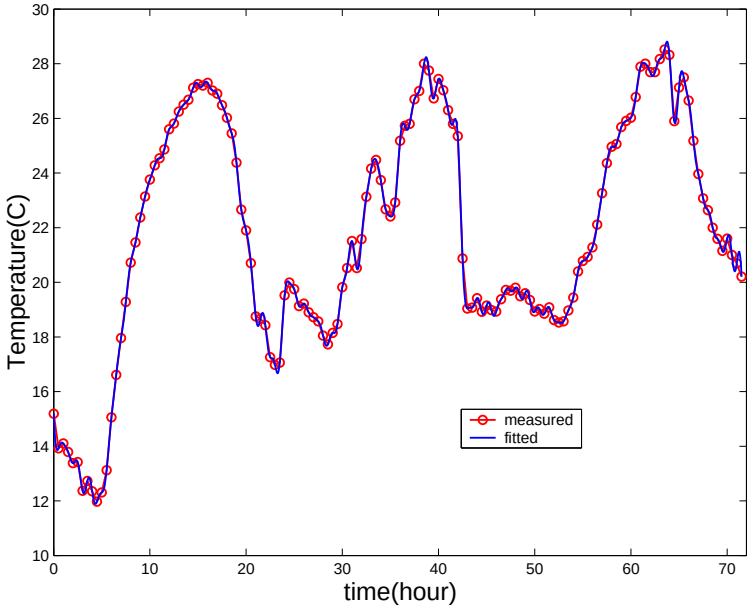

Figure 3.4: Measured and fitted air temperature for three days in June 2003

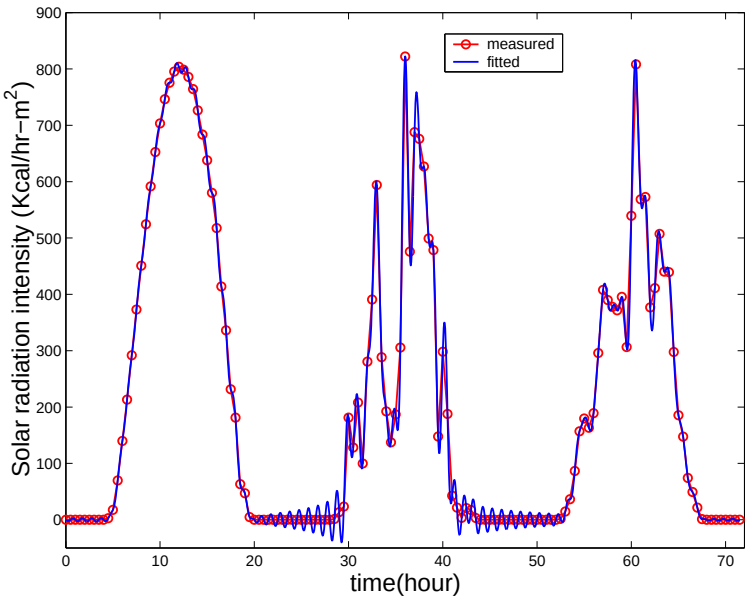

Figure 3.5: Measured and fitted solar radiation intesities for three days in June 2003

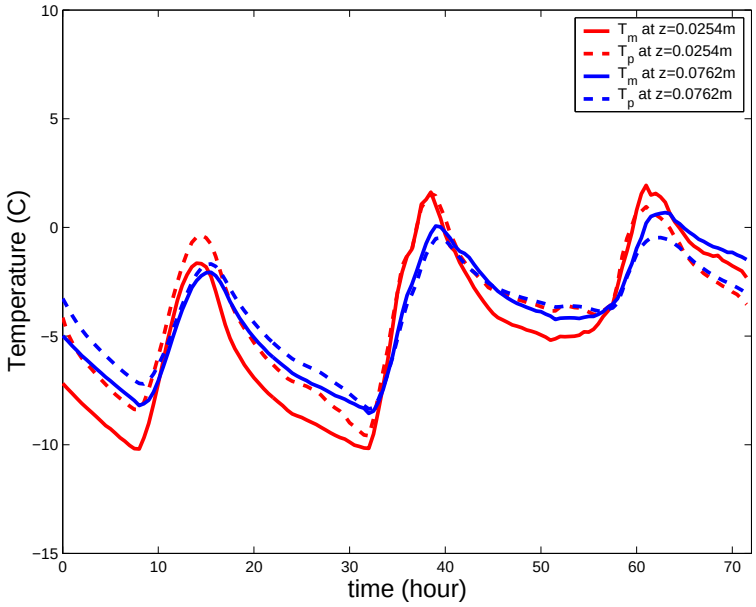

Figure 3.6: Predicted (T_p) and measured (T_m) temperature for z=0.0254 m and z=0.0762 m in Jan. 2003

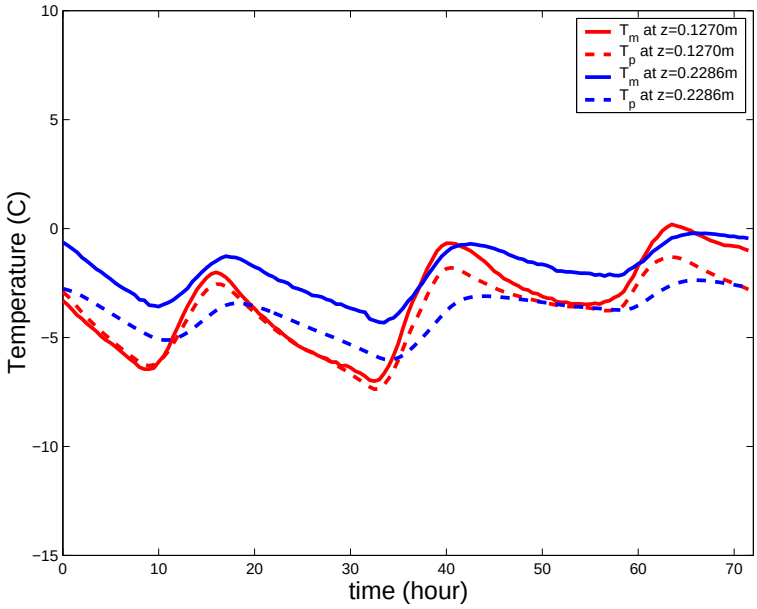

Figure 3.7: Predicted (T_p) and measured (T_m) temperature for z=0.1270 m and z=0.2286 m in Jan. 2003

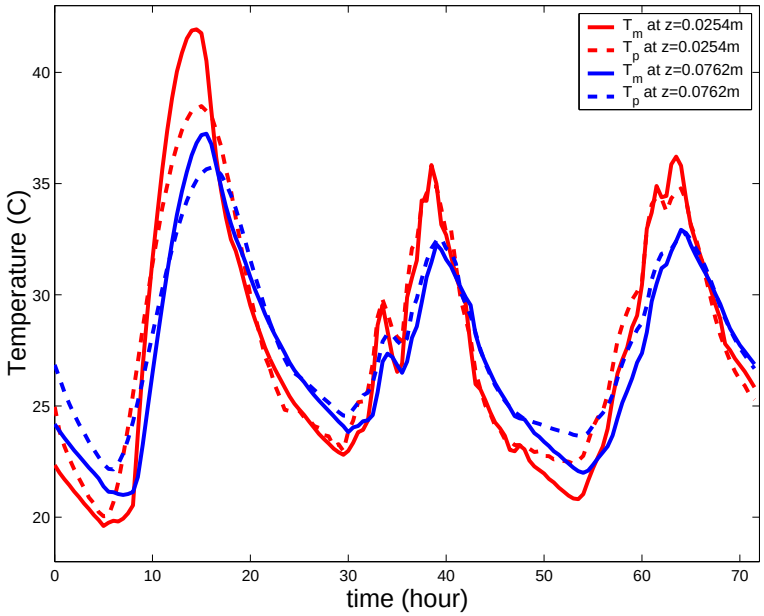

Figure 3.8: Predicted (T_p) and measured (T_m) temperature for z=0.0254 m and z=0.0762 m in June 2003

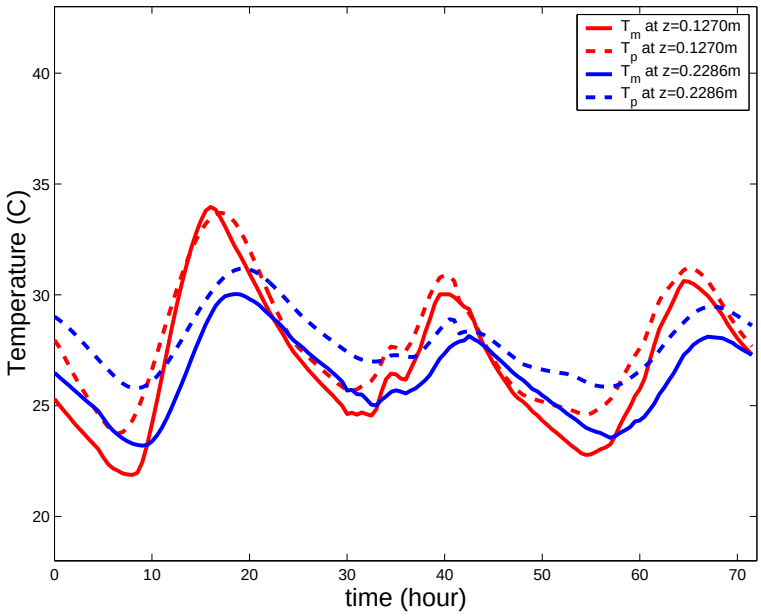

Figure 3.9: Predicted (T_p) and measured (T_m) temperature for z=0.1270 m and z=0.2286 m in June 2003

Table 3.3: Thermal input parameters in 2-D axisymmetric temperature model verification.

Parameters	Value
Thermal conductivity, λ (Kcal/h m C)	
PCC slab	1.85
Asphalt concrete base	1.38
Aggregate subbase	2.58
Subgrade	1.00
Thermal diffusivity, α (m^2/h)	
PCC slab	0.0035
Asphalt concrete base	0.0021
Aggregate subbase	0.0030
Subgrade	0.0030
Effective absorptivity, $\widetilde{a_s}$	0.50
Parameter μ	0.002
Radial coordinate, r	0
Pavement surface convection coefficient, B (Kcal/m^2 h C)	16.29

Table 3.4: Mean errors between predicted and measured temperature at different depths (C), i.e., $T_p - T_m$

Date	Slab depth location z (m)				
	0.0254	0.0762	0.1270	0.1778	0.2286
Jan. 12-14, 2003	0.80	0.12	-0.53	-1.19	-1.91
	(0.97)	(0.74)	(0.57)	(0.43)	(0.34)
June 28-30, 2003	0.31	0.68	1.06	1.37	1.63
	(1.36)	(0.92)	(0.74)	(0.64)	(0.60)

Note: Values in parentheses denote standard deviations of temperature prediction error.

The predicted and measured pavement temperatures are plotted in Figs. 3.6 and 3.7 for January, and in Figs. 3.8 and 3.9 for June 2003, respectively, at $z = 0.0254$ m, $z = 0.0762$ m, $z = 0.1270$ m, and $z = 0.2286$ m. It is observed that the derived theoretical solution predicts reasonably good pavement temperature profile compared to the measured data. The maximum error between the predicted and measured temperature is around 3 C for these two, 3-day testing results except for one particular case, i.e., in predicting the temperature at $z = 0.0254$ m from the pavement surface at 8:00 a.m. on June 28, 2003, where the error between the predicted and measured temperature is around 5 C.

Table 3.4 presents the mean errors and standard deviations between the predicted (T_p) and measured (T_m) temperature for each of five different slab depth locations. The mean error is the greatest near the bottom of the slab but the standard deviation is the largest near the top of the slab where temperature fluctuations are the greatest. The temperature discrepancy between the predicted and measured values come from many factors, such as the errors involved in selecting the appropriate material thermal parameters, e.g., thermal conductivity and thermal diffusivity; errors involved in the continuous interfacial heat flux assumptions, since different levels of heat flow resistance may exist in the interface of two consecutive pavement layers; deep soil temperature effects; irradiation occurring at night and temperature measurement error. The irradiation at night and the effect of the deep soil temperature are likely the major reasons for the temperature discrepancy between the predicted and measured values. The irradiation in this study is considered only by adjusting the absorptivity of the concrete and convection coefficient. Furthermore, the unknown deep soil temperature cannot be currently considered with the proposed analytical approach.

3.4 Chapter Summary

In this chapter, the analytical solution of a 2-D axisymmetric temperature field in a multi-layered pavement system is successfully derived. The temperature at any pavement location (r, z) and time t in an N-layered pavement system can be calculated using this solution under the cylindrical coordinate system. Hankel

transform with respect to the radial coordinate is employed in the derivation of the solution. The interpolatory trigonometric polynomials are used to fit the measured air temperature and solar radiation intensities during a day, which are essential components in the boundary condition for the underlying heat transfer problem. Field temperature testing results demonstrate that the derived analytical solution generates realistic temperature profiles in a concrete slab for a four-layered rigid pavement system. The advantage of this formulation is that it can rapidly predict the pavement temperature profile for short time durations with limited input data.

Chapter 4

Analytical Solutions of Pavement Temperature Fields Under Rapid Transient Thermal Loadings

New generation military aircraft are being developed to take-off and land vertically resulting in large thermal loads on the pavement surface. This fast transient thermal loads will produce a rapidly varying temperature profile through the depth of the concrete slab as well as radially. Traditional paving materials such as concrete and asphalt concrete will not have the same longevity under this repeated thermal loading condition [21, 22, 23, 26, 27, 40]. Accurately predicting this transient high temperature profile is crucial and a prerequisite to further determining the thermal stress fields in the material design of this new type of airfield pavement application.

4.1 1-D Temperature Field in Homogeneous Half-Space Subjected to Fast, Transient Thermal Loadings

4.1.1 Specified Pavement Surface Temperature

The governing equation for this heat conduction problem without internal heat source/sink is the classic 1-D heat equation

$$\frac{\partial T}{\partial t} = \alpha \frac{\partial^2 T}{\partial z^2} \qquad \text{for} \quad 0 < z < \infty \quad \text{and} \quad t > 0 \tag{4.1}$$

where α = thermal diffusivity of material (m^2/h).

One way to consider rapidly transient thermal loadings, i.e., energy emanated from vertical take-off/landing aircraft with fast heating rate (say, 500 C/min. used in Ju and Zhang [27]), is to use measured transient surface temperatures $F(t)$ (if available) in the area where the temperature is the highest. Mathematically, the following initial boundary value problem needs to be solved

$$
\begin{aligned}
\frac{\partial T}{\partial t}(z,t) &= \alpha \frac{\partial^2 T}{\partial z^2}(z,t) \qquad 0 < z < \infty \quad \text{and} \quad 0 < t < \infty \\
T(0,t) &= F(t) \qquad \text{for} \quad z = 0 \\
T(z,0) &= G(z) \qquad \text{for} \quad t = 0
\end{aligned} \tag{4.2}
$$

The analytical solution for the above initial boundary value problem (4.2) can be obtained using the method of odd extension discussed in Section 3.1 in Strauss [47], or by summing up solutions of two relatively simpler initial boundary value problems outlined on Page 64 in Carslaw and Jaeger [9]. The complete solution of (4.2) is

$$
\begin{aligned}
T(z,t) &= \frac{1}{\sqrt{4\pi\alpha t}} \int_0^\infty \left[e^{-\frac{(z-y)^2}{4\alpha t}} - e^{-\frac{(z+y)^2}{4\alpha t}} \right] G(y) dy \\
&\quad + \frac{2}{\sqrt{\pi}} \int_{\frac{z}{\sqrt{4\alpha t}}}^\infty F\left(t - \frac{z^2}{4\alpha y^2} \right) e^{-y^2} dy
\end{aligned} \tag{4.3}
$$

provided the improper integrals in Eq. (4.3) converge.

In Ju and Zhang [27], $F(t)$ and $G(z)$ take the following forms

$$
\begin{aligned}
F(t) &= T_s(t) \\
&= 285 + 49.5 \ln(t + 0.00554) \qquad (4.4) \\
G(z) &= T_0 \\
&= 25 \qquad (4.5)
\end{aligned}
$$

where t in Eq. (4.4) is measured in seconds, and T_0 in Celsius degree in Eq. (4.5).

Substituting Eqs. (4.4) and (4.5) into Eq. (4.3) gives

$$
T(z,t) = \frac{2}{\sqrt{\pi}} \int_{\frac{z}{\sqrt{4\alpha t}}}^\infty T_s\left(t - \frac{z^2}{4\alpha y^2} \right) e^{-y^2} dy + \frac{2}{\sqrt{\pi}} T_0 \int_0^{\frac{z}{\sqrt{4\alpha t}}} e^{-y^2} dy \tag{4.6}
$$

which is in agreement with Eq. (5) in Ju and Zhang [27].

It is noted that for arbitrary $z > 0$ and $t > 0$, the improper intergral in Eq. (4.6) can be shown to be convergent to a finite value by using Lebesgue dominated convergence theorem from real analysis. The time-dependent surface temperature described by Eq. (4.4) is plotted in Fig. 4.1.

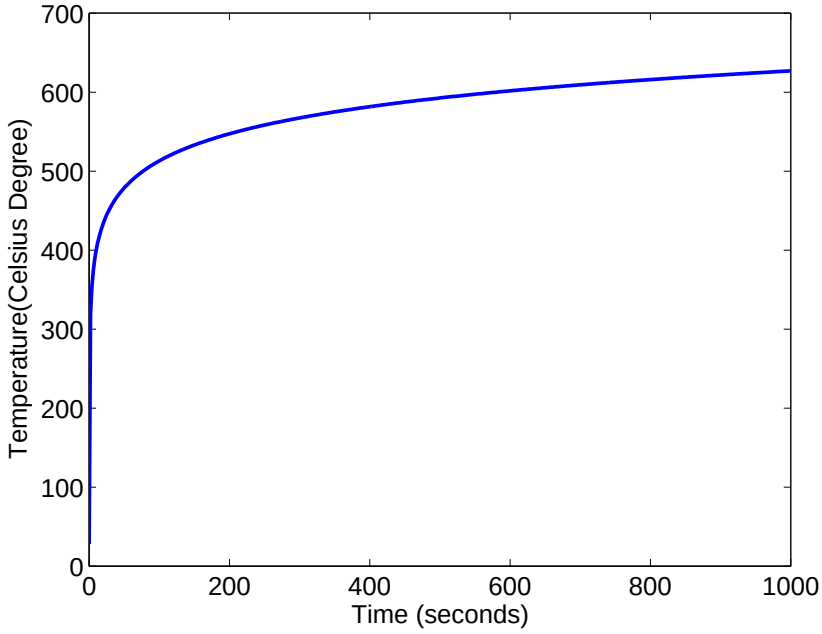

Figure 4.1: Time-dependent surface temperature due to transient high temperature loadings

Due to the complexities of integrands in the integrals in Eq. (4.6), the closed-form solution of integrals in Eq. (4.6) are hard to be derived, thus numerical approximation to Eq. (4.6) is employed in this study.

Steen et al. developed efficient Gauss-type integration formulas to approximate integrals of the forms

$$\int_0^\infty e^{-x^2} f(x)dx \qquad \text{and} \qquad \int_0^1 e^{-x^2} f(x)dx,$$

and their formulas are given as follows

$$\int_0^\infty e^{-x^2} f(x)dx \approx \sum_{k=1}^{N} w_k f(x_k) \tag{4.7}$$

$$\int_0^1 e^{-x^2} f(x)dx \approx \sum_{k=1}^{M} w_k f(x_k) \tag{4.8}$$

where $N \in \{k \text{ is a positive integer} : 2 \leq k \leq 15\}$; $M \in \{k \text{ is a positive integer} : 2 \leq k \leq 10\}$; weights w_k and abscissae $x_k, k = 1, 2, \ldots, N$ or M are listed in [46].

In order to apply Eqs. (4.7) and (4.8), the integrals in Eq. (4.6) have to be transformed into the standard integral form $\int_0^\infty e^{-x^2} f(x)dx$ or $\int_0^1 e^{-x^2} f(x)dx$. This can be easily obtained using change of variable as follows:

Table 4.1: Weights and abscissae used in Eq. (4.7), $N = 15$ [46, p. 668]

k	w_k	x_k
1	5.54433663102343d-02	2.16869474675590d-02
2	1.24027738987730d-01	1.12684220347775d-01
3	1.75290943892075d-01	2.70492671421899d-01
4	1.91488340747342d-01	4.86902370381935d-01
5	1.63473797144070d-01	7.53043683072978d-01
6	1.05937637278492d-01	1.06093100362236d+00
7	5.00270211534535d-02	1.40425495820363d+00
8	1.64429690052673d-02	1.77864637941183d+00
9	3.57320421428311d-03	2.18170813144494d+00
10	4.82896509305201d-04	2.61306084533352d+00
11	3.74908650266318d-05	3.07461811380851d+00
12	1.49368411589636d-06	3.57140815113714d+00
13	2.55270496934465d-08	4.11373608977209d+00
14	1.34217679136316d-10	4.72351306243148d+00
15	9.56227446736465d-14	5.46048893578335d+00

Let $\eta = \frac{z}{\sqrt{4\alpha t}}$ and $y = \eta + \xi$, then the improper integral in Eq. (4.6) becomes

$$\int_{\eta}^{\infty} T_s \left(t - \frac{z^2}{4\alpha y^2} \right) e^{-y^2} dy = \int_{0}^{\infty} e^{-\xi^2} e^{-\eta(\eta+2\xi)} T_s \left(t - \frac{z^2}{4\alpha(\eta+\xi)^2} \right) d\xi \tag{4.9}$$

on the other hand, let $y = \eta\xi$, the definite integral in Eq. (4.6) becomes

$$\int_{0}^{\eta} e^{-y^2} dy = \eta \int_{0}^{1} e^{-\xi^2} e^{(1-\eta^2)\xi^2} d\xi \tag{4.10}$$

Fix $z > 0, t > 0$, the temperature $T(z,t)$ can be approximated by applying Steen et al's integral formulas to Eq. (4.6). To investigate effects of concrete diffusivity coefficient α on temperature profile, $\alpha = 1.3$ mm^2/sec and $\alpha = 1.0$ mm^2/sec used in [27] are adopted in this study, and $N = 15, M = 10$ are employed in Steen et al's integral formulas. For the sake of completeness Tables 4.1 and 4.2 list the weights w_k and abscissae x_k used in Eqs. (4.7) and (4.8), respectively.

Fig. 4.2 plots effects of concrete diffusivity coefficient α on concrete pavement temperature profile at t=10 second and t=600 second due to transient high temperature loadings. Fig. 4.3 presents effects of concrete diffusivity coefficient α on transient temperature values at z=1 mm and z=20 mm at different times. These results are consistent with the graphical solutions presented by Ju and Zhang [27].

Table 4.2: Weights and abscissae used in Eq. (4.8), $M = 10$ [46, p. 670]

k	w_k	x_k
1	3.25319695101801d-02	1.27378499713740d-02
2	7.24838964037449d-02	6.58023279743935d-02
3	1.04004662155270d-01	1.56155783059660d-01
4	1.21594475562980d-01	2.75890718366863d-01
5	1.22093608318116d-01	4.14966322218475d-01
6	1.07195747923389d-01	5.62009142193357d-01
7	8.30779890294863d-02	7.04832804690269d-01
8	5.69285988401857d-02	8.30893869740303d-01
9	3.33982919934992d-02	9.28057569743495d-01
10	1.35148930755755d-02	9.85992766817013d-01

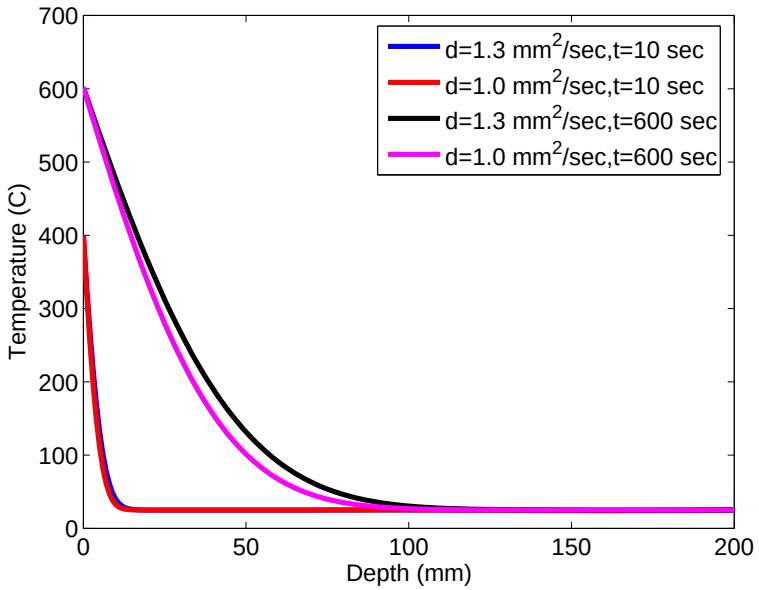

Figure 4.2: Concrete pavement temperature profile at t=10 sec. and t=600 sec. due to fast transient thermal loadings

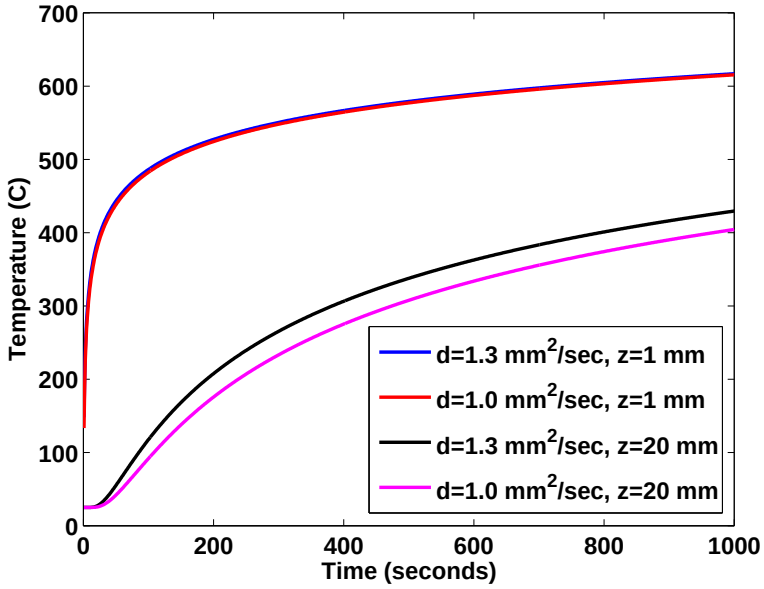

Figure 4.3: Transient temperature values at z=1 mm and z=20 mm at different times due to fast transient thermal loadings

4.1.2 Section Summary

In this section, 1-D rapidly varying temperature profiles in homogeneous half-space subjected to transient thermal loadings are investigated. The well-known general solution for this problem is numerically evaluated using an efficient Gaussian-type integration formulas developed by Steen et al. Numerical calculations based on the uniform initial pavement temperature profile and a model surface temperature history are carried out, matching well with the published results.

4.2 1-D Temperature Field in Two-Layered Pavement Systems Subjected to High Temperature Transient Loadings

The 1-D time-dependent temperature profile in a homogeneous half space can be exteneded to a two-layered pavement system, shown in Fig. 4.4. This idealized two-layered system can be eventually used to analyze a heat resistant concrete layer over a conventional concrete layer. The two-layered system can be modeled as a boundary value problem, where h_1 = thickness of Portland cement concrete (m); h_2 = thickness of the base layer (m); λ_j = thermal conductivity of the jth layer (Kcal/m h C); α_j = thermal diffusivity of the jth layer (m^2/h); and $T_j(z,t)$ = temperature function for layer j (C). The material in each layer is assumed to be continuous, homogeneous, and isotropic. The temperature $T_2(z,t)$ is assumed to be constant for $z \geq H_2$ and $t > 0$.

4.2.1 Specified Pavement Surface Temperature

Similar to Section 4.1, suppose that the measured transient surface temperature data is available, then 1-D time-dependent temperature profile in a two-layered pavement system subjected to this high temperature transient loadings can be modeled as the following initial boundary value problem

$$\begin{aligned}
\frac{\partial T_j}{\partial t}(z,t) &= \alpha_j \frac{\partial^2 T_j}{\partial z^2}(z,t) \qquad 0 < t < \infty, \qquad H_{j-1} < z < H_j, \qquad j = 1,2 \\
T_j(z,0) &= G_j(z), \qquad j = 1,2 \qquad \text{(initial condition)} \\
T_1(0,t) &= F(t) \qquad \text{(first boundary condition)} \\
T_2(H_2,t) &= \text{constant} \qquad \text{(second boundary condition)} \\
T_1(H_1,t) &= T_2(H_1,t) \qquad \text{(first interface condition)} \\
\lambda_1 \frac{\partial T_1}{\partial z}(H_1,t) &= \lambda_2 \frac{\partial T_2}{\partial z}(H_1,t) \qquad \text{(second interface condition)}
\end{aligned} \tag{4.11}$$

where $H_0 = 0,\ H_1 = h_1$ and $H_2 = h_1 + h_2$.

The main mathematical tool used for solving the system (4.11) is Laplace integral transform. To facilitate the derivation of the solution, we introduce the variable $U_j(z,t),\ j = 1,2$ below

$$U_j(z,t) = T_j(z,t) - T_j(z,0) \tag{4.12}$$

For simplicity, we assume that the initial temperature, $T_j(z,0),\ j = 1,2$ is a constant. In view of Eq. (4.12),

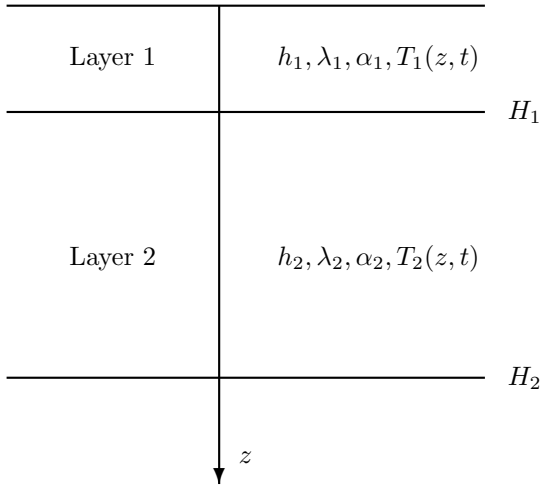

Figure 4.4: Two-layered pavement system

the system (4.11) can be written as the following initial boundary value problem

$$\frac{\partial U_i}{\partial t}(z,t) = \alpha_i \frac{\partial^2 U_i}{\partial z^2}(z,t) \qquad 0 < t < \infty, \qquad H_{i-1} < z < H_i, \quad i = 1,2 \tag{4.13}$$

$$U_i(z,0) = 0 \tag{4.14}$$

$$U_1(0,t) = F(t) - T_1(0,0) \tag{4.15}$$

$$U_2(H_2,t) = 0 \tag{4.16}$$

$$U_1(H_1,t) = U_2(H_1,t) \tag{4.17}$$

$$\lambda_1 \frac{\partial U_1}{\partial z}(H_1,t) = \lambda_2 \frac{\partial U_2}{\partial z}(H_1,t) \tag{4.18}$$

where we assume that $T_2(H_2,t) = T_2(H_2,0)$ for all $t > 0$.

Let $\mathcal{L}$ denote the Laplace transform operator and $\hat{U}_i(z,s)$ be the Laplace transform of $U_i(z,t)$ with respect to time t. Furthermore, the following operational property of Laplace transform is needed [43, p. 148]

$$\mathcal{L}\left[f'(t)\right] = s\hat{f}(s) - f(0) \tag{4.19}$$

where $\hat{f}(s)$ is assumed to exist.

Applying Laplace transform with respect to t to Eq. (4.13) in conjunction with Eqs. (4.14) and (4.19)

yields

$$\frac{\partial^2 \hat{U}_j(z,s)}{\partial z^2} - \frac{s}{\alpha_j}\hat{U}_j(z,s) = 0, \qquad H_{j-1} < z < H_j,\ j = 1,2 \tag{4.20}$$

Let $r_j(s) = \sqrt{\frac{s}{\alpha_j}}$, then the solution of Eq. (4.20) is

$$\hat{U}_j(z,s) = A_j(s)e^{-r_j z} + B_j(s)e^{r_j z},\ j = 1,2 \tag{4.21}$$

where $A_j(s),\ B_j(s),\ j = 1,2$ are to be determined using Laplace transforms of boundary and interface conditions. Applying Laplace transform with respect to t to the boundary and interface conditions in Eqs. (4.15)-(4.18) yields Eqs. (4.22)-(4.25), respectively

$$\hat{U_1}(0,s) = \hat{F}(s) - \frac{c}{s} \tag{4.22}$$

$$\hat{U_2}(H_2,s) = 0 \tag{4.23}$$

$$\hat{U_1}(H_1,s) = \hat{U_2}(H_1,s) \tag{4.24}$$

$$\lambda_1 \frac{\partial \hat{U_1}}{\partial z}(H_1,s) = \lambda_2 \frac{\partial \hat{U_2}}{\partial z}(H_1,s) \tag{4.25}$$

where constant c stands for $T_1(0,0)$.

From Eq. (4.21), we know

$$\frac{\partial \hat{U_j}}{\partial z}(z,s) = -r_j A_j(s)e^{-r_j z} + r_j B_j(s)e^{r_j z},\ j = 1,2 \tag{4.26}$$

Substituting Eqs. (4.21) and (4.26) into Eqs. (4.22)-(4.25) yields the following linear system with $A_j(s), B_j(s),\ j = 1,2$ being unknown variables

$$\begin{bmatrix} a_{11} & a_{12} & 0 & 0 \\ a_{21} & a_{22} & a_{23} & a_{24} \\ a_{31} & a_{32} & a_{33} & a_{34} \\ 0 & 0 & a_{43} & a_{44} \end{bmatrix} \begin{bmatrix} A_1(s) \\ B_1(s) \\ A_2(s) \\ B_2(s) \end{bmatrix} = \begin{bmatrix} C_1 \\ 0 \\ 0 \\ 0 \end{bmatrix} \tag{4.27}$$

where

$$
\begin{array}{llll}
a_{11} = 1 & a_{12} = 1 & & \\
a_{21} = e^{-r_1 H_1} & a_{22} = e^{r_1 H_1} & a_{23} = -e^{-r_2 H_1} & a_{24} = -e^{r_2 H_1} \\
a_{31} = -\lambda_1 r_1 e^{-r_1 H_1} & a_{32} = \lambda_1 r_1 e^{r_1 H_1} & a_{33} = \lambda_2 r_2 e^{-r_2 H_1} & a_{34} = -\lambda_2 r_2 e^{r_2 H_1} \\
a_{43} = e^{-r_2 H_2} & a_{44} = e^{r_2 H_2} & & \\
C_1 = \hat{F}(s) - \frac{c}{s} & & &
\end{array}
\tag{4.28}
$$

Linear system (4.27) can be easily solved by using Cramer's rule and its solutions are

$$
\begin{aligned}
A_1(s) &= \frac{C_1}{\Delta} I_1 \\
B_1(s) &= -\frac{C_1}{\Delta} I_2 \\
A_2(s) &= 2\frac{C_1}{\Delta} \lambda_1 r_1 e^{r_2 H_2} \\
B_2(s) &= -2\frac{C_1}{\Delta} \lambda_1 r_1 e^{-r_2 H_2}
\end{aligned}
\tag{4.29}
$$

where

$$
\begin{aligned}
I_1 &= e^{r_1 h_1} \left[\lambda_1 r_1 \sinh(r_2 h_2) + \lambda_2 r_2 \cosh(r_2 h_2)\right] \\
I_2 &= e^{-r_1 h_1} \left[-\lambda_1 r_1 \sinh(r_2 h_2) + \lambda_2 r_2 \cosh(r_2 h_2)\right] \\
\Delta &= 2\left[\lambda_1 r_1 \sinh(r_2 h_2)\cosh(r_1 h_1) + \lambda_2 r_2 \cosh(r_2 h_2)\sinh(r_1 h_1)\right] \\
h_2 &= H_2 - H_1
\end{aligned}
$$

From Eq. (4.4) in Section 4.1, it is clear that $T_s(t)$ can be well approximated for large t by

$$
F(t) = 285 + 49.5 \ln(t), \quad t > 1 \tag{4.30}
$$

Since Laplace transform of Eq. (4.30) is much simpler than that of (4.4), Eq. (4.30) will be used in the following sample calculation. Laplace transform of $\ln(t)$ takes the form [45]

$$
L[\ln(t)] = -\frac{\gamma + \ln(s)}{s} \tag{4.31}
$$

where $\gamma \approx 0.5772156$ is Euler's constant.

In view of Eq. (4.31), Laplace transform of Eq. (4.30) is

$$\hat{F}(s) = \frac{285 - 49.5(\gamma + \ln(s))}{s} \tag{4.32}$$

Based on $T_j(z,0) = 25,\ j = 1,2$ (see Eq. (4.5)) and Eq. (4.32), C_1 can be obtained as

$$C_1 = \frac{1}{s}\left[260 - 49.5(\gamma + \ln(s))\right] \tag{4.33}$$

Substituting $A_j(s), B_j(s),\ j = 1,2$ in Eq. (4.29) into Eq. (4.21) and using the inverse Laplace transform yields

$$U_1(z,t) = \frac{1}{2\pi i}\int_{\nu-i\infty}^{\nu+i\infty} \hat{U}_1(z,s)e^{st}ds, \quad 0 < z < H_1 \tag{4.34}$$

$$U_2(z,t) = \frac{1}{2\pi i}\int_{\nu-i\infty}^{\nu+i\infty} \hat{U}_2(z,s)e^{st}ds, \quad H_1 < z < H_2 \tag{4.35}$$

where ν is some real number such that $\hat{U}_j(z,s)$, $j = 1,2$ converges absolutely along the line $\mathrm{Re}(s) = \nu$, where $\mathrm{Re}(s)$ denotes the real part of a complex number s [15].

Due to the complexities of $\hat{U}_j(z,s)$, $j = 1,2$, the closed-form solutions of Eqs. (4.34) and (4.35) are difficult to derive, so we seek numerical inversion of the Laplace transform. In this study, Gaussian quadrature formula for evaluating the following integral of functions of complex variables is employed [48]

$$\frac{1}{2\pi i}\int_{\nu-i\infty}^{\nu+i\infty} \frac{e^p}{p}F(p)\,dp \approx \sum_{j=1}^{N} w_j F(p_j) \tag{4.36}$$

where $N \geq 2$ is an integer; $w_j, p_j, j = 1,2,\ldots,N$ are weights and abscissae, respectively, as shown in Table 2.5 in Section 2.3. For fixed z and t, let $st = p$, then complex integrals in Eqs. (4.34) and (4.35) can be written in the form of the integrals in Eq. (4.36) as follows:

$$U_1(z,t) = \frac{1}{2\pi i}\int_{\gamma-i\infty}^{\gamma+i\infty} \frac{e^p}{p}F_1(p)\,dp, \quad 0 < z < H_1 \tag{4.37}$$

$$U_2(z,t) = \frac{1}{2\pi i}\int_{\gamma-i\infty}^{\gamma+i\infty} \frac{e^p}{p}F_2(p)\,dp, \quad H_1 < z < H_2 \tag{4.38}$$

where $F_j(p) = \hat{U}_j(z, \frac{p}{t})\frac{p}{t},\ j = 1,2$, then Eqs. (4.37) and (4.38) are ready to be approximated using Eq. (4.36). To verify the validity of applying Eq. (4.36) to evaluate Eqs. (4.37) and (4.38), a sample calculation was performed using parameters given in Table 4.3 below.

In the sample calculation, it is assumed that $T_j(z,0) = 25$ C, $j = 1,2$, thus in view of Eq. (4.12), the

Table 4.3: Geometry and material parameters used in the sample calculation

Parameters	Value
Layer thickness (m)	
h_1	0.4
h_2	2.0
Thermal conductivity, λ (Kcal/m h C)	
PCC slab	1.85
Base layer	1.20
Thermal diffusivity, α (m^2/h)	
PCC slab	0.00468
Base layer	0.00360

final solution $T_j(z,t),\ j = 1, 2$ is

$$T_j(z,t) = U_j(z,t) + 25 \tag{4.39}$$

Fig. 4.5 plots temperature profiles in the concrete slab at time t = 10, 60, 180, 360 and 600 seconds using temperature solutions for a two-layered system; while Fig. 4.6 illustrates transient temperature histories from t = 1 to 1000 seconds at z = 1, 10, 20, 50, 100 and 200 mm measured from pavement surface.

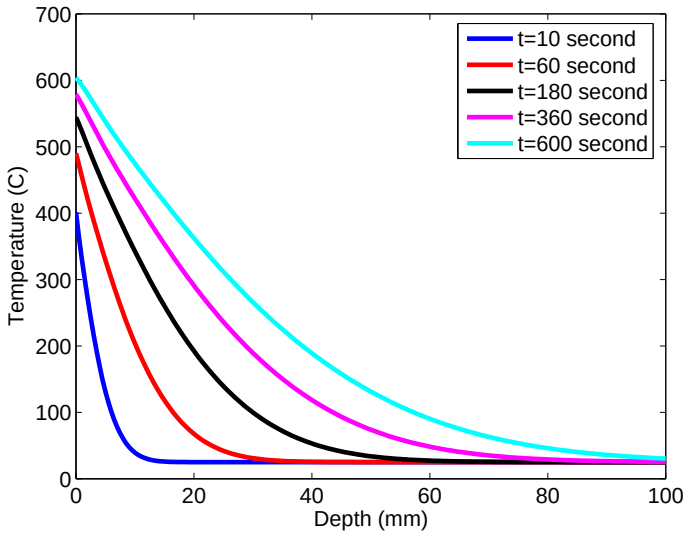

Figure 4.5: Transient concrete slab temperature profile for a two-layered system subjected to transient thermal loading

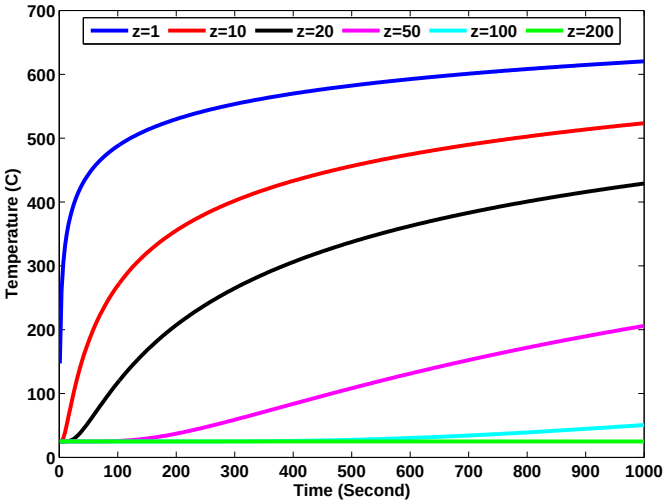

Figure 4.6: Transient temperature values evaluated at different depths in the concrete slab for a two-layered system subjected to thermal loading

4.2.2 Specified Heat Flux from Aircraft Engine, $Q(t)$

In this case, we assume that if the heat flux emanating from aircraft engine, $Q(t)$, is known, then the underlying mathematical model to estimate 1-D temperature field in a two-layered pavement system, as shown in Fig. 4.4, is given by the following equations

$$\begin{aligned}
\frac{\partial T_j}{\partial t}(z,t) &= \alpha_j \frac{\partial^2 T_j}{\partial z^2}(z,t) \qquad 0<t<\infty, \qquad H_{j-1}<z<H_j, \qquad j=1,2 \\
T_j(z,0) &= G_j(z), \qquad j=1,2 \qquad \text{(initial condition)} \\
-\lambda_1 \frac{\partial T_1}{\partial z}(0,t) &= B\left[\frac{Q(t)}{B} + T_{\text{air}}(t) - T_1(0,t)\right] \qquad \text{(first boundary condition)} \\
T_2(H_2,t) &= \text{constant} \qquad \text{(second boundary condition)} \\
T_1(H_1,t) &= T_2(H_1,t) \qquad \text{(first interface condition)} \\
\lambda_1 \frac{\partial T_1}{\partial z}(H_1,t) &= \lambda_2 \frac{\partial T_2}{\partial z}(H_1,t) \qquad \text{(second interface condition)}
\end{aligned} \tag{4.40}$$

where B = pavement surface convection coefficient (Kcal/m^{2}hr C); $T_{\text{air}}(t)$ = air temperature (C); and the other variables are defined in Section 4.2.1. Note that the heat input from direct solar radiation discussed in Chapters 2 and 3 is ignored in this problem due to the rapid transient heating of the surface by the aircraft engine. The only difference between Systems (4.11) and (4.40) is the first boundary condition.

Similar to Section 4.2.1, let $U_j(z,t) = T_j(z,t) - T_j(z,0),\ j=1,2$ and suppose that $T_j(z,0)$ is a constant, then the first boundary condition in System (4.40) becomes

$$-\lambda_1 \frac{\partial U_1}{\partial z}(0,t) = B\left[\frac{Q(t)}{B} + T_{\text{air}}(t) - T_1(0,0) - U_1(0,t)\right] \tag{4.41}$$

Since $\frac{Q(t)}{B} \gg T_{\text{air}}(t) - T_1(0,0)$, we drop $T_{\text{air}}(t) - T_1(0,0)$ for simplicity. Thus System (4.40) can be rewritten in terms of $U_j(z,t), j=1,2$ as follows:

$$\frac{\partial U_j}{\partial t}(z,t) = \alpha_j \frac{\partial^2 U_j}{\partial z^2}(z,t) \qquad 0<t<\infty, \qquad H_{j-1}<z<H_j, \quad j=1,2 \tag{4.42}$$

$$U_j(z,0) = 0 \tag{4.43}$$

$$-\lambda_1 \frac{\partial U_1}{\partial z}(0,t) = Q(t) - BU_1(0,t) \tag{4.44}$$

$$U_2(H_2,t) = 0 \tag{4.45}$$

$$U_1(H_1,t) = U_2(H_1,t) \tag{4.46}$$

$$\lambda_1 \frac{\partial U_1}{\partial z}(H_1,t) = \lambda_2 \frac{\partial U_2}{\partial z}(H_1,t) \tag{4.47}$$

where it is assumed that $T_2(H_2, t) = T_2(H_2, 0)$ for all t.

Similar to Section 4.2.1, the main mathematical tools employed to resolve the system in equation (4.40) are again Laplace transform and the numerical inversion of Laplace transform. Refering to Section 4.2.1, $\hat{U_j}(z, s), j = 1, 2$ are given by Eq. (4.21) with $A_j(s), B_j(s), j = 1, 2$ determined using Laplace transformations of boundary and interlayer contact conditions. Applying Laplace transform to Eq. (4.44) with respect to t gives

$$-\lambda_1 \frac{\partial \hat{U_1}}{\partial z}(0, s) = \hat{Q}(s) - B\hat{U_1}(0, s) \tag{4.48}$$

In the following sample calculation, $Q(t)$, the step function representing the heat flux of the engine, is assumed to be given by

$$Q(t) = \begin{cases} Q_0 & \text{if } t_1 \leq t \leq t_2 \\ 0 & \text{if } 0 \leq t < t_1 \text{ or } t > t_2 \end{cases} \tag{4.49}$$

where Q_0 is a constant heat flux; t_1, t_2 are two time values. Thus Laplace transform of Eq. (4.49) is

$$\hat{Q}(s) = \frac{Q_0}{s}\left(e^{-st_1} - e^{-st_2}\right) \tag{4.50}$$

As in Section 4.2.1, $A_j(s)$, $B_j(s)$, $j = 1, 2$ can be determined using the linear system (4.27) with all the symbols defined in Eq. (4.28) except the following ones

$$\begin{aligned} a_{11} &= B + \lambda_1 r_1 \\ a_{12} &= B - \lambda_1 r_1 \\ C_1 &= \frac{Q_0}{s}\left(e^{-st_1} - e^{-st_2}\right) \end{aligned} \tag{4.51}$$

and $A_j(s)$, $B_j(s)$, $j = 1, 2$ are given as follows:

$$\begin{aligned} A_1(s) &= \frac{C_1}{\widetilde{\Delta}}\widetilde{I_1} \\ B_1(s) &= -\frac{C_1}{\widetilde{\Delta}}\widetilde{I_2} \\ A_2(s) &= 2\frac{C_1}{\widetilde{\Delta}}\lambda_1 r_1 e^{h_1(r_2 - r_1)} \\ B_2(s) &= -2\frac{C_1}{\widetilde{\Delta}}\lambda_1 r_1 e^{-2r_2 h_2 - h_1(r_1 + r_2)} \end{aligned} \tag{4.52}$$

Table 4.4: Additional parameters assumed in the sample calculation.

Parameters	Value
B (Kcal/m^2 h C)	16.29
Q_0 (Kcal/m^2 h)	9.0e+4
$T_j(z,0)$, $j=1,2$ (C)	25
Time variables used in $Q(t)$ (second)	
t_1	10
t_2	130

where

$$\begin{aligned}
\widetilde{I}_1 &= \lambda_1 r_1 + \lambda_2 r_2 + (\lambda_2 r_2 - \lambda_1 r_1)\, e^{-2r_2 h_2} \\
\widetilde{I}_2 &= (\lambda_2 r_2 - \lambda_1 r_1)\, e^{-2r_1 h_1} + (\lambda_1 r_1 + \lambda_2 r_2)\, e^{-2(r_1 h_1 + r_2 h_2)} \\
\widetilde{\Delta} &= (B + \lambda_1 r_1)\left[\lambda_1 r_1 + \lambda_2 r_2 + (\lambda_2 r_2 - \lambda_1 r_1) e^{-2r_2 h_2}\right] \\
&\quad + (B - \lambda_1 r_1) e^{-2r_1 h_1}\left[\lambda_1 r_1 - \lambda_2 r_2 - (\lambda_1 r_1 + \lambda_2 r_2) e^{-2r_2 h_2}\right]
\end{aligned} \tag{4.53}$$

Furthermore, inserting Eq. (4.52) into Eq. (4.21) yields $\hat{U}_j(z,s)$, $j=1,2$ below

$$\begin{aligned}
\hat{U}_1(z,s) &= \frac{C_1}{\widetilde{\Delta}}\Big\{(\lambda_1 r_1 + \lambda_2 r_2) e^{-r_1 z}\left[1 - e^{-2(r_1 h_1 + r_2 h_2 - r_1 z)}\right] \\
&\quad + (\lambda_2 r_2 - \lambda_1 r_1)\left[e^{-(2r_2 h_2 + r_1 z)} - e^{-2r_1 h_1 + r_1 z}\right]\Big\} \qquad (4.54) \\
\hat{U}_2(z,s) &= \frac{C_1}{\widetilde{\Delta}} 2\lambda_1 r_1 e^{-r_2(z-h_1) - r_1 h_1}\left[1 - e^{-2r_2(H_2 - z)}\right] \qquad (4.55)
\end{aligned}$$

where C_1 is given in Eq. (4.51).

As in Section 4.2.1, $U_j(z,t)$, $j=1,2$ can be determined by inverse Laplace transform as in Eqs. (4.34) and (4.35). The numerical inversion can be estimated using the 10-point Gaussian quadrature formula shown in Eq. (4.36). In the sample calculation, the parameters from Table 4.3 are selected in addition to those given in Table 4.4.

Fig. 4.7 plots temperature profiles in the concrete slab at time t = 15, 30, 60, 90, 120, 150, and 210 seconds using temperature solutions for a two-layered pavement system in this section, while Fig. 4.8 illustrates transient temperature histories from t = 1 to 1000 seconds at z = 0, 1, 3, 5, 8, 10, 20, 30, and 40 mm measured from pavement surface.

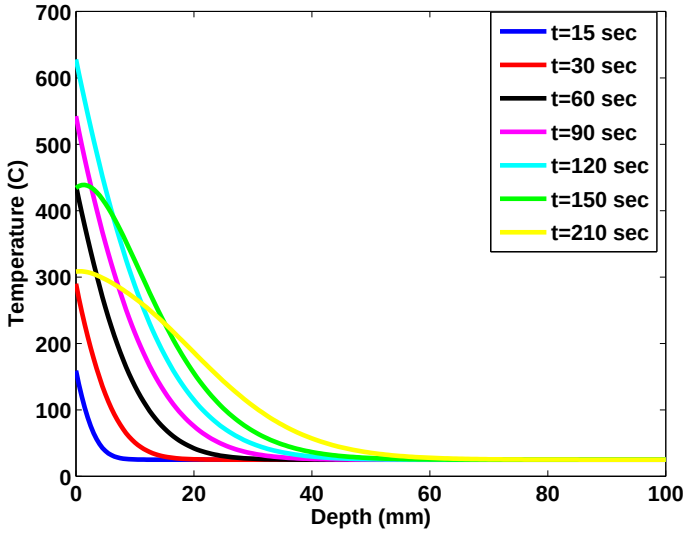

Figure 4.7: Transient concrete slab temperature profile in the first layer for a two-layered pavement system subjected to specified heat flux from aircraft

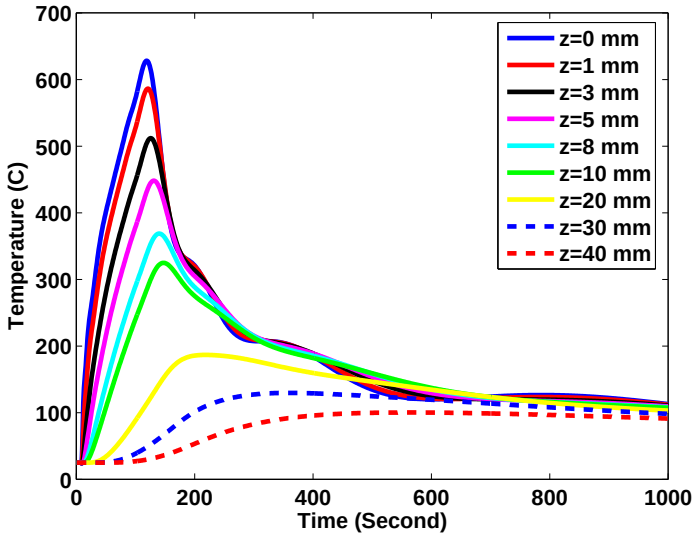

Figure 4.8: Transient temperature values evaluated at different depths in the first layer for a two-layered pavement system subjected to specified heat flux from aircraft

Table 4.5: Geometry and material parameters used in the sensitivity study

Parameters	Value
Layer thickness (mm)	
h_1	60,100
h_2	400
Thermal conductivity, λ (Kcal/mm sec C)	
Geopolymer paste	0.2E-6
PCC slab	0.51E-6
Thermal diffusivity, α (mm^2/sec)	
Geopolymer	0.2
PCC slab	1.3

4.2.3 Sensitivity Study

In this subsection, we conduct brief sensitivity study of effects of thermal properties and the thickness of first layer on temperature profile in a two-layered system. This will give some clues to select appropriate materials having heat resistant properties for the surface layer in airfield concrete pavement. Since geopolymer materials have desired properties for serving as an alternative binder to traditional Portland Cement in producing paving concrete, such as lower thermal conductivity and diffusivity values, high compressive strength at early-age, non-flammability, and high thermal stability, it is possible to construct paving concrete made from geopolymer binder on top of the ordinary concrete slab in order to limit the temperature penetration in the ordinary concrete layer [14]. The following sensitivity study gives an example of such two-layered system.

The parameters used in the sensitivity study are given in Tables 4.4 and 4.5. Figs. 4.9 and 4.10 plot temperatue profiles at different times, and Figs. 4.11 and 4.12 plot transient temperature values evaluated at different depths, for a two-layered system with $h_1 = 60$ mm and $h_1 = 100$ mm, respectively. Actual calculations show that there are no differences in the first nine significant digits between calculated temperature values in generating Figs. 4.9 to 4.12, i.e., fixing all the other parameters and replacing h_1=60 mm by $h_1 = 100$ mm does not change temperature profiles in the two-layered system under the rapidly imposed thermal loading case. However, Figs. 4.8 and 4.11 demonstrate that the peak temperature values in the two-layered system containing geopolymer materials are lower than those in the ordinary concrete two-layered system at all depths except the surface, as expected. In particular, at $z = 40$ mm, the peak temperature drops from around 100 C in Fig. 4.8 to about 37 C in Fig. 4.11.

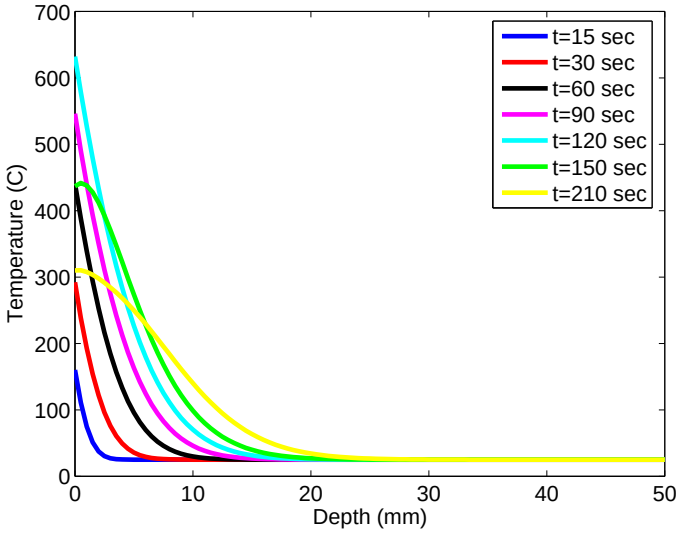

Figure 4.9: Transient temperature profile for a geopolymer-concrete system ($h_1 = 60$ mm) subjected to specified heat flux from aircraft

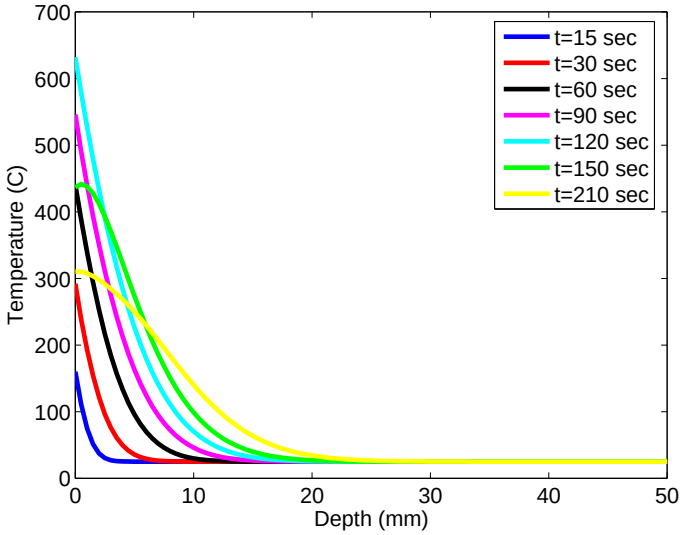

Figure 4.10: Transient temperature profile for a geopolymer-concrete system ($h_1 = 100$ mm) subjected to specified heat flux from aircraft

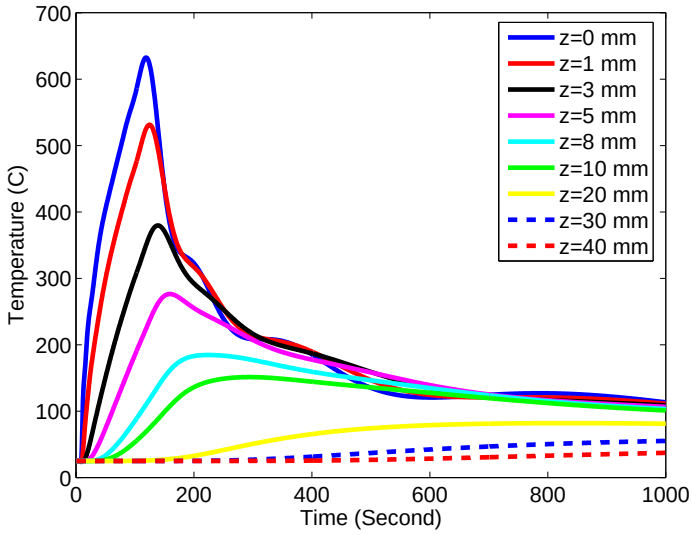

Figure 4.11: Transient temperature values evaluated at different depths in a geopolymer-concrete system ($h_1 = 60$ mm) subjected to specified heat flux from aircraft

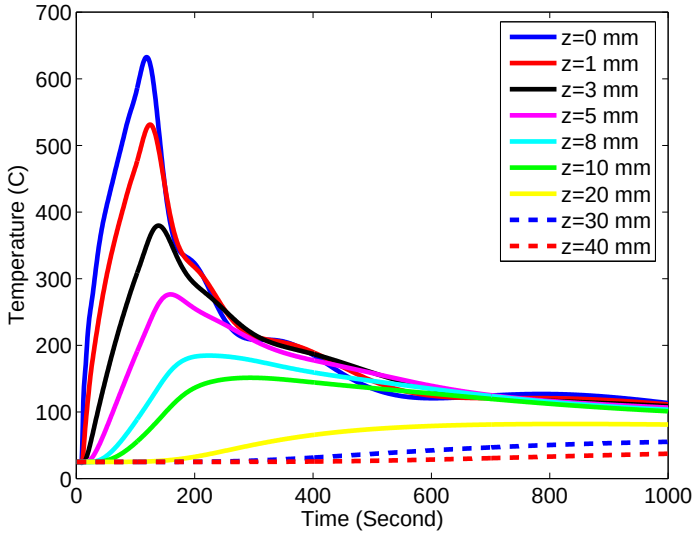

Figure 4.12: Transient temperature values evaluated at different depths in a geopolymer-concrete system ($h_1 = 100$ mm) subjected to specified heat flux from aircraft

4.2.4 Section Summary

In this section, 1-D rapidly varying temperature profiles in two-layered pavement systems subjected to transient thermal loadings are studied. The underlying solution techniques are Laplace transform and numerical inverse Laplace transform. Analytical solutions are derived for both specified surface temperature history and heat flux from aircraft engine conditions. Numerical calculations are carried out to illustrate the derived solutions. Also, a brief sensitivity study of effects of material thermal properties and the thickness of first layer on temperature profile in a two-layered system is conducted.

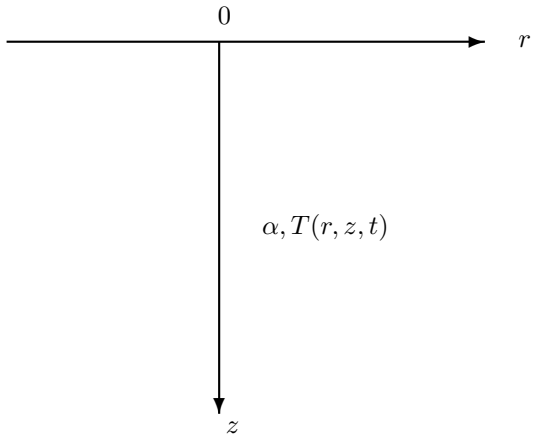

Figure 4.13: Cylindrical coordinate system

4.3 2-D Axisymmetric Temperature Field in Homogeneous Half-Space with Specified Surface Temperature

In this section, analytical solutions of 2-D axisymmetric transient temperature field are derived under the assumption that the thermal loadings and surface boundary conditions are axisymmetric. To take advantage of axisymmetry, the cylindrical coordinate system is used, as shown in Fig. 4.13, where α = thermal diffusivity (m^2/h) and $T(r, z, t)$ = the temperature function. Here, we assume that the surface temperatures are available during the period of interest. The mathematical formulation of this problem is given as

$$\frac{\partial T}{\partial t} = \alpha\left(\frac{\partial^2 T}{\partial r^2} + \frac{1}{r}\frac{\partial T}{\partial r} + \frac{\partial^2 T}{\partial z^2}\right), \qquad 0 < t < \infty, \qquad 0 < z < \infty \tag{4.56}$$

$$T(r, 0, t) = F(r, t), \qquad \text{(boundary condition)} \tag{4.57}$$

$$T(r, z, 0) = G(r, z), \qquad \text{(initial condition)} \tag{4.58}$$

where F and G are assumed to be continuous.

Let the time period of interest be $[0, t_e]$, and m a positive integer. Suppose that $[0, t_e]$ is divided into $2m$ sub-intervals of equal lengths, and that the surface temperature at $r = 0$ are measured at two end points of

each sub-interval except at time t_e, then the interpolatory trigonometric polynomials, based on the discrete least squares approximation, can be obtained to approximate $F(0,t)$ as follows [5]

$$F(0,t) = \frac{a_0}{2} + \frac{a_m}{2}\cos(m\bar{t}) + \sum_{k=1}^{m-1}\left[a_k\cos(k\bar{t}) + b_k\sin(k\bar{t})\right], \qquad 0 \le t \le t_e - \frac{t_e}{2m} \tag{4.59}$$

with

$$\bar{t} = \pi\left(\frac{2t}{t_e} - 1\right) \tag{4.60}$$

$$a_k = \frac{1}{m}\sum_{l=0}^{2m-1} T_l \cos\left[\frac{k\pi}{m}(l-m)\right] \quad \text{for each} \quad k = 0, 1, \ldots, m \tag{4.61}$$

$$b_k = \frac{1}{m}\sum_{l=0}^{2m-1} T_l \sin\left[\frac{k\pi}{m}(l-m)\right] \quad \text{for each} \quad k = 1, 2, \ldots, m-1 \tag{4.62}$$

where T_l = measured surface temperature at $r = 0$ at l^{th} partitioning point of $[0, t_e]$, i.e., at time $t_l = \frac{l}{2m}t_e$ for each $l = 0, 1, 2, \ldots, 2m-1$. In the following, $F(r,t)$ is assumed to have the form

$$F(r,t) = e^{-\mu r}F(0,t) \tag{4.63}$$

where μ is some parameter.

For simplicity, we assume that $T(r,z,0)$ is independent of z. Also, the compatibilities of initial and boundary conditions at $z = 0, t = 0$ impose that $F(r,0) = G(r,0)$, which yields $T(r,z,0) = F(r,0)$.

In view of the above discussion, the following focuses on the derivation of the analytical solution for $T(r,z,t)$ satisfying the PDE given in Eq. (4.56) with the boundary and initial conditions given by

$$\begin{aligned} T(r,0,t) = {} & e^{-\mu r}\left\{\frac{a_0}{2} + \frac{a_m}{2}\sin\left[\frac{2m\pi}{t_e}t + \pi\left(\frac{1}{2} - m\right)\right]\right. \\ & \left. + \sum_{k=1}^{m-1}\left[a_k\sin\left(\frac{2k\pi}{t_e}t + \pi\left(\frac{1}{2} - k\right)\right) + b_k\sin\left(\frac{2k\pi}{t_e}t - k\pi\right)\right]\right\}, \end{aligned} \tag{4.64}$$

where $0 \le t \le t_e\left(1 - \frac{1}{2m}\right)$; and

$$T(r,z,0) = e^{-\mu r}\left\{\frac{a_0}{2} + \frac{a_m}{2}\sin\left[\pi\left(\frac{1}{2} - m\right)\right] + \sum_{k=1}^{m-1}\left[a_k\sin\left(\pi\left(\frac{1}{2} - k\right)\right) + b_k\sin\left(-k\pi\right)\right]\right\}, \tag{4.65}$$

where Eq. (4.65) is obtained by setting $t = 0$ in Eq. (4.64). It is noted that Eq. (4.56) is linear, the principle of linear superposition implies that the final solution satisfying the Eqs. (4.56), (4.64) and (4.65)

can be obtained by summing up each solution satifying Eq. (4.56) and the following boundary and initial conditions

$$T(r,0,t) = e^{-\mu r} A \sin(\omega t + \phi) \tag{4.66}$$

$$T(r,z,0) = e^{-\mu r} A \sin\phi \tag{4.67}$$

where $e^{-\mu r} A \sin(\omega t + \phi), e^{-\mu r} A \sin(\phi)$ resemble each term in the right hand side of Eqs. (4.64) and (4.65), respectively. Hence, the model initial boundary value problem consisting of Eqs. (4.56), (4.66) and (4.67) will be considered.

4.3.1 Separation of Variables

The method of separation of variables has been employed to predict time-dependent temperature profile in multilayered pavement systems using the measured air temperature, solar radiation intensity and material parameters in the previous two chapters. To facilitate the derivation of analytical solution, the complex-valued function of real variables, $Y(r,z,t)$ is introduced, which is the solution of the following boundary value problem

$$\frac{\partial Y}{\partial t} = \alpha\left(\frac{\partial^2 Y}{\partial r^2} + \frac{1}{r}\frac{\partial Y}{\partial r} + \frac{\partial^2 Y}{\partial z^2}\right), \qquad 0 < t < \infty, \qquad 0 < z < \infty \tag{4.68}$$

$$Y(r,0,t) = A e^{-\mu r + j(\omega t + \phi)} \tag{4.69}$$

$$Y(r,z,t) \quad \text{is bounded} \tag{4.70}$$

where j is the imaginary unit number with $j^2 = -1$.

It is clear that the imaginary part of $Y(r,z,t)$ satisfies the Eqs. (4.56) and (4.66), and in general does not satisfy the Eq. (4.67). However, the influence of initial data $T(r,z,0)$ on transient temperature distributions gradually decays as time increases [47], and thus the solution based on the method of separation of variable can still give reasonable approximation to temperature at the point $Q(r,z,t)$ with small z and large t.

The following outlines the main steps involved in solving Eqs. (4.68) and (4.69) based on the method of separation of variables:

1. We assume that

$$Y(r,z,t) = u(r,z) e^{j(\omega t + \phi)} \tag{4.71}$$

then, it follows that

$$\frac{\partial Y}{\partial t} = j\omega Y \tag{4.72}$$

2. Inserting Eqs. (4.71) and (4.72) into Eq. (4.68) yields

$$j\omega u = \alpha \left(\frac{\partial^2 u}{\partial r^2} + \frac{1}{r}\frac{\partial u}{\partial r} + \frac{\partial^2 u}{\partial z^2} \right) \tag{4.73}$$

3. We assume that u_r is bounded at $r = 0$, $u(r, z)$ is $O(r^{-k})$ [1] and $u_r(r, z)$ is $O(r^{-k+1})$ as $r \to \infty$ for each $z > 0$ with $k > \frac{3}{2}$, then the Hankel transform of order zero of $u(r, z)$ with respect to r, $\bar{u}(\xi, z)$ defined below exists [11]

$$\bar{u}(\xi, z) = \int_0^\infty r u(r, z) J_0(\xi r) dr \tag{4.74}$$

where $J_0(\xi r)$ is the first kind of Bessel function of order zero.

Applying the Hankel transform on r to both sides of Eq. (4.73), we obtain formally the following equation

$$\frac{\partial^2 \bar{u}}{\partial z^2}(\xi, z) - \left(\xi^2 + \frac{\omega}{\alpha} j \right) \bar{u}(\xi, z) = 0 \tag{4.75}$$

Note that the following fact was used in deriving Eq. (4.75) when u and u_r satisfy the above-mentioned conditions [11]

$$\int_0^\infty r \left(\frac{d^2}{dr^2} + \frac{1}{r}\frac{d}{dr} \right) u(r, z) J_0(\xi r) dr = -\xi^2 \bar{u}(\xi, z) \tag{4.76}$$

4. Solving Eq. (4.75), we find that

$$\bar{u}(\xi, z) = C e^{-\xi z(M + jN)} + D e^{\xi z(M + jN)} \tag{4.77}$$

where $M = \sqrt{\frac{V+1}{2}}$, $N = \sqrt{\frac{V-1}{2}}$, $V = \sqrt{1 + \left(\frac{\omega}{\alpha \xi^2} \right)^2}$; and C, D are constants of integration which are determined using the boundary condition.

5. The boundedness of $Y(r, z, t)$ implies $D = 0$ in Eq. (4.77), and the inverse Hankel transform of $\bar{u}$ gives [11]

$$Y(r, z, t) = \int_0^\infty \xi C(\xi) e^{-\xi M z + j(\omega t - \xi N z + \phi)} J_0(\xi r) d\xi \tag{4.78}$$

[1] The order symbol O is defined as [60, pp. 570-571]

$$f(k) = O[G(K)], \quad k \to a \ \text{ (here } a \text{ may be } \pm\infty) \ \text{ if}$$

$$\text{absolute value of } \frac{F(k)}{G(k)} \text{ approaches to } A \text{ as } \ k \to a, \ \text{ where } A \text{ is a nonzero constant}$$

6. Setting $z = 0$ in Eq. (4.78) and considering Eq. (4.69), we find that [11]

$$\begin{aligned} C(\xi) &= \int_0^\infty rAe^{-\mu r} J_0(\xi r) dr \\ &= A\mu(\xi^2 + \mu^2)^{-\frac{3}{2}} \end{aligned} \tag{4.79}$$

7. Substituting Eq. (4.79) into Eq. (4.78) yields the complete expression for $Y(r, z, t)$ whose imaginary part, $T(r, z, t)$ being the desired solution solving Eqs. (4.56) and (4.66)

$$T(r, z, t) = A\mu \int_0^\infty \frac{\xi}{(\xi^2 + \mu^2)^{3/2}} e^{-\xi M z} \sin(\omega t - \xi N z + \phi) J_0(\xi r) d\xi \tag{4.80}$$

It can be shown that for fixed t the improper integral in Eq. (4.80) converges uniformly with respect to r and z, where $r \in [\,0, \infty\,)$ and $z \in [\,0, \infty\,)$ by using the Wererstrass criterion on uniform convergence of improper integrals involving parameters [11].

In practice, the improper integral can be approximated using numerical integration schemes such as Gaussian Quadrature formulas. Since the assumption in Eq. (4.71) may not be valid even for moderate value of z under the rapidly changed thermal loadings condition, for example $z = 40$ mm as illustrated in Fig. (4.18) below. Therefore, we propose another solution method based on integral transforms such as Laplace and Hankel transforms.

4.3.2 Integral Transforms

In this section, we seek the analytical solution satifying Eqs. (4.56), (4.66) and (4.67) based on Laplace and Hankel integral transforms. The main steps involved in the derivation of solution are summarized as follows:

1. Refer to Section (4.2.1), Let $\hat{T}(r,z,s)$ denote the Laplace transform of $T(r,z,t)$ with respect to time t. Applying the Laplace transform with respect to t to the both sides of Eq. (4.56) yields

$$\frac{s}{\alpha}\hat{T}(r,z,s) - \frac{A}{\alpha}e^{-\mu r}\sin\phi = \frac{\partial^2\hat{T}}{\partial r^2} + \frac{1}{r}\frac{\partial\hat{T}}{\partial r} + \frac{\partial^2\hat{T}}{\partial z^2} \tag{4.81}$$

2. We assume that T_r is bounded at $r=0$, T is $O(r^{-k})$ and T_r is $O(r^{-k+1})$ as $r\to\infty$ for each $z>0$, $t>0$ with $k>\frac{3}{2}$. Applying the Hankel transform of order zero on r to both sides of Eq. (4.81) produces the ordinary differential equation

$$\frac{d^2\bar{\hat{T}}}{dz^2} - \left(\xi^2 + \frac{s}{\alpha}\right)\bar{\hat{T}} = -\frac{A}{\alpha}\mu(\xi^2+\mu^2)^{-\frac{3}{2}}\sin\phi \tag{4.82}$$

   where $\bar{\hat{T}}(\xi,z,s)$ denote the Hankel transform of order zero of $\hat{T}(r,z,s)$.

3. The solution of Eq. (4.82) is

$$\bar{\hat{T}}(\xi,z,s) = C(\xi,s)e^{-\beta z} + D(\xi,s)e^{\beta z} + \bar{\hat{T}}_p \tag{4.83}$$

   where $\beta = \sqrt{\xi^2+\frac{s}{\alpha}}$, $C(\xi,s)$ and $D(\xi,s)$ are constants of integration, and $\bar{\hat{T}}_p$ stands for a particular solution of Eq. (4.82) and is given by

$$\bar{\hat{T}}_p = \frac{A\mu(\xi^2+\mu^2)^{-3/2}}{\alpha\xi^2+s}\sin\phi \tag{4.84}$$

4. Boundedness of $T(r,z,t)$ implies that for fixed complex number s with $\mathrm{Re}(s)>0$, $\hat{T}(r,z,s)$ is bounded for $r>0$, $z>0$, and it follows that $D(\xi,s)=0$. Thus

$$\bar{\hat{T}}(\xi,z,s) = C(\xi,s)e^{-\beta z} + \bar{\hat{T}}_p \tag{4.85}$$

   where $C(\xi,s)$ is to be determined using the BC.

5. Applying the Laplace transform on t to the both sides of Eq. (4.66) yields $\hat{T}(r,0,s)$

$$\hat{T}(r,0,s) = Ae^{-\mu r}\left(\frac{\omega}{\omega^2+s^2}\cos\phi + \frac{s}{\omega^2+s^2}\sin\phi\right) \tag{4.86}$$

Applying the Hankel transform of order zero on r to the both sides of Eq. (4.86) gives

$$\bar{\hat{T}}(\xi,0,s) = A\mu(\xi^2+\mu^2)^{-3/2}\left(\frac{\omega}{\omega^2+s^2}\cos\phi + \frac{s}{\omega^2+s^2}\sin\phi\right) \tag{4.87}$$

6. Setting $z = 0$ in Eq. (4.85) and comparing with Eq. (4.87) gives

$$C(\xi,s) = A\mu(\xi^2+\mu^2)^{-3/2}\left[\frac{\omega}{\omega^2+s^2}\cos\phi + \left(\frac{s}{\omega^2+s^2} - \frac{1}{\alpha\xi^2+s}\right)\sin\phi\right] \tag{4.88}$$

7. Substituting Eq. (4.88) into Eq. (4.85) and performing the inverse Hankel transform of order zero of $\bar{\hat{T}}(\xi,z,s)$ yields

$$\begin{aligned}\hat{T}(r,z,s) &= A\mu\int_0^\infty \xi(\xi^2+\mu^2)^{-3/2}\left\{\left[\frac{\omega}{\omega^2+s^2}\cos\phi + \left(\frac{s}{\omega^2+s^2} - \frac{1}{\alpha\xi^2+s}\right)\sin\phi\right]e^{-\beta z}\right. \\ &\quad \left. + \frac{1}{\alpha\xi^2+s}\sin\phi\right\} J_0(\xi r)d\xi\end{aligned} \tag{4.89}$$

8. Referring to Section 4.2.1, the final solution of $T(r,z,t)$ can be approximated using Eq. (4.89) by numerical inverse Laplace transform methods such as Gaussian-Quadrature-type formulas.

4.3.3 Numerical Results

In this section, numerical results based on the above-mentioned two solution methods are presented. In the following calculation, α = 0.35E-2 m^2/h and μ = 0.1E-1 1/m, and temperatures at $r = 0$ with $z =$ 0, 1, 5, 10, 20, 40, 60 mm are calculated starting from $t = 0$ until $t = 1475$ second with the increment of 25 seconds.

The surface temperature at $r = 0$ for every 25 seconds from $t = 0$ until $t = 1475$ second are generated using Figure 3.1 in [26]. The prescribed surface temperature values $T(0,0,t)$ at $t = 0, 25, 50, \ldots, 1475$ seconds and those generated using the above-mentioned interpolatory trigonometric polynomials are presented in Fig. 4.14. When the approximation based on the method of separation of variables are used, the surface temperatures $T(0,0,t)$ is assumed to be $T(0,0,0)$ at each time $t = -300, -275, -250, \ldots, -50, -25$ second in order to get more accurate solution of $T(r,z,0)$ with $r \geq 0$ and $z > 0$.

For the numerical results based on the method of separation variables, the composite 16-point Gaussian quadrature formula is employed to evaluate Eq. (4.80) where the upper limit ∞ is replaced by $\xi = 30$, which is determined using an error analysis. The length of each subinterval equals 0.2 in the composite Gaussian integration scheme. While the 10-point Guassian quadrature formula used for resolving inverse Laplace transform in Section 4.2.1 is employed again to obtain numerical values of $T(r, z, t)$.

Fig. 4.15 shows the prescribed temperature $T(0, 0, t)$ at $t = 0, 25, 50, \ldots, 1475$ seconds and the predicted ones based on the methods of separation of variables and Laplace transforms, respectively. Fig. 4.15 indicates that the surface temperatures at $r = 0$ were almost exactly recovered by the results based on the method of separation of variables (SV), and well approximated for $t \leq 450$ seconds by results based on the Laplace transforms (LT). The artificial oscillation of temperature for the large t exhibited in the approximation based on the Laplace transforms is probably caused by the error associated with the numerical inverse Laplace transforms.

Figs. 4.16 to 4.18 present the predicted transient temperature $T(0, z, t)$ at $z = 1, 5, 10, 20, 40, 60$ mm using the methods of separation of variables and Laplace transforms, respectively. Note that in the Figs. 4.15 to 4.18, "LT" stands for the results based on the Laplace transform, and "SV" for the method of separation of variables. Figs. 4.16 to 4.18 reveal that for $z = 1, 5, 10$ mm, the method of separation of variables gives reasonable prediction of temperature except for small values of t; while the method of Laplace transforms generates reasonable approximation except for artificial oscillations exhibited at $t > 700$ seconds, which are suspected to be caused by the numerical inverse Laplace transform. For $z = 20, 40, 60$ mm, the method of Laplace transform gives better results than separation of variables does. The reason behind this fact is that the latter does not use the initial temperature values and the assumption made in Eq. (4.71) may not be valid in general.

To take advantge of the reasonable temperature prediction generated by each solution method, a combined solution technique is proposed in this study. For example, using the results presented in Figs. 4.15 to 4.18, we proposed that the final approximation for the transient temperature at $z = 0, 1, 5, 10, 20, 40, 60$ mm, as shown in Fig. 4.19, were generated using the approach given in Table 4.6.

4.3.4 Section Summary

In this section, 2-D axisymmetric temperature field with specified surface temperature history in a homogeneous half-space due to transient thermal loading is studied. Two solution methods, one based on the method of separation of variables and Hankel transform, another Laplace and Hankel transforms, are proposed. Inverse Hankel and Laplace transforms can be resolved numerically. A combined solution approach is

Table 4.6: Proposed transient temperature prediction using combined solution technique

z (mm)	$T(0,z,t)$
0	based on SV
1	$T(0,1,0), T(0,1,25)$ based on LT, the others based on SV
5	$T(0,5,0), T(0,5,25), T(0,5,50)$ based on LT, the others based on SV
10	$T(0,10,0), T(0,10,25)$ based on LT, the others based on SV
20	based on LT
40	based on LT
60	based on LT

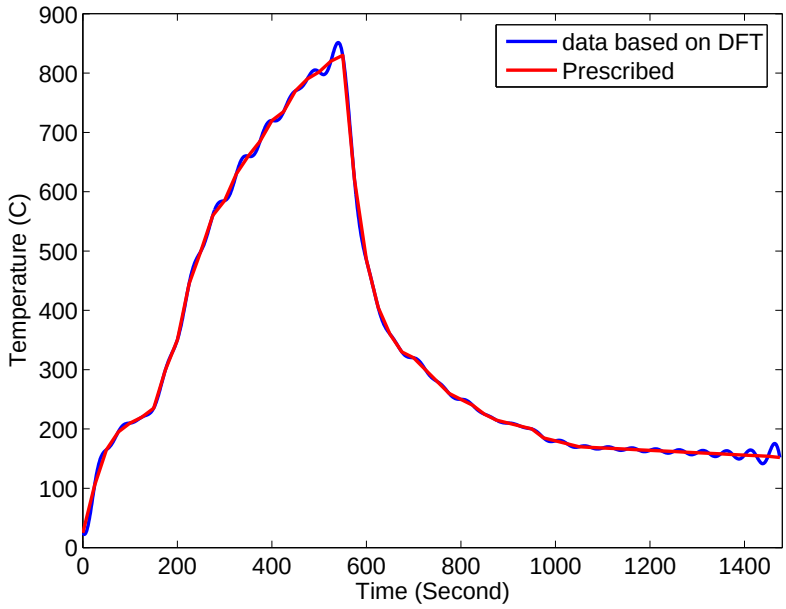

Figure 4.14: Prescribed $T(0,0,t)$ at $t = 0, 25, 50, \ldots, 1475$ seconds and its predicted values based on the interpolatory trigonometric polynomials

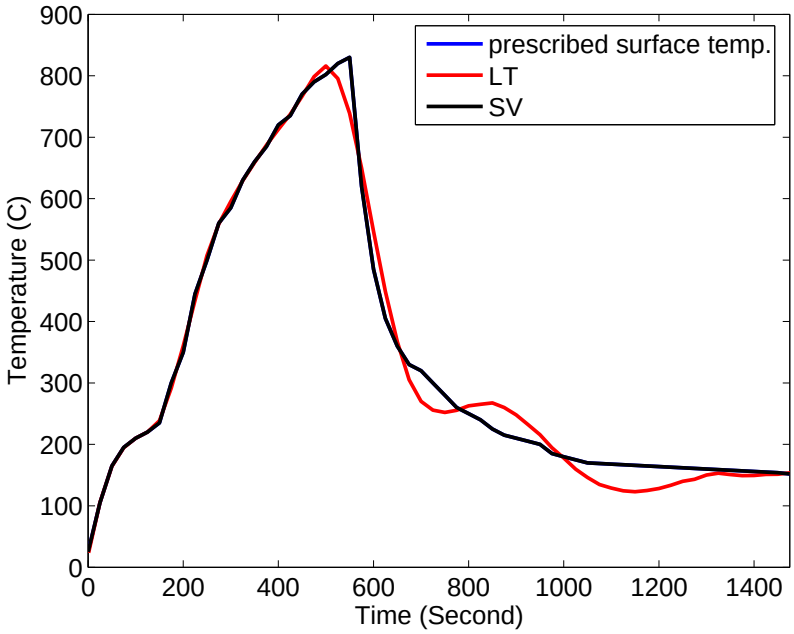

Figure 4.15: Prescribed and predicted surface temperatures at $r = 0$ for different times based on Laplace transform (LT) and separation of variables (SV) method

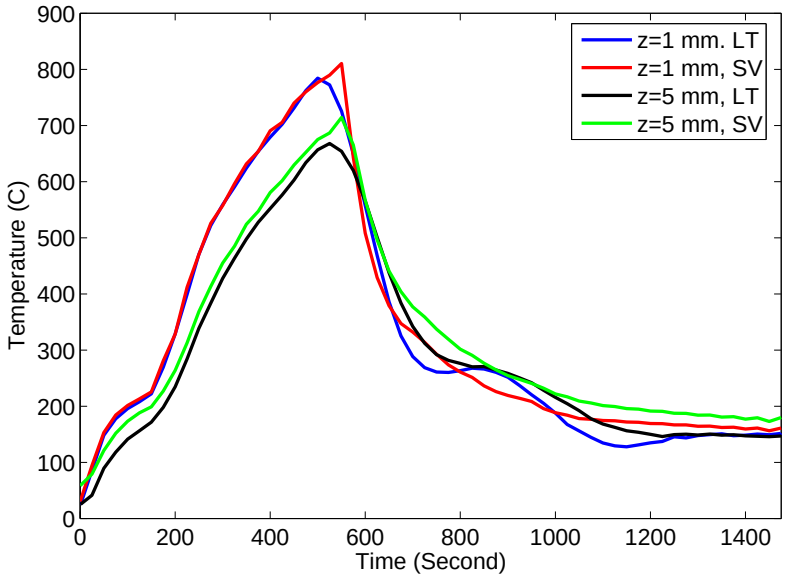

Figure 4.16: Predicted temperatures at $r = 0,\ z = 1$ mm and $r = 0,\ z = 5$ mm for different times

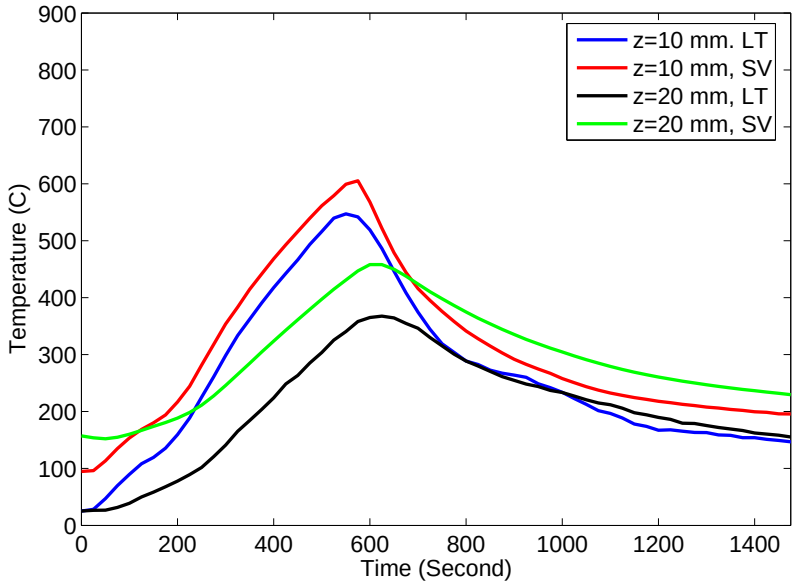

Figure 4.17: Predicted temperatures at $r = 0,\ z = 10$ mm and $r = 0,\ z = 20$ mm for different times

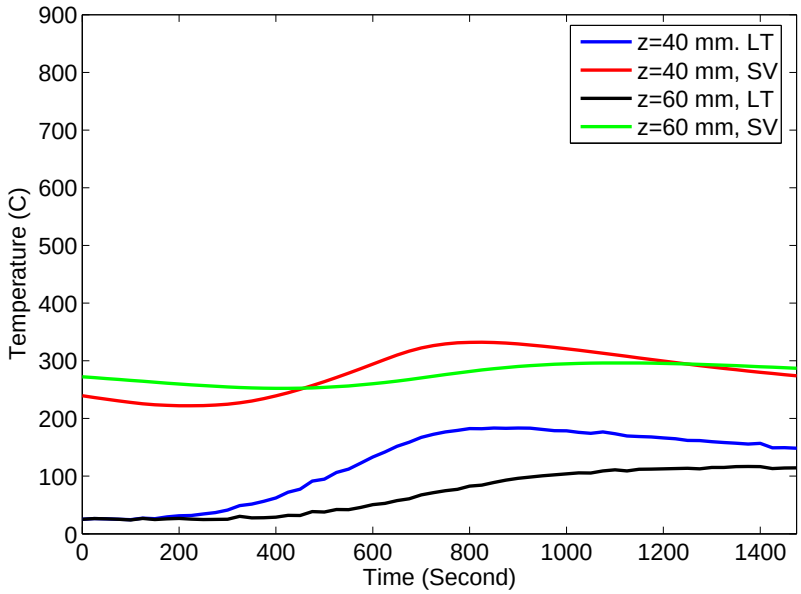

Figure 4.18: Predicted temperatures at $r = 0,\ z = 40$ mm and $r = 0,\ z = 60$ mm for different times

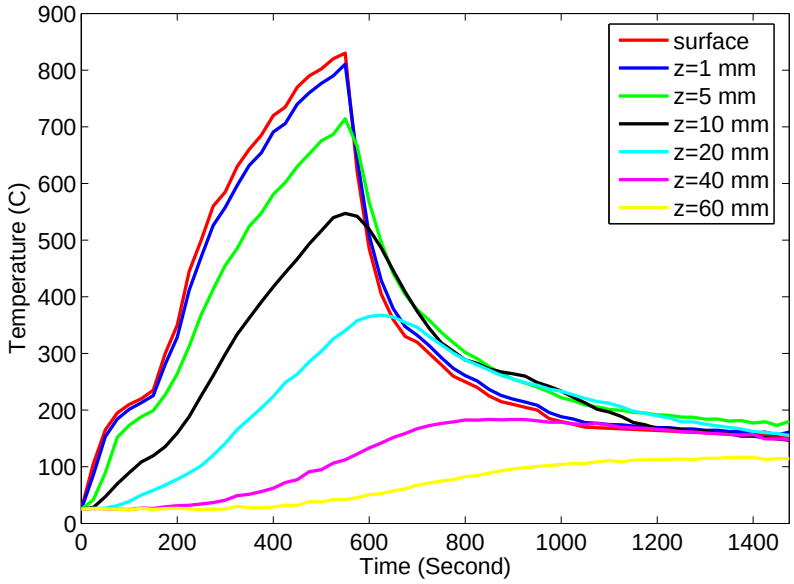

Figure 4.19: Predicted transient temperatures at different depths using results based on two methods described in this section

proposed using the results based on these two methods. Model calculations show that the combined solution approach gives reasonable approximation to the rapidly varying temperature profile.

Chapter 5

Innovative Algorithm to Solve Axisymmetric Displacement and Stress Fields

This chapter presents an innovative algorithm to calculate the displacement and stress fields within a multi-layered pavement system using Layered Elastic Theory and Hankel and Laplace integral transforms. In particular, a recurrence relationship, which links the Hankel transform of displacements and stresses at any point $P(r, z)$ within a multi-layered pavement system with those at the surface point, $Q(r, 0)$, is systematically derived. The Hankel transforms of displacements and stresses at any point within a multi-layered pavement system can be explicitly determined using the derived recurrence relationships, and the subsequent inverse Hankel transforms give the displacements and stresses at the point of interest. Theoretical and computational verification of the proposed algorithm justify its correctness. The proposed algorithm does not use a numerical linear system solver employed in the traditional approach to solve the axisymmetric problems in multi-layered pavement systems. Due to the explicitly derived recurrence relationships for displacements and stresses, the proposed algorithm provides a more rapid solution time than the stress-function-based approach utilized in existing layered elastic theory programs.

5.1 Introduction

Layered Elastic Theory (LET) has been widely used to develop numerous programs to analyze multi-layered pavement systems throughout the world, such as BISAR [16], JULEA [51], DIPLOMAT [29], Kenlayer [19], LEAF [24], etc. The displacement and stress fields, generated from vertical, circular surface loads, are the main quantities to be determined in the analysis of a multi-layered pavement system. There are two major classes of methods for calculating the displacements and stresses within a multi-layered pavement using LET. The traditional one is based on the classical solution of an axisymmetric problem via stress function approach, and they are expressed in the forms of inverse Hankel transforms of certain functions [33]. For example, Burmister solved displacements and stresses in two- and three-layered soil systems by using an ingenious stress function [6, 7, 8]. Matsui, Maina and Inoue calculated the displacements and stresses in multi-layered pavement systems subject to interface slips using Michell function [37]. By using Michell and

Boussinesq functions, Maina and Matsui solved elastic responses of a pavement structure due to vertical and horizontal surface loading [36].

There are $4N-2$ constants of integration in a N-layered pavement system, which are usually approximated using a numerical linear system solver for each given Hankel parameter in the stress-function-based method. Although some solution strategies can be manipulated so that only two equations need solving, but this requires successive matrix multiplications to be performed in order to obtain those two equations [19]. Furthermore, linear systems of four equations need to be solved successively using inter-layer contact condition in order to determine all the constants of integration for each Hankel parameter [19].

This traditional approach is a straight forward, but time-consuming since a large number of Hankel parameters are required to evaluate displacements and stresses at a point within a multi-layered pavement system. This problem becomes more evident in developing sophisticated flexible pavement design tools based on LET, such as the Interim AASHTO Mechanistic-Empirical Design Guide, since tremendously large numbers of displacement and stress calculations are required in order to fully simulate the responses of a flexible pavement during its entire design life [1, 2, 28]. Recently, Khazanovich and Wang proposed several approaches aimed to specifically speed up the numerical evaluation of the inverse Hankel transforms in the layered elastic solutions [28].

Another class of solution methods is based on integral transform techniques, such as Laplace and Hankel transforms, etc.. These methods directly deal with the governing partial differential equations (PDEs) via appropriate integral transforms with respect to various independent variables, transforming complicated PDEs into easily handled equations without resorting to certain stress functions. Furthermore, corresponding inverse integral transforms give rise to the desired displacements and stresses in the form of integral equations, which can be resolved analytically for certain problems or numerically for complex ones [53]. The integral transformation approach has been previously used to solve multi-layered pavement system problems in China [52, 61]. Additionally, Wong and Zhong [56] applied an integral transform method to calculate the thermal stresses due to temperature variation in multi-layered pavement systems . One prominent advantage of these integral transform approaches is the constants of integration involved in the integral equations can be explicitly solved using boundary and inter-layer contact conditions, making the use of a numerical linear system solver unnecessary and thus the solution process should be more efficient.

This chapter presents an innovative algorithm to calculate displacement and stress fields within a multi-layered pavement system based on Hankel and Laplace integral transforms similar to the work proposed by Zhong et al. [61], but with a explicitly-defined recurrence relationship linking the Hankel transform of displacements and stresses at any point $P(r,z)$ with those at surface point $Q(r,0)$. Firstly, the underlying

problems and assumptions used in this study are introduced followed secondly by derivations of the displacements and stresses in a homogeneous half-space for an axisymmetric problem using an integral transform technique. Thirdly, the extension of the solutions for a homogeneous half-space to a multi-layer case is systematically presented. The theoretical justification of proposed algorithm for homogeneous half-space under concentrated and uniformly circular loading are given next and finally, the computational justification for a three-layer system under uniformly circular loading is performed.

5.2 General Multi-Layered Pavement System and Assumptions

The displacement and stress fields in a multi-layered pavement system can be reasonably assumed to be axisymmetric provided the external loading is axisymmetric [6, 7, 8]. A typical $N-$Layer pavement system is shown in Fig. 5.1, where integer $n \geq 2$, h_i, ν_i and G_i are thickness, Poisson's ratio and the modulus of rigidity of the ith layer (thickness of the last layer is assumed to be infinite, i.e. $h_n = \infty$), respectively; p and δ are uniform pressure and radius of circular loading, respectively. The cylindrical coordinate system is used in this study.

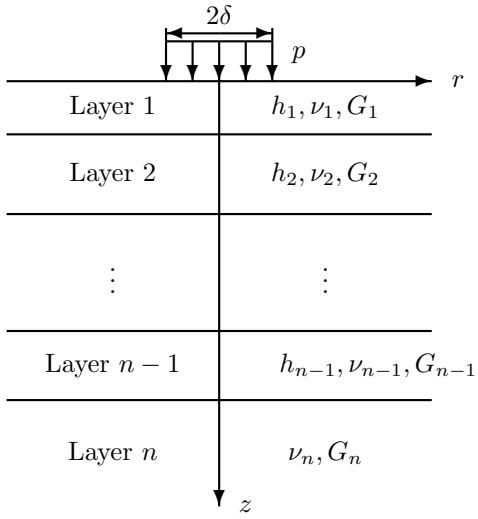

Figure 5.1: Multi-layered pavement system

The mathematical model to solve the displacements and stresses in a multi-layered pavement system is based on LET, and the basic assumptions used in LET are as follows:

- Each layer is assumed to be linear elastic, homogeneous and isotropic.
- Each layer has infinite extent in r- direction. The thickness of each layer is finite except for the last layer.

- Fully bonded inter-layer contact conditions are assumed.
- Body forces are ignored.
- Only vertical traffic loading is considered and assumed to be axisymmetric about the z-axis.
- Strains and displacements are assumed to be small.
- All stress and displacement components vanish as $r \to \infty$ and $z \to \infty$.

In view of the above assumptions, the displacement and stress fields are axisymmetric about z-axis. To facilitate the presentation of proposed algorithm for solving the axisymmetric problems in multi-layered pavement systems, displacement and stress fields in the homogeneous half-space are first determined.

5.3 Displacements and Stresses in a Homogeneous Half-Space

5.3.1 Governing Equations

For a homogeneous half-space, the material parameters are defined as $\nu_i = \nu, G_i = G$ for $i = 1, \cdots, n$ in Fig. 5.1. We denote the displacement along the radial r- direction as u, and vertical z- direction as w. The normal stress components are denoted as $\sigma_r, \sigma_\theta, \sigma_z$, shear stress components as $\tau_{zr}, \tau_{r\theta}, \tau_{\theta z}$, normal strain components as $\varepsilon_r, \varepsilon_\theta, \varepsilon_z$, and shear strain components as $\gamma_{zr}, \gamma_{r\theta}, \gamma_{\theta z}$, respectively. Due to axisymmetric assumption, the displacement along the circumferential θ- direction, shear stress components $\tau_{r\theta}, \tau_{\theta z}$ and shear strain components $\gamma_{r\theta}, \gamma_{\theta z}$ all vanish.

By virtue of the classical theory of linear elasticity [33, p. 274], the governing equations for the axisymmetric problem are as follows:

- Equations of equilibrium

$$\frac{\partial \sigma_r}{\partial r} + \frac{\partial \tau_{zr}}{\partial z} + \frac{\sigma_r - \sigma_\theta}{r} = 0 \tag{5.1}$$

$$\frac{\partial \sigma_z}{\partial z} + \frac{\partial \tau_{zr}}{\partial r} + \frac{\tau_{zr}}{r} = 0 \tag{5.2}$$

- Stress-strain relationships

$$\begin{aligned} \varepsilon_r &= \frac{1}{E}\left[\sigma_r - \nu\left(\sigma_\theta + \sigma_z\right)\right] \\ \varepsilon_\theta &= \frac{1}{E}\left[\sigma_\theta - \nu\left(\sigma_r + \sigma_z\right)\right] \\ \varepsilon_z &= \frac{1}{E}\left[\sigma_z - \nu\left(\sigma_r + \sigma_\theta\right)\right] \\ \gamma_{zr} &= \frac{\tau_{zr}}{G} \end{aligned} \tag{5.3}$$

- Strain-displacement relationships

$$\begin{aligned} \varepsilon_r &= \frac{\partial u}{\partial r} \\ \varepsilon_\theta &= \frac{u}{r} \\ \varepsilon_z &= \frac{\partial w}{\partial z} \\ \gamma_{zr} &= \frac{\partial u}{\partial z} + \frac{\partial w}{\partial r} \end{aligned} \tag{5.4}$$

The equations of equilibrium can be further written in terms of u and w

$$G\left(\nabla^2 u - \frac{u}{r^2}\right) + (\lambda + G)\frac{\partial e}{\partial r} = 0 \tag{5.5}$$

$$G\nabla^2 w + (\lambda + G)\frac{\partial e}{\partial z} = 0 \tag{5.6}$$

where the modulus of rigidity $G = \frac{E}{2(1+\nu)}$, $E =$ the modulus of elasticity, $\nu =$ Poisson's ratio, Lame constant $\lambda = \frac{2\nu G}{1-2\nu}$, the first strain invariant $e = \varepsilon_r + \varepsilon_\theta + \varepsilon_z$, and Laplacian for the axisymmetric problem in cylindrical coordinate system $\nabla^2 = \frac{\partial^2}{\partial r^2} + \frac{1}{r}\frac{\partial}{\partial r} + \frac{\partial^2}{\partial z^2}$.

Furthermore, the stress components can be expressed in terms of u and w by substituting Eq. (5.4) into Eq. (5.3)

$$\sigma_r = 2G\frac{\partial u}{\partial r} + \lambda e \tag{5.7}$$

$$\sigma_\theta = 2G\frac{u}{r} + \lambda e \tag{5.8}$$

$$\sigma_z = 2G\frac{\partial w}{\partial z} + \lambda e \tag{5.9}$$

$$\tau_{zr} = G\left(\frac{\partial u}{\partial z} + \frac{\partial w}{\partial r}\right) \tag{5.10}$$

5.3.2 Integral Transform Techniques

Hankel and Laplace integral transforms are employed to derive displacement and stress fields in a homogeneous half-space. To derive the solutions, some useful formulas involving these integral transforms are presented next:

Let $\widetilde{\phi}^m(\xi)$ be the Hankel transform of order m of a function $\phi(r)$, where m is zero or half of positive integer and ξ is the Hankel parameter. In view of reference [43, p. 299],

$$\widetilde{\phi}^m(\xi) = \int_0^\infty r\phi(r)J_m(\xi r)dr \tag{5.11}$$

and $\phi(r)$ can be represented as the inverse Hankel transform of $\widetilde{\phi}^m(\xi)$

$$\phi(r) = \int_0^\infty \xi\widetilde{\phi}^m(\xi)J_m(\xi r)d\xi \tag{5.12}$$

Also, from reference [43, pp. 310-311]

$$\int_0^\infty r\frac{d\phi}{dr}J_1(\xi r)dr = -\xi\widetilde{\phi}^0(\xi) \tag{5.13}$$

$$\int_0^\infty r\left[\left(\frac{d}{dr}+\frac{1}{r}\right)\phi(r)\right]J_0(\xi r)dr = \xi\widetilde{\phi}^1(\xi) \tag{5.14}$$

$$\int_0^\infty r\left[\left(\frac{d^2}{dr^2}+\frac{1}{r}\frac{d}{dr}\right)\phi(r)\right]J_0(\xi r)dr = -\xi^2\widetilde{\phi}^0(\xi) \tag{5.15}$$

$$\int_0^\infty r\left[\left(\frac{d^2}{dr^2}+\frac{1}{r}\frac{d}{dr}-\frac{1}{r^2}\right)\phi(r)\right]J_1(\xi r)dr = -\xi^2\widetilde{\phi}^1(\xi) \tag{5.16}$$

Denote $\overline{f}(s)$ as the Laplace transform of function $f(z)$, where s is the Laplace parameter. Referring to reference [43, p. 136],

$$\overline{f}(s) = \int_0^\infty f(z)e^{-sz}dz \qquad (z>0)$$

and its inverse Laplace transform gives

$$f(z) = \frac{1}{2\pi i}\int_{\beta-i\infty}^{\beta+i\infty}\overline{f}(s)e^{sz}ds \qquad (\beta>0, z>0)$$

where i = pure imaginary number with $i^2=-1$.

The following outlines the main steps involved in using integral transformation techniques to solve an elastic half-space problem

- Applying Hankel transform of order one to the both sides of Eq. (5.5) with respect to r and in

conjunction with Eqs. (5.13) and (5.16), and order zero to Eq. (5.6) in conjunction with Eqs. (5.14) and (5.15) yields, respectively

$$(1-2\nu)\frac{\partial^2 \widetilde{u}^1}{\partial z^2} - \xi\frac{\partial \widetilde{w}^0}{\partial z} - 2(1-\nu)\xi^2\widetilde{u}^1 = 0 \tag{5.17}$$

$$2(1-\nu)\frac{\partial^2 \widetilde{w}^0}{\partial z^2} + \xi\frac{\partial \widetilde{u}^1}{\partial z} - (1-2\nu)\xi^2\widetilde{w}^0 = 0 \tag{5.18}$$

- Applying Laplace transform to both sides of Eqs. (5.17) and (5.18) with respect to z yields, respectively

$$\left[(1-2\nu)s^2 - 2(1-\nu)\xi^2\right]\overline{\widetilde{u}^1} - \xi s\overline{\widetilde{w}^0} = (1-2\nu)s\widetilde{u}^1(\xi,0) - \xi\widetilde{w}^0(\xi,0) + (1-2\nu)\frac{\partial \widetilde{u}^1}{\partial z}(\xi,0) \tag{5.19}$$

$$\xi s\overline{\widetilde{u}^1} + \left[2(1-\nu)s^2 - (1-2\nu)\xi^2\right]\overline{\widetilde{w}^0} = \xi\widetilde{u}^1(\xi,0) + 2(1-\nu)s\widetilde{w}^0(\xi,0) + 2(1-\nu)\frac{\partial \widetilde{w}^0}{\partial z}(\xi,0) \tag{5.20}$$

- Applying Hankel transform of order zero to the both sides of Eq. (5.9) with respect to r , and order one to Eq. (5.10) gives, respectively

$$\frac{\partial \widetilde{w}^0}{\partial z}(\xi,z) = \frac{1}{1-\nu}\left[\frac{1-2\nu}{2G}\widetilde{\sigma_z}^0(\xi,z) - \nu\xi\widetilde{u}^1(\xi,z)\right] \tag{5.21}$$

$$\frac{\partial \widetilde{u}^1}{\partial z}(\xi,z) = \frac{1}{G}\widetilde{\tau_{zr}}^1(\xi,z) + \xi\widetilde{w}^0(\xi,z) \tag{5.22}$$

- Setting $z = 0$ in Eqs. (5.21) and (5.22) yields $\frac{\partial \widetilde{w}^0}{\partial z}(\xi,0)$ and $\frac{\partial \widetilde{u}^1}{\partial z}(\xi,0)$, respectively. Substituting $\frac{\partial \widetilde{u}^1}{\partial z}(\xi,0)$ into Eq. (5.19), $\frac{\partial \widetilde{w}^0}{\partial z}(\xi,0)$ into Eq. (5.20), respectively, leads to a linear system of two equations involving two unknowns $\overline{\widetilde{u}^1}(\xi,s)$ and $\overline{\widetilde{w}^0}(\xi,s)$, which can be easily determined in terms of $\widetilde{u}^1(\xi,0), \widetilde{w}^0(\xi,0), \widetilde{\tau_{zr}}^1(\xi,0)$ and $\widetilde{\sigma_z}^0(\xi,0)$ as

$$\begin{Bmatrix} \overline{\widetilde{u}^1}(\xi,s) \\ \\ \\ \overline{\widetilde{w}^0}(\xi,s) \end{Bmatrix} = \begin{bmatrix} P_{11} & P_{12} & P_{13} & P_{14} \\ & & & \\ & & & \\ P_{21} & P_{22} & P_{23} & P_{24} \end{bmatrix} \begin{Bmatrix} \widetilde{u}^1(\xi,0) \\ \widetilde{w}^0(\xi,0) \\ \widetilde{\tau_{zr}}^1(\xi,0) \\ \widetilde{\sigma_z}^0(\xi,0) \end{Bmatrix} \tag{5.23}$$

where $P_{ij}, i = 1,2$ and $j = 1,2,3,4$ are given in Appendix C.

- Performing inverse Laplace transforms of $\overline{\widetilde{u}^1}(\xi,s)$ and $\overline{\widetilde{w}^0}(\xi,s)$ in Eq. (5.23) with respect to s yield

$\widetilde{u}^1(\xi,z)$ and $\widetilde{w}^0(\xi,z)$. Furthermore, $\widetilde{\sigma_z}^0(\xi,z)$ and $\widetilde{\tau_{zr}}^1(\xi,z)$ are ready to be obtained using Eqs. (5.21) and (5.22). We list $\widetilde{u}^1(\xi,z), \widetilde{w}^0(\xi,z), \widetilde{\tau_{zr}}^1(\xi,z)$ and $\widetilde{\sigma_z}^0(\xi,z)$ using the following vector-matrix form

$$\begin{Bmatrix} \widetilde{u}^1(\xi,z) \\ \widetilde{w}^0(\xi,z) \\ \widetilde{\tau_{zr}}^1(\xi,z) \\ \widetilde{\sigma_z}^0(\xi,z) \end{Bmatrix} = e^{\xi z} \begin{bmatrix} G_{11} & G_{12} & G_{13} & G_{14} \\ G_{21} & G_{22} & G_{23} & G_{24} \\ G_{31} & G_{32} & G_{33} & G_{34} \\ G_{41} & G_{42} & G_{43} & G_{44} \end{bmatrix} \begin{Bmatrix} \widetilde{u}^1(\xi,0) \\ \widetilde{w}^0(\xi,0) \\ \widetilde{\tau_{zr}}^1(\xi,0) \\ \widetilde{\sigma_z}^0(\xi,0) \end{Bmatrix} \tag{5.24}$$

where $G_{ij}, i,j = 1,2,3,4$ are given in Appendix C.

- Since only vertical traffic loading applied on top of the half-space is considered, i.e. $\sigma_z(r,0)$ is known and $\tau_{zr}(r,0) = 0$, it follows that $\widetilde{\tau_{zr}}^1(\xi,0) = 0$ and $\widetilde{\sigma_z}^0(\xi,0)$ is also known. Furthermore, the last assumption used in LET above, i.e. all stress and displacement components vanish as $r \to \infty$ and $z \to \infty$ implies

$$\lim_{z\to\infty} \widetilde{u}^1(\xi,z) = 0 \qquad \text{and} \qquad \lim_{z\to\infty} \widetilde{w}^0(\xi,z) = 0. \tag{5.25}$$

  Hence, $\widetilde{u}^1(\xi,0)$ and $\widetilde{w}^0(\xi,0)$ can be solved using the first two equations in Eq. (5.24) in conjunction with Eq. (5.25).

- Next, $\widetilde{u}^1(\xi,z), \widetilde{w}^0(\xi,z), \widetilde{\tau_{zr}}^1(\xi,z)$ and $\widetilde{\sigma_z}^0(\xi,z)$ are ready to be solved using Eq. (5.24), and $u(r,z), w(r,z), \tau_{zr}(r,z)$ and $\sigma_z(r,z)$ can be formulated using the appropriate inverse Hankel transforms of Eq. (5.24) as follows:

$$\begin{aligned} u(r,z) &= \int_0^\infty \xi \widetilde{u}^1(\xi,z) J_1(\xi r) d\xi \\ w(r,z) &= \int_0^\infty \xi \widetilde{w}^0(\xi,z) J_0(\xi r) d\xi \\ \tau_{zr}(r,z) &= \int_0^\infty \xi \widetilde{\tau_{zr}}^1(\xi,z) J_1(\xi r) d\xi \\ \sigma_z(r,z) &= \int_0^\infty \xi \widetilde{\sigma_z}^0(\xi,z) J_0(\xi r) d\xi \end{aligned} \tag{5.26}$$

- Combining the first two equations in Eq. (5.26) and the first three equations in Eq. (5.4) with Eqs. (5.7) and (5.8) gives $\sigma_r(r,z)$ and $\sigma_\theta(r,z)$, respectively.

5.4 Displacements and Stresses in a Multi-Layered Pavement System

Referring to Fig. 5.1, according to LET, the governing equations for the i-th layer in a multi-layered pavement system are the same as those for a half-space case except that in the constitutive law, i.e. Eq. (5.3), E, ν and G should be replaced by E_i, ν_i and G_i, respectively, in order to distinguish between material properties of different layers. Let h_i be the thickness of ith layer, where $i = 1, \cdots, n-1$. Define

$$\begin{aligned} H_0 &= 0 \\ H_i &= \sum_{k=1}^{i} h_k \end{aligned}$$

Let Q(r, z) be the point where the displacements and stresses are evaluated, and assume that Q is located in the ith layer, where z is measured from the upper boundary of the i-th layer. Let

$$\widetilde{\Phi}_i(\xi, z) = \left[\widetilde{u}_i^1(\xi, z), \widetilde{w}_i^0(\xi, z), \widetilde{\tau_{zr}}_i^1(\xi, z), \widetilde{\sigma_z}_i^0(\xi, z)\right]^T$$

where the subscript i indicates that the point Q is located in the i-th layer and the superscript T stands for matrix transposition. Let $[G(\xi, z)]_i$ denote the 4 x 4 matrix in Eq. (5.24), where subscript i indicates E_i, ν_i and G_i replacing E, ν and G respectively in Appendix C. The following illustrates how to generalize the results for a half-space problem to a multi-layered system

- In view of Eq. (5.24), the relationship between Hankel transform of displacements and stresses at point with coordinate (r, z) and those at point with coordinate $(r, 0)$ can be expressed as

$$\widetilde{\Phi}_i(\xi, z) = e^{\xi z} \left[G(\xi, z)\right]_i \widetilde{\Phi}_i(\xi, 0) \tag{5.27}$$

  where $i = 1, 2, \cdots, n$.

- Fully bonded conditions at the layer interfaces imply that

$$\widetilde{\Phi}_i(\xi, 0) = \widetilde{\Phi}_{i-1}(\xi, h_{i-1}) \tag{5.28}$$

  where $i = 2, 3, \cdots, n$.

- Substituting Eq. (5.28) into Eq. (5.27) yields

$$\widetilde{\Phi}_i(\xi, z) = e^{\xi z} \left[G(\xi, z)\right]_i \widetilde{\Phi}_{i-1}(\xi, h_{i-1}) \tag{5.29}$$

where $i = 2, 3, \cdots, n$.

- Repeatedly applying the recurrence relation in Eq. (5.29) for $i = n-1, n-2, \cdots, 1$ and $z = h_{n-1}, h_{n-2}, \cdots, h_1$ yields

$$\widetilde{\Phi}_i(\xi, h_i) = e^{\xi H_i} \left[F(\xi, h_i)\right] \widetilde{\Phi}_1(\xi, 0) \tag{5.30}$$

where $i = 1, 2, \cdots, n-1$, and $[F(\xi, h_i)]$ is a 4 x 4 matrix whose components $[F(\xi, h_i)]_{kl}$, $k, l = 1, 2, 3, 4$ are

$$[F(\xi, h_i)]_{kl} = \begin{cases} ([G(\xi, h_1)]_1)_{kl} & \text{if } i = 1 \\ \sum_{j=1}^{4} ([G(\xi, h_i)]_i)_{kj} \cdot [F(\xi, h_{i-1})]_{jl} & \text{otherwise} \end{cases} \tag{5.31}$$

- Setting $i = i - 1$ in Eq. (5.30), then substituting $\widetilde{\Phi}_{i-1}(\xi, h_{i-1})$ into Eq. (5.29) yields

$$\widetilde{\Phi}_i(\xi, z) = e^{\xi(H_{i-1}+z)} \left[G(\xi, z)\right]_i \cdot [F(\xi, h_{i-1})] \widetilde{\Phi}_1(\xi, 0) \tag{5.32}$$

- Since $\sigma_{z1}(r, 0)$ is given and $\tau_{zr1}(r, 0) = 0$, Hankel integral transforms of $\sigma_{z1}(r, 0)$, $\tau_{zr1}(r, 0)$ yields $\widetilde{\sigma}^0_{z1}(\xi, 0)$ and $\widetilde{\tau}^1_{zr1}(\xi, 0)$ respectively, where $\widetilde{\tau}^1_{zr1}(\xi, 0) = 0$. Analogous to the homogeneous half-space case, $\widetilde{u}^1_1(\xi, 0)$ and $\widetilde{w}^0_1(\xi, 0)$ can be determined by using the first two equations in Eq. (5.32) with $i = n$ in conjunction with

$$\lim_{z\to\infty} \widetilde{u}^1_n(\xi, z) = 0 \qquad \text{and} \qquad \lim_{z\to\infty} \widetilde{w}^0_n(\xi, z) = 0 \tag{5.33}$$

The final solutions for $\widetilde{u}^1_1(\xi, 0)$ and $\widetilde{w}^0_1(\xi, 0)$ are

$$\begin{aligned} \widetilde{u}^1_1(\xi, 0) &= \frac{T_{12}}{\Delta} \widetilde{\sigma_{z1}}^0(\xi, 0) \\ \widetilde{w}^0_1(\xi, 0) &= \frac{T_{22}}{\Delta} \widetilde{\sigma_{z1}}^0(\xi, 0) \end{aligned} \tag{5.34}$$

where Δ, T_{12} and T_{22} are given in Appendix C.

- Since $\widetilde{\Phi}_1(\xi, 0) = \left[\widetilde{u}^1_1(\xi, 0), \widetilde{w}^0_1(\xi, 0), \widetilde{\tau_{zr1}}^1(\xi, 0), \widetilde{\sigma_{z1}}^0(\xi, 0)\right]^T$ is known, we can use Eq. (5.32) to calculate $\widetilde{\Phi}_i(\xi, z)$ for $i = 1, 2, \cdots, n$. Note, $[F(\xi, h_{i-1})]$ will becomes a 4 x 4 identity matrix when Q is located in the first layer, i.e. $i = 1$. Furthermore when Q is located in the last layer, i.e. $i = n$, the last

assumption used in LET, i.e., all stress and displacement components are vanished as $r \to \infty$ and $z \to \infty$, indicates that the coefficients of $e^{\xi z}$ terms in the propagating matrix $[G(\xi, z)]_n$ must vanish.

- The inverse Hankel transforms of components of $\widetilde{\Phi}_i(\xi, z)$ give rise to $u_i(r, z), w_i(r, z), \tau_{zri}(r, z)$ and $\sigma_{zi}(r, z)$, see Appendix C for the complete expressions.
- Finally, $\sigma_r(r, z)$ and $\sigma_\theta(r, z)$ can be determined using Eqs. (5.7) and (5.8), respectively, and the complete expressions can be found in Appendix C.

5.5 Theoretical and Computational Justifications of Proposed Algorithm

5.5.1 Theoretical Justification for Homogeneous Half-Space Under Concentrated Vertical Loading

When a concentrated vertical force P is applied on the boundary plane boundary, Hankel transform of order zero of $\sigma_z(r, 0)$ and order one of $\tau_{zr}(r, 0)$ with respect to r yields, respectively

$$\widetilde{\sigma_z}^0(\xi, 0) = -\frac{P}{2\pi} \qquad \text{and} \qquad \widetilde{\tau_{zr}}^1(\xi, 0) = 0 \tag{5.35}$$

Referring to the results for a half-space problem, we can now deduce that

$$\widetilde{u}^1(\xi, 0) = -\frac{(1-2\nu)P}{4\pi\xi G} \qquad \text{and} \qquad \widetilde{w}^0(\xi, 0) = \frac{(1-\nu)P}{2\pi\xi G} \tag{5.36}$$

Substituting Eqs. (5.35) and (5.36) into Eq. (5.24) gives rise to $\widetilde{u}^1(\xi, z)$, $\widetilde{w}^0(\xi, z)$, $\widetilde{\tau_{zr}}^1(\xi, z)$ and $\widetilde{\sigma_z}^0(\xi, z)$ whose inverse Hankel transforms generate the following classical Boussinesq solutions [49, pp. 401-402]

$$\begin{aligned}
u(r, z) &= \frac{(1+\nu)Pr}{2\pi ER}\left(\frac{z}{R^2} - \frac{1-2\nu}{R+z}\right) \\
w(r, z) &= \frac{(1+\nu)P}{2\pi ER}\left[2(1-\nu) + \frac{z^2}{R^2}\right] \\
\sigma_z(r, z) &= -\frac{3Pz^3}{2\pi R^5} \\
\tau_{zr}(r, z) &= -\frac{3Pz^2 r}{2\pi R^5}
\end{aligned}$$

where $R = \sqrt{r^2 + z^2}$.

5.5.2 Theoretical Justification for Homogeneous Half-Space Under Uniform Vertical Circular Loading

Consider circular loading with uniform pressure P and radius of δ (see Fig. 5.1), i.e.

$$\sigma_z(r,0) = \begin{cases} -p & \text{if } r < \delta \\ 0 & \text{otherwise} \end{cases} \qquad \text{and} \qquad \tau_{zr}(r,0) = 0$$

then

$$\widetilde{\sigma_z}^0(\xi,0) = -\frac{P\delta J_1(\xi\delta)}{\xi} \qquad \text{and} \qquad \widetilde{\tau_{zr}}^1(\xi,0) = 0$$

Following the derivation in solving a half-space problem above, we have

$$\widetilde{u}^1(\xi,0) = -\frac{(1-2\nu)P\delta J_1(\xi\delta)}{2G\xi^2} \qquad \text{and} \qquad \widetilde{w}^0(\xi,0) = \frac{(1-\nu)P\delta J_1(\xi\delta)}{G\xi^2}$$

and

$$\begin{aligned}
\sigma_z(r,z) &= -p\int_0^\infty (1+\frac{z}{\delta}x)e^{-\frac{z}{\delta}x}J_1(x)J_0(\frac{r}{\delta}x)dx \\
\sigma_r(r,z) &= p\int_0^\infty \left[(1-2\nu-\frac{z}{\delta}x)\frac{\delta}{rx}J_1(\frac{r}{\delta}x) - (1-\frac{z}{\delta}x)J_0(\frac{r}{\delta}x)\right]e^{-\frac{z}{\delta}x}J_1(x)dx \\
w(r,z) &= \frac{p}{2G}\int_0^\infty \left[z+\frac{2(1-\nu)\delta}{x}\right]e^{-\frac{z}{\delta}x}J_1(x)J_0(\frac{r}{\delta}x)dx
\end{aligned}$$

In particular, setting $r = 0$ in these formulas and using the following results of infinite integrals [54, p. 386]

$$\begin{aligned}
\int_0^\infty e^{-\frac{z}{\delta}x}J_1(x)dx &= 1-\frac{z}{\delta}\left(1+\frac{z^2}{\delta^2}\right)^{-\frac{1}{2}} \\
\int_0^\infty xe^{-\frac{z}{\delta}x}J_1(x)dx &= \left(1+\frac{z^2}{\delta^2}\right)^{-\frac{3}{2}} \\
\int_0^\infty \frac{1}{x}e^{-\frac{z}{\delta}x}J_1(x)dx &= \left(1+\frac{z^2}{\delta^2}\right)^{\frac{1}{2}} - \frac{z}{\delta}
\end{aligned}$$

We recover the following special formulas [19, p. 50]

$$
\begin{aligned}
\sigma_z(0,z) &= -p\left[1-\frac{z^3}{\sqrt{(z^2+\delta^2)^3}}\right] \\
\sigma_r(0,z) &= -\frac{p}{2}\left[1+2\nu-\frac{2(1+\nu)z}{\sqrt{z^2+\delta^2}}+\frac{z^3}{\sqrt{(z^2+\delta^2)^3}}\right] \\
w(0,z) &= \frac{p}{2G}\left[\frac{\delta^2}{\sqrt{z^2+\delta^2}}+(1-2\nu)\left(\sqrt{z^2+\delta^2}-z\right)\right]
\end{aligned}
$$

5.5.3 Computational Justification for Three-Layered Elastic Systems Under Uniform Vertical Circular Loading

The three-layer elastic system is shown in Fig. 5.2. Due to the complexities of integrands involved in the infinite integrals for solutions of stresses and displacements in three-layer elastic systems, the closed-form solutions are rarely available. Instead, numerical integration technologies, such as Gaussian quadrature formulas can be applied to evaluate the infinite integrals [48].

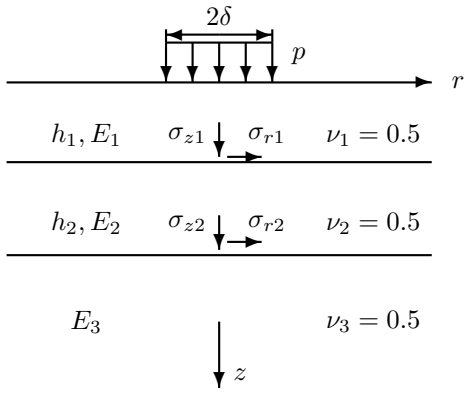

Figure 5.2: Three-layered pavement system

In this case, the stress values calculated using the proposed algorithms are compared with the widely used Jones' Tables of stresses in three-layer elastic system [25]. As shown in Fig. 5.2, the vertical and radial stresses in the bottom of the first and second layer on the axis of symmetry ($r = 0$), denoted by σ_{z1}, σ_{r1}, σ_{z2} and σ_{r2}, respectively, are calculated.

The following parameters are used in Jones' Table:

$$
k_1 = \frac{E_1}{E_2} \qquad k_2 = \frac{E_2}{E_3} \qquad a_1 = \frac{\delta}{h_2} \quad \text{and} \quad H = \frac{h_1}{h_2}
$$

Table 5.1: Calculated stress values using the proposed algorithm and those in Jones' table printed in parentheses (stress values being expressed as a fraction of the applied vertical loading P)

a_1	H	k_1	k_2	σ_{z1}	σ_{r1}	σ_{z2}	σ_{r2}
0.1	0.125	2	2	4.294983e-1	-2.765433e-1	8.960207e-3	-8.199295e-3
				(4.2950e-1)	(-2.7672e-1)	(8.96e-3)	(-8.2e-3)
0.2	0.25	2	2	4.246671e-1	-2.466141e-1	7.061373e-3	-1.000422e-1
				(4.2462e-1)	(-2.4653e-1)	(7.06e-3)	(-1.0004e-1)
0.4	0.5	20	20	1.144855e-1	-2.080734e0	9.882485e-3	-1.312787e-1
				(1.1448e-1)	(-2.08072e0)	(9.88e-3)	(-1.3128e-1)
0.8	1	200	20	1.235930e-2	-4.249169e0	4.361452e-3	-3.389900e-2
				(1.236e-2)	(-4.24864e0)	(4.36e-3)	(-3.389e-2)
1.6	2	2	2	3.663678e-1	-3.843012e-1	2.014516e-1	-1.536974e-1
				(3.6644e-1)	(-3.8443e-1)	(2.0145e-1)	(-1.5370e-1)
3.2	4	20	20	3.257526e-2	-3.077159e0	2.061185e-2	-1.884397e-1
				(3.258e-2)	(-3.07722e0)	(2.061e-2)	(-1.8845e-1)

Table 5.1 lists the calculated stress values corresponding to different parameters using the proposed algorithms and those values from Jones' Table[1], suggesting that at least three significant digits are agreeable between our results and those values from Jones' Table.

5.6 Discussion and Chapter Summary

5.6.1 Discussion

As shown in solving axisymmetric problems in a multi-layered pavement system, the main unknowns $\widetilde{u}_1^1(\xi,0), \widetilde{w}_1^0(\xi,0)$ are solved explicitly using the recurrence relationship defined in Eq. (5.32). Once $\widetilde{u}_1^1(\xi,0), \widetilde{w}_1^0(\xi,0)$ are known, $\widetilde{u}_i^1(\xi,z)$, $\widetilde{w}_i^0(\xi,z)$, $\widetilde{\tau_{zr}}_i^1(\xi,z)$ and $\widetilde{\sigma_z}_i^0(\xi,z)$ are ready to be obtained. Appropriate inverse Hankel transforms of those quantities give the desired solutions for u, w, τ_{zr} and σ_z at any point within a multi-layered pavement system, and solutions for σ_r and σ_θ can be easily solved using Eqs. (5.7) and (5.8). In the paper authored by Zhong, Wang and Guo [61], $\widetilde{u}_1^1(\xi,0)$ and $\widetilde{w}_1^0(\xi,0)$ are solved numerically using a quadratic equation which is obtained by successively performing numerical matrix multiplications. This is the main difference between Reference [61] and this study.

Since all the integrands in the inverse Hankel transforms, which give the desired displacements and stresses, are determined explicitly using the proposed algorithm and all the variables are presented in the appendices of this paper, researchers and engineers can write a computer code to implement, check, and expand this layered elastic theory algorithm.

[1]The stress sign convention used in Jones' Table is applied, i.e., compression stress is positive.

5.6.2 Chapter Summary

In this chapter, application of integral transform techniques, specifically Hankel and Laplace transforms, in solving axisymmetric problem in multi-layered pavement systems is introduced. The desired displacements and stresses evaluated at any point within a N-layered pavement system are formulated in terms of appropriate inverse Hankel transforms. Let $Q(r, z)$ be an evaluation point located in the ith layer, a vector $\widetilde{\Phi}_i(\xi, z)$ consisting of appropriate Hankel transforms of $u_i(r, z), w_i(r, z), \tau_{zri}(r, z)$ and $\sigma_{zi}(r, z)$ is formed. Furthermore, $\widetilde{\Phi}_i(\xi, z)$ and $\widetilde{\Phi}_1(\xi, 0)$ are related using inter-layer contact conditions, and explicit expressions for $\widetilde{u}_1^1(\xi, 0)$ and $\widetilde{w}_1^0(\xi, 0)$ are successfully derived in terms of the solvable quantities $\widetilde{\tau_{zr}}_1^1(\xi, 0)$ and $\widetilde{\sigma_{z}}_1^0(\xi, 0)$ using the assumptions for LET. Theoretical and computational verifications demonstrate the correctness of the proposed algorithm. The proposed algorithm does not use a numerical linear system solver employed in the traditional approach to solving these problems, which should produce faster solutions times.

Chapter 6

Summary and Future Works

6.1 Summary

This thesis extends existing analytical solutions for two common types of problems in pavement engineering, i.e., heat conduction and axisymmetric displacement and stress fields in multi-layered pavement systems. There are two sets of solutions for the first problem. Among them, one set of solutions deals with prediction of time-dependent temperature profile in multi-layered pavement systems based on layer thicknesses, material thermal properties, climatic data (i.e., air temperature and solar radiation intensity), pavement surface absorptivity and convection coefficients. Temperature profile is modeled as an initial boundary value problem where the governing equation is the heat equation. To take account of measured air temperature and solar radiation intensity values, we use the interpolatory trigonometric polynomials, which are based on the discrete least squares approximation, to generate continuous functions to facilitate the derivation of theoretical solutions. Furthermore, a mixed-type boundary condition is considered using energy balances at the pavement surface.

Analytical solutions for 1-D temperature profile in multi-layered pavement systems, i.e., temperature only varies along pavement depth, were derived using the methods of separation of variables and Laplace transform method, respectively. In the latter method, temperature profile is represented in the form of inverse Laplace transform, which is carried out numerically using a Gaussian-Quadrature-type method. Under the assumption of axisymmetric thermal conditions, analytical solution for axisymmetric 2-D temperature profile in a multi-layered pavement system is also derived using Hankel integral transform and the method of separation of variables. Comparisons between model calculated temperature profile based on 1-D and axisymmetric 2-D results and measured field data demonstrate that these analytical solutions give reasonable temperature profiles in the concrete slab of a four-layered CRCP test section. The main advantage of these analytical solutions is that they are easily implementable and can rapidly generate pavement temperature profile with limited inputs. In particular, 1-D analytical solutions can be easily programmed and should be of interest to pavement engineers in characterizing field temperature profile. The 2-D axisymmetric

temperature solution has laid the foundations for further studies of axisymmetric low-temperature thermal stress fields in asphalt pavements based on layered elastic theory.

Another set of solutions is to determine the rapidly varying temperature profile in a two-layer pavement system due to transient thermal loading. Again, analytical 1-D and axisymmetric 2-D solutions are developed in this thesis. For the 1-D solutions, the main mathematical tools employed are Laplace transform and numerical inversion of Laplace transform. 1-D solutions are derived for both specified surface temperature and heat flux from aircraft engines conditions. Model calculations suggest that the derived 1-D analytical solutions can capture the rapidly changing transient pavement temperature profile. For the 2-D axisymmetric Dirichlet problem in homogeneous half-space, specified axisymmetric transient surface temperatures are assumed and two solution methods are proposed. The first method is based on Hankel integral transform and the method of separation of variables, while the other is based on Laplace and Hankel integral transforms. Numerical experiments suggest that a combined result based on these two analytical solutions can give reasonable predictions for the rapidly varying temperature profile.

The second type of problem solved in this thesis was development of an innovative algorithm to calculate axisymmetric displacement and stress fields in multi-layered pavement systems under traffic loading using integral transform techniques and the theory of layered elasticity. All the integration constants arising in the solution of the field equations are explicitly derived in terms of pavement geometric and material parameters as well as Hankel variables. Thus the proposed method does not use any numerical linear system solver which is usually employed in the traditional stress-function-based approaches to solving the same problem. The proposed algorithm will be of interests to researchers working on pavement stress prediction based on the theory of layered elasticity. Under the assumption of axisymmetric pavement temperature profile, e.g., pavement temperature fields under rapid transient thermal loadings discussed in this thesis, the proposed algorithm can be applied to predict thermal stress fields in pavements using the theory of thermomechanics.

6.2 Future Works

The following lists possible future research works relative to this thesis topic:

- The Green's function methods have been proven to be elegant approaches to tackle linear boundary value problems. Application of such methods to solve pavement temperature profile problems is promising.
- In this thesis, the irradiation energy emitted by pavement surface is nonlinear, which is only indirectly considered by reducing the total amount of solar radiation intensity, and hence introduce errors in

calculating pavement temperature profile at night. To directly take this nonlinear term into account, the theory of nonlinear partial differential equations may be applied to derive analytical solutions.

- Within the framework of thermomechanics, thermal stress analysis in pavements can be conducted based on layered elastic or viscoelastic theory.
- Sensitivity studies can be carried out to investigate the effects of initial pavement temperature profile, thermal properties of pavement layer materials, surface absorptivity and convection coefficient on pavement temperature profiles.

Appendix A

This appendix lists the main variables and symbols used in Section 2.2. The superscripts l, m range from 1 to 2 with the understanding that they are not taken as exponents; a symbol such as $(CH)_i$ means CH for the ith layer.

$$\begin{aligned} H_i &= \sum_{k=1}^{i} h_k, \qquad i = 1, 2, \ldots, n-1. \\ (CH)_i &= -2H_i v_i + H_{i-1}(v_i + v_{i-1}), \qquad i = 2, 3, \ldots, n-1. \\ (CK)_i &= -H_{i-1}(v_i - v_{i-1}), \qquad i = 2, 3, \ldots, n-1. \end{aligned}$$

1. Formulas in determining P_i^{lm} and R_i^{lm} for $i = 1, 2, \ldots, n-1$

$$\begin{aligned} P_i^{lm} &= F_i^{lm} e^{j\beta_i^{lm}} \\ F_i^{11} &= \frac{1}{2}\left(1 + \frac{\lambda_i v_i}{\lambda_{i+1} v_{i+1}}\right) \\ F_i^{22} &= F_i^{11} \\ \beta_i^{11} &= -(v_i - v_{i+1}) H_i \\ \beta_i^{22} &= -\beta_i^{11} \end{aligned}$$

There are two cases in determining $F_i^{12}, F_i^{21}, \beta_i^{12}$ and β_i^{21} as follows:

- Case 1: If $1 - \frac{\lambda_i v_i}{\lambda_{i+1} v_{i+1}} < 0$, then

$$\begin{aligned} F_i^{12} &= \frac{1}{2}\left(\frac{\lambda_i v_i}{\lambda_{i+1} v_{i+1}} - 1\right) \\ F_i^{21} &= F_i^{12} \\ \beta_i^{12} &= (v_i + v_{i+1}) H_i + \pi \\ \beta_i^{21} &= -(v_i + v_{i+1}) H_i + \pi \end{aligned}$$

- Case 2: If $1 - \frac{\lambda_i v_i}{\lambda_{i+1} v_{i+1}} \geq 0$, then

$$\begin{aligned} F_i^{12} &= \frac{1}{2}\left(1 - \frac{\lambda_i v_i}{\lambda_{i+1} v_{i+1}}\right) \\ F_i^{21} &= F_i^{12} \\ \beta_i^{12} &= (v_i + v_{i+1}) H_i \\ \beta_i^{21} &= -\beta_i^{12} \end{aligned}$$

$$\begin{aligned} R_i^{lm} &= K_i^{lm} e^{j\psi_i^{lm}} \\ K_1^{lm} &= F_1^{lm} \\ \psi_1^{lm} &= \beta_1^{lm} \end{aligned}$$

$$\begin{aligned} K_i^{11} &= \left\{ \left[e^{(CH)_i} F_i^{11} K_{i-1}^{11} \cos\left(\beta_i^{11} + \psi_{i-1}^{11}\right) + e^{(CK)_i} F_i^{12} K_{i-1}^{21} \cos\left(\beta_i^{12} + \psi_{i-1}^{21}\right) \right]^2 \right. \qquad \text{(A.1)} \\ &\quad \left. + \left[e^{(CH)_i} F_i^{11} K_{i-1}^{11} \sin\left(\beta_i^{11} + \psi_{i-1}^{11}\right) + e^{(CK)_i} F_i^{12} K_{i-1}^{21} \sin\left(\beta_i^{12} + \psi_{i-1}^{21}\right) \right]^2 \right\}^{\frac{1}{2}} \\ K_i^{12} &= \left\{ \left[e^{(CH)_i} F_i^{11} K_{i-1}^{12} \cos\left(\beta_i^{11} + \psi_{i-1}^{12}\right) + e^{(CK)_i} F_i^{12} K_{i-1}^{22} \cos\left(\beta_i^{12} + \psi_{i-1}^{22}\right) \right]^2 \right. \qquad \text{(A.2)} \\ &\quad \left. + \left[e^{(CH)_i} F_i^{11} K_{i-1}^{12} \sin\left(\beta_i^{11} + \psi_{i-1}^{12}\right) + e^{(CK)_i} F_i^{12} K_{i-1}^{22} \sin\left(\beta_i^{12} + \psi_{i-1}^{22}\right) \right]^2 \right\}^{\frac{1}{2}} \\ K_i^{21} &= \left\{ \left[e^{(CH)_i} F_i^{21} K_{i-1}^{11} \cos\left(\beta_i^{21} + \psi_{i-1}^{11}\right) + e^{(CK)_i} F_i^{22} K_{i-1}^{21} \cos\left(\beta_i^{22} + \psi_{i-1}^{21}\right) \right]^2 \right. \qquad \text{(A.3)} \\ &\quad \left. + \left[e^{(CH)_i} F_i^{21} K_{i-1}^{11} \sin\left(\beta_i^{21} + \psi_{i-1}^{11}\right) + e^{(CK)_i} F_i^{22} K_{i-1}^{21} \sin\left(\beta_i^{22} + \psi_{i-1}^{21}\right) \right]^2 \right\}^{\frac{1}{2}} \\ K_i^{22} &= \left\{ \left[e^{(CH)_i} F_i^{21} K_{i-1}^{12} \cos\left(\beta_i^{21} + \psi_{i-1}^{12}\right) + e^{(CK)_i} F_i^{22} K_{i-1}^{22} \cos\left(\beta_i^{22} + \psi_{i-1}^{22}\right) \right]^2 \right. \qquad \text{(A.4)} \\ &\quad \left. + \left[e^{(CH)_i} F_i^{21} K_{i-1}^{12} \sin\left(\beta_i^{21} + \psi_{i-1}^{12}\right) + e^{(CK)_i} F_i^{22} K_{i-1}^{22} \sin\left(\beta_i^{22} + \psi_{i-1}^{22}\right) \right]^2 \right\}^{\frac{1}{2}} \end{aligned}$$

where $i = 2, 3, \ldots, n-1$ in Eqs. (A.1)–(A.4).

Argument ψ_i^{11} associated with K_i^{11} can be determined as follows: Let

$$\begin{aligned} \Phi &= e^{(CH)_i} F_i^{11} K_{i-1}^{11} \cos\left(\beta_i^{11} + \psi_{i-1}^{11}\right) + e^{(CK)_i} F_i^{12} K_{i-1}^{21} \cos\left(\beta_i^{12} + \psi_{i-1}^{21}\right) \\ \Psi &= e^{(CH)_i} F_i^{11} K_{i-1}^{11} \sin\left(\beta_i^{11} + \psi_{i-1}^{11}\right) + e^{(CK)_i} F_i^{12} K_{i-1}^{21} \sin\left(\beta_i^{12} + \psi_{i-1}^{21}\right) \end{aligned}$$

(a) If $\Phi > 0$ and $\Psi \geq 0$ or $\Phi > 0$ and $\Psi \leq 0$, then $\psi_i^{11} = \arctan \frac{\Psi}{\Phi}$.

(b) If $\Phi < 0$ and $\Psi \geq 0$ or $\Phi < 0$ and $\Psi \leq 0$, then $\psi_i^{11} = \arctan\frac{\Psi}{\Phi} + \pi$.

(c) If $\Phi = 0$ and $\Psi > 0$, then $\psi_i^{11} = \frac{\pi}{2}$.

(d) If $\Phi = 0$ and $\Psi < 0$, then $\psi_i^{11} = \frac{3\pi}{2}$.

(e) If $\Phi = 0$ and $\Psi = 0$, then $\psi_i^{11} = 0$.

and $\psi_i^{12}, \psi_i^{21}, \psi_i^{22}$ can be determined analogously.

2. Formulas in determining C_1 and D_1

$$\delta = \sqrt{\left(1 - \frac{\lambda_1 v_1}{B}\right)^2 + \left(\frac{\lambda_1 v_1}{B}\right)^2}$$

Let $\Phi = 1 - \frac{\lambda_1 v_1}{B}$, $\Psi = -\frac{\lambda_1 v_1}{B}$, the argument γ associated with δ can be obtained by using the formulas for solving ψ_i^{11} above.

$$\begin{aligned}
G_1 &= 1 + \frac{\lambda_1 v_1}{B} - e^{-2H_1 v_1}\delta\frac{K_{n-1}^{21}}{K_{n-1}^{22}}\cos\left(\psi_{n-1}^{21} - \psi_{n-1}^{22} + \gamma\right) \\
G_2 &= \frac{\lambda_1 v_1}{B} - e^{-2H_1 v_1}\delta\frac{K_{n-1}^{21}}{K_{n-1}^{22}}\sin\left(\psi_{n-1}^{21} - \psi_{n-1}^{22} + \gamma\right) \\
C_1 &= \Delta_{11}e^{j\delta_{11}} \\
D_1 &= \Delta_{12}e^{j\delta_{12}} \\
\Delta_{11} &= \frac{A}{\sqrt{G_1^2 + G_2^2}} \\
\delta_{11} &= -\tau_1 \\
\Delta_{12} &= \Delta_{11}e^{-2H_1 v_1}\frac{K_{n-1}^{21}}{K_{n-1}^{22}} \\
\delta_{12} &= \psi_{n-1}^{21} - \psi_{n-1}^{22} + \delta_{11} + \pi
\end{aligned}$$

where τ_1 can be determined by putting $\Phi = G_1$ and $\Psi = G_2$ and using the formulas for solving ψ_i^{11} above.

3. Formulas in determining C_i and D_i for $i = 2, 3, \ldots, n$:

$$
\begin{aligned}
(SC)_i &= e^{-2H_1 v_1} K_{i-1}^{11} \Delta_{11} \\
(SD)_i &= K_{i-1}^{12} \Delta_{12} \\
(SE)_i &= \psi_{i-1}^{12} + \delta_{12} \\
(SF)_i &= \psi_{i-1}^{11} + \delta_{11} \\
(SG)_i &= e^{-2H_1 v_1} K_{i-1}^{21} \Delta_{11} \\
(SH)_i &= K_{i-1}^{22} \Delta_{12} \\
(SK)_i &= \psi_{i-1}^{22} + \delta_{12} \\
(SJ)_i &= \psi_{i-1}^{21} + \delta_{11} \\
\Delta_{i1} &= \Big\{ [(SC)_i \cos(SF)_i + (SD)_i \cos(SE)_i]^2 \\
&\quad + [(SC)_i \sin(SF)_i + (SD)_i \sin(SE)_i]^2 \Big\}^{\frac{1}{2}} \\
\Delta_{i2} &= \Big\{ [(SG)_i \cos(SJ)_i + (SH)_i \cos(SK)_i]^2 \\
&\quad + [(SG)_i \sin(SJ)_i + (SH)_i \sin(SK)_i]^2 \Big\}^{\frac{1}{2}}
\end{aligned}
$$

where the argument δ_{i1} associated with Δ_{i1} can be determined by setting

$$
\begin{aligned}
\Phi &= (SC)_i \cos(SF)_i + (SD)_i \cos(SE)_i \\
\Psi &= (SC)_i \sin(SF)_i + (SD)_i \sin(SE)_i
\end{aligned}
$$

and using the formulas for solving ψ_i^{11} above. Similarly, the argument δ_{i2} associated with Δ_{i2} can be determined by using

$$
\begin{aligned}
\Phi &= (SG)_i \cos(SJ)_i + (SH)_i \cos(SK)_i \\
\Psi &= (SG)_i \sin(SJ)_i + (SH)_i \sin(SK)_i
\end{aligned}
$$

$$
\begin{aligned}
C_i &= \Delta_{i1} e^{j\delta_{i1}} e^{H_{i-1}(v_i + v_{i-1})}, \qquad i = 2, 3, \ldots, n. \\
D_i &= \Delta_{i2} e^{j\delta_{i2}} e^{-H_{i-1}(v_i - v_{i-1})}, \qquad i = 2, 3, \ldots, n-1. \\
D_n &= 0
\end{aligned}
$$

Appendix B

This appendix lists the main variables and symbols used in Section 3.2. In the following, the suscript i runs from 1 to n except stated explicitly otherwise, the superscripts k, l range from 1 to 2 with the understanding that they are not taken as exponents; a symbol such as $(CH)_i$ means CH for the ith layer.

$$
\begin{aligned}
v_i &= \sqrt{1+\frac{\omega^2}{\alpha_i^2\xi^4}} \\
M_i &= \sqrt{\frac{v_i+1}{2}} \\
N_i &= \sqrt{\frac{v_i-1}{2}} \\
\gamma_i &= \arctan\left(\sqrt{\frac{v_i-1}{v_i+1}}\right) \\
(CA)_i &= \xi H_i(N_{i+1}-N_i),\ i=1,2,\ldots,n-1 \\
(CB)_i &= \xi H_i(N_{i+1}+N_i),\ i=1,2,\ldots,n-1 \\
(CC)_i &= \gamma_i-\gamma_{i+1},\ i=1,2,\ldots,n-1 \\
(CD)_i &= \frac{\lambda_i}{\lambda_{i+1}}\sqrt{\frac{v_i}{v_{i+1}}},\ i=1,2,\ldots,n-1 \\
(CK)_i &= -\xi H_{i-1}(M_i-M_{i-1}),\ i=2,3,\ldots,n \\
(CH)_i &= (CK)_i-2\xi h_i M_i,\ i=2,3,\ldots,n-1
\end{aligned}
$$

$$
P_i^{11} = \frac{1}{2}\left[e^{j\xi H_i(N_{i+1}-N_i)}+(CD)_i e^{j(\xi H_i(N_{i+1}-N_i)+\gamma_i-\gamma_{i+1})}\right] \tag{B.1}
$$

$$
P_i^{12} = \frac{1}{2}\left[e^{j\xi H_i(N_{i+1}+N_i)}+(CD)_i e^{j(\xi H_i(N_{i+1}+N_i)+\gamma_i-\gamma_{i+1})}\right] \tag{B.2}
$$

$$
P_i^{21} = \frac{1}{2}\left[e^{-j\xi H_i(N_{i+1}+N_i)}-(CD)_i e^{j(-\xi H_i(N_{i+1}+N_i)+\gamma_i-\gamma_{i+1})}\right] \tag{B.3}
$$

$$
P_i^{22} = \frac{1}{2}\left[e^{j\xi H_i(N_i-N_{i+1})}+(CD)_i e^{j(\xi H_i(N_i-N_{i+1})+\gamma_i-\gamma_{i+1})}\right] \tag{B.4}
$$

where $i=1,2,\ldots,n-1$ in Eqs. (B.1)–(B.4).

P_i^{kl} can also be written as

$$P_i^{kl} = F_i^{kl} e^{j\beta_i^{kl}}, \;\; i = 1, 2, \ldots, n-1$$

where

$$\begin{aligned} F_i^{11} &= \frac{1}{2}\sqrt{1 + (CD)_i^2 + 2(CD)_i \cos(CC)_i} \\ F_i^{12} &= \frac{1}{2}\sqrt{1 + (CD)_i^2 - 2(CD)_i \cos(CC)_i} F_i^{11} \\ F_i^{21} &= F_i^{12} \\ F_i^{22} &= F_i^{11} \end{aligned}$$

Argument β_i^{11} associated with F_i^{11}, $i = 1, 2, \ldots, n-1$ can be determined as follows: Let $\Phi = \cos(CA)_i + (CD)_i \cos[(CA)_i + (CC)_i]$, $\Psi = \sin(CA)_i + (CD)_i \sin[(CA)_i + (CC)_i]$,

1. If $\Phi > 0$ and $\Psi \geq 0$ or $\Phi > 0$ and $\Psi \leq 0$, then

$$\beta_i^{11} = \arctan \frac{\Psi}{\Phi} \tag{B.5}$$

2. If $\Phi < 0$ and $\Psi \geq 0$ or $\Phi < 0$ and $\Psi \leq 0$, then

$$\beta_i^{11} = \arctan \frac{\Psi}{\Phi} + \pi \tag{B.6}$$

3. If $\Phi = 0$ and $\Psi > 0$, then

$$\beta_i^{11} = \frac{\pi}{2} \tag{B.7}$$

4. If $\Phi = 0$ and $\Psi < 0$, then

$$\beta_i^{11} = \frac{3\pi}{2} \tag{B.8}$$

5. If $\Phi = 0$ and $\Psi = 0$, then

$$\beta_i^{11} = 0 \tag{B.9}$$

and $\beta_i^{12}, \beta_i^{21}, \beta_i^{22}$ can be otained analogously.

$$R_1^{kl} = P_1^{kl}$$

$$R_i^{11} = e^{(CK)_i}\left[e^{-2\xi h_i M_i}P_i^{11}R_{i-1}^{11} + P_i^{12}R_{i-1}^{21}\right] \tag{B.10}$$

$$R_i^{12} = e^{(CK)_i}\left[e^{-2\xi h_i M_i}P_i^{11}R_{i-1}^{12} + P_i^{12}R_{i-1}^{22}\right] \tag{B.11}$$

$$R_i^{21} = e^{(CK)_i}\left[e^{-2\xi h_i M_i}P_i^{21}R_{i-1}^{11} + P_i^{22}R_{i-1}^{21}\right] \tag{B.12}$$

$$R_i^{22} = e^{(CK)_i}\left[e^{-2\xi h_i M_i}P_i^{21}R_{i-1}^{12} + P_i^{22}R_{i-1}^{22}\right] \tag{B.13}$$

where $i = 2, 3, \ldots, n-1$ in Eqs. (B.10)–(B.13). Also, R_i^{kl} can be written as

$$R_i^{kl} = K_i^{kl}e^{j\psi_i^{kl}}$$

where $K_i^{kl},\ i = 2, 3, \ldots, n-1$ can be determined as follows:

$$K_i^{11} = e^{(CK)_i}\left[e^{-4\xi h_i M_i}(F_i^{11}K_{i-1}^{11})^2 + (F_i^{12}K_{i-1}^{21})^2 + 2e^{-2\xi h_i M_i}F_i^{11}F_i^{12}K_{i-1}^{11}K_{i-1}^{21}\cos(\beta_i^{11} - \beta_i^{12} + \psi_{i-1}^{11} - \psi_{i-1}^{21})\right]^{\frac{1}{2}}$$

$$K_i^{12} = e^{(CK)_i}\left[e^{-4\xi h_i M_i}(F_i^{11}K_{i-1}^{12})^2 + (F_i^{12}K_{i-1}^{22})^2 + 2e^{-2\xi h_i M_i}F_i^{11}F_i^{12}K_{i-1}^{12}K_{i-1}^{22}\cos(\beta_i^{11} - \beta_i^{12} + \psi_{i-1}^{12} - \psi_{i-1}^{22})\right]^{\frac{1}{2}}$$

$$K_i^{21} = e^{(CK)_i}\left[e^{-4\xi h_i M_i}(F_i^{21}K_{i-1}^{11})^2 + (F_i^{22}K_{i-1}^{21})^2 + 2e^{-2\xi h_i M_i}F_i^{21}F_i^{22}K_{i-1}^{11}K_{i-1}^{21}\cos(\beta_i^{21} - \beta_i^{22} + \psi_{i-1}^{11} - \psi_{i-1}^{21})\right]^{\frac{1}{2}}$$

$$K_i^{22} = e^{(CK)_i}\left[e^{-4\xi h_i M_i}(F_i^{21}K_{i-1}^{12})^2 + (F_i^{22}K_{i-1}^{22})^2 + 2e^{-2\xi h_i M_i}F_i^{21}F_i^{22}K_{i-1}^{12}K_{i-1}^{22}\cos(\beta_i^{21} - \beta_i^{22} + \psi_{i-1}^{12} - \psi_{i-1}^{22})\right]^{\frac{1}{2}}$$

while argument ψ_i^{kl} associated with $K_i^{kl},\ i = 2, 3, \ldots, n-1$ can be obtained analogously in determining β_i^{11} above.

$$G_1 = -\xi\sqrt{v_1}e^{-2\xi H_1 M_1}\frac{K_{n-1}^{21}}{K_{n-1}^{22}}\cos(\psi_{n-1}^{21} - \psi_{n-1}^{22} + \gamma_1) - \xi\sqrt{v_1}\cos\gamma_1 + \frac{B}{\lambda_1}\frac{K_{n-1}^{21}}{K_{n-1}^{22}}e^{-2\xi H_1 M_1}\cos(\psi_{n-1}^{21} - \psi_{n-1}^{22}) - \frac{B}{\lambda_1}$$

$$G_2 = -\xi\sqrt{v_1}e^{-2\xi H_1 M_1}\frac{K_{n-1}^{21}}{K_{n-1}^{22}}\sin(\psi_{n-1}^{21} - \psi_{n-1}^{22} + \gamma_1) - \xi\sqrt{v_1}\sin\gamma_1 + \frac{B}{\lambda_1}\frac{K_{n-1}^{21}}{K_{n-1}^{22}}e^{-2\xi H_1 M_1}\sin(\psi_{n-1}^{21} - \psi_{n-1}^{22})$$

Argument τ_1 associated with G_1 and G_2 can be obtained analogously in determining β_i^{11} above by setting

$\Phi = G_1$ and $\Psi = G_2$.

$$
\begin{aligned}
\Gamma_1 &= -\frac{\mu AB}{\lambda_1}\frac{\sqrt{(\mu^2+\xi^2)(G_1^2+G_2^2)}}{(\mu_2+\xi^2)^2(G_1^2+G_2^2)} \\
\Gamma_2 &= -\frac{K_{n-1}^{21}}{K_{n-1}^{22}}\Gamma_1 e^{-2\xi H_1 M_1} \\
(SC)_i &= K_{i-1}^{11}\Gamma_1 e^{-2\xi H_1 M_1} && \text{(B.14)} \\
(SD)_i &= K_{i-1}^{12}\Gamma_2 && \text{(B.15)} \\
(SE)_i &= \psi_{i-1}^{12} + \psi_{n-1}^{21} - \psi_{n-1}^{22} - \tau_1 && \text{(B.16)} \\
(SF)_i &= \psi_{i-1}^{11} - \tau_1 && \text{(B.17)} \\
(SG)_i &= K_{i-1}^{21}\Gamma_1 e^{-2\xi H_1 M_1} && \text{(B.18)} \\
(SH)_i &= K_{i-1}^{22}\Gamma_2 && \text{(B.19)} \\
(SK)_i &= \psi_{i-1}^{22} + \psi_{n-1}^{21} - \psi_{n-1}^{22} - \tau_1 && \text{(B.20)} \\
(SJ)_i &= \psi_{i-1}^{21} - \tau_1 && \text{(B.21)}
\end{aligned}
$$

where $i = 2, 3, \ldots, n$ in Eqs. (B.14)–(B.21).

$$
\begin{aligned}
\Delta_{11} &= \Gamma_1 \\
\delta_{11} &= -\tau_1 \\
\Delta_{12} &= \Gamma_2 \\
\delta_{12} &= \psi_{n-1}^{21} - \psi_{n-1}^{22} - \tau_1
\end{aligned}
$$

$$
\Delta_{i1} = \sqrt{\left[(SC)_i\cos(SF)_i + (SD)_i\cos(SE)_i\right]^2 + \left[(SC)_i\sin(SF)_i + (SD)_i\sin(SE)_i\right]^2} \quad \text{(B.22)}
$$

$$
\Delta_{i2} = \sqrt{\left[(SG)_i\cos(SJ)_i + (SH)_i\cos(SK)_i\right]^2 + \left[(SG)_i\sin(SJ)_i + (SH)_i\sin(SK)_i\right]^2} \quad \text{(B.23)}
$$

where $i = 2, 3, \ldots, n$ in Eq. (B.22) and $i = 2, 3, \ldots, n-1$ in Eq. (B.23).

$$\begin{aligned}
\Delta_{n2} &= 0 \\
C_1 &= \Gamma_1 e^{-j\tau_1} \\
D_1 &= \Gamma_2 e^{j\left(\psi_{n-1}^{21} - \psi_{n-1}^{22} - \tau_1\right)} \\
C_i &= \Delta_{i1} e^{j\delta_{i1}} e^{\xi H_{i-1}(M_i + M_{i-1})} \qquad \text{(B.24)} \\
D_i &= \Delta_{i2} e^{j\delta_{i2}} e^{-\xi H_{i-1}(M_i - M_{i-1})} \qquad \text{(B.25)} \\
D_n &= 0
\end{aligned}$$

where $i = 2, 3, \ldots, n$ in Eq. (B.24) and $i = 2, 3, \ldots, n-1$ in Eq. (B.25), and arguments δ_{i1}, δ_{i2} can be obtained analogously in determining β_i^{11}; for example, to determine δ_{i1}, replacing Φ, Ψ by

$$\begin{aligned}
\Phi &= (SC)_i \cos(SF)_i + (SD)_i \cos(SE)_i \\
\Psi &= (SC)_i \sin(SF)_i + (SD)_i \sin(SE)_i
\end{aligned}$$

Appendix C

This appendix lists some variables and symbols used in Sections 5.3.2 and 5.4.

1. P_{ij}, $i,j=1,2,3,4$ in Eq. (5.23) and G_{ij}, $i,j=1,2,3,4$ in Eq. (5.24)

$$
\begin{aligned}
P_{11} &= \frac{s}{\left(s^2-\xi^2\right)^2}\left(s^2+\frac{\nu\xi^2}{1-\nu}\right)\\
P_{12} &= \frac{\xi}{\left(s^2-\xi^2\right)^2}\left(s^2+\frac{\nu\xi^2}{1-\nu}\right)\\
P_{13} &= \frac{1}{2\left(s^2-\xi^2\right)^2 G}\left[2s^2-\frac{(1-2\nu)\xi^2}{1-\nu}\right]\\
P_{14} &= \frac{\xi s}{2(1-\nu)\left(s^2-\xi^2\right)^2 G}\\
P_{21} &= -\frac{\xi}{\left(s^2-\xi^2\right)^2}\left[\xi^2+\frac{\nu s^2}{1-\nu}\right]\\
P_{22} &= \frac{s}{\left(s^2-\xi^2\right)^2}\left[s^2-\frac{(2-\nu)\xi^2}{1-\nu}\right]\\
P_{23} &= -P_{14}\\
P_{24} &= -\frac{1}{2\left(s^2-\xi^2\right)^2 G}\left[2\xi^2-\frac{(1-2\nu)s^2}{1-\nu}\right]\\
G_{11} &= \frac{1}{4(1-\nu)}\left\{2(1-\nu)+\xi z+\left[2(1-\nu)-\xi z\right]e^{-2\xi z}\right\}\\
G_{12} &= \frac{1}{4(1-\nu)}\left[1-2\nu+\xi z-(1-2\nu-\xi z)\,e^{-2\xi z}\right]\\
G_{13} &= \frac{1}{8(1-\nu)\xi G}\left[3-4\nu+\xi z-(3-4\nu-\xi z)\,e^{-2\xi z}\right]\\
G_{14} &= \frac{z}{8(1-\nu)G}\left(1-e^{-2\xi z}\right)\\
G_{21} &= \frac{1}{4(1-\nu)}\left[1-2\nu-\xi z-(1-2\nu+\xi z)\,e^{-2\xi z}\right]\\
G_{22} &= \frac{1}{4(1-\nu)}\left\{2(1-\nu)-\xi z+\left[2(1-\nu)+\xi z\right]e^{-2\xi z}\right\}\\
G_{23} &= -G_{14}\\
G_{24} &= \frac{1}{8(1-\nu)\xi G}\left[3-4\nu-\xi z-(3-4\nu+\xi z)\,e^{-2\xi z}\right]
\end{aligned}
$$

$$
\begin{aligned}
G_{31} &= \frac{\xi G}{2(1-\nu)}\left[1+\xi z-(1-\xi z)\,e^{-2\xi z}\right] \\
G_{32} &= \frac{\xi^2 G z}{2(1-\nu)}\left(1-e^{-2\xi z}\right) \\
G_{33} &= G_{11} \\
G_{34} &= -G_{21} \\
G_{41} &= -G_{32} \\
G_{42} &= \frac{\xi G}{2(1-\nu)}\left[1-\xi z-(1+\xi z)e^{-2\xi z}\right] \\
G_{43} &= -G_{12} \\
G_{44} &= G_{22}
\end{aligned}
$$

2. Δ, T_{12} & T_{22} in Eq. (5.34)

$$
\begin{aligned}
\Delta &= a_{11}a_{22}-a_{12}a_{21}+\frac{1-2\nu_n}{2\xi G_n}\left(a_{12}a_{31}+a_{21}a_{42}\right. \\
&\quad \left.-a_{11}a_{32}-a_{22}a_{41}\right)+\frac{1-\nu_n}{\xi G_n}\left(a_{11}a_{42}+a_{22}a_{31}\right. \\
&\quad \left.-a_{12}a_{41}-a_{21}a_{32}\right)+\frac{3-4\nu_n}{4\xi^2(G_n)^2}\left(a_{31}a_{42}-a_{32}a_{41}\right) \\
T_{12} &= a_{12}a_{24}-a_{14}a_{22}+\frac{1-2\nu_n}{2\xi G_n}\left(a_{22}a_{44}+a_{14}a_{32}\right. \\
&\quad \left.-a_{12}a_{34}-a_{24}a_{42}\right)+\frac{1-\nu_n}{\xi G_n}\left(a_{12}a_{44}+a_{24}a_{32}\right. \\
&\quad \left.-a_{14}a_{42}-a_{22}a_{34}\right)+\frac{3-4\nu_n}{4\xi^2(G_n)^2}\left(a_{32}a_{44}-a_{34}a_{42}\right) \\
T_{22} &= a_{14}a_{21}-a_{11}a_{24}+\frac{1-2\nu_n}{2\xi G_n}\left(a_{11}a_{34}+a_{24}a_{41}\right. \\
&\quad \left.-a_{21}a_{44}-a_{14}a_{31}\right)+\frac{1-\nu_n}{\xi G_n}\left(a_{14}a_{41}+a_{21}a_{34}\right. \\
&\quad \left.-a_{11}a_{44}-a_{24}a_{31}\right)+\frac{3-4\nu_n}{4\xi^2(G_n)^2}\left(a_{34}a_{41}-a_{31}a_{44}\right)
\end{aligned}
$$

where $a_{ij}=[F(\xi,h_{n-1})]_{ij}$.

3. $u(r,z), w(r,z), \tau_{zr}(r,z)$ & $\sigma_z(r,z)$ when Q is located in the i-th layer

(a) When $i = 1, 2, \cdots, n-1$

$$
\begin{aligned}
u &= \int_0^\infty \xi e^{\xi(H_{i-1}+z)} \left[G_{11}\ G_{12}\ G_{13}\ G_{14}\right]_i \cdot [F(\xi, h_{i-1})]\widetilde{\Phi}_1(\xi, 0) J_1(\xi r) d\xi \\
w &= \int_0^\infty \xi e^{\xi(H_{i-1}+z)} \left[G_{21}\ G_{22}\ G_{23}\ G_{24}\right]_i \cdot [F(\xi, h_{i-1})]\widetilde{\Phi}_1(\xi, 0) J_0(\xi r) d\xi \\
\tau_{zr} &= \int_0^\infty \xi e^{\xi(H_{i-1}+z)} \left[G_{31}\ G_{32}\ G_{33}\ G_{34}\right]_i \cdot [F(\xi, h_{i-1})]\widetilde{\Phi}_1(\xi, 0) J_1(\xi r) d\xi \\
\sigma_z &= \int_0^\infty \xi e^{\xi(H_{i-1}+z)} \left[G_{41}\ G_{42}\ G_{43}\ G_{44}\right]_i \cdot [F(\xi, h_{i-1})]\widetilde{\Phi}_1(\xi, 0) J_0(\xi r) d\xi
\end{aligned}
$$

(b) When $i = n$

$$
\begin{aligned}
u &= \int_0^\infty \xi e^{\xi(H_{n-1}-z)} \left[b_{11}\ b_{12}\ b_{13}\ b_{14}\right] \cdot [F(\xi, h_{n-1})]\widetilde{\Phi}_1(\xi, 0) J_1(\xi r) d\xi \\
w &= \int_0^\infty \xi e^{\xi(H_{n-1}-z)} \left[b_{21}\ b_{22}\ b_{23}\ b_{24}\right] \cdot [F(\xi, h_{n-1})]\widetilde{\Phi}_1(\xi, 0) J_0(\xi r) d\xi \\
\tau_{zr} &= \int_0^\infty \xi e^{\xi(H_{n-1}-z)} \left[b_{31}\ b_{32}\ b_{33}\ b_{34}\right] \cdot [F(\xi, h_{n-1})]\widetilde{\Phi}_1(\xi, 0) J_1(\xi r) d\xi \\
\sigma_z &= \int_0^\infty \xi e^{\xi(H_{n-1}-z)} \left[b_{41}\ b_{42}\ b_{43}\ b_{44}\right] \cdot [F(\xi, h_{n-1})]\widetilde{\Phi}_1(\xi, 0) J_0(\xi r) d\xi
\end{aligned}
$$

where

$$
\begin{aligned}
b_{11} &= \frac{2(1-\nu_n)-\xi z}{4(1-\nu_n)} \\
b_{12} &= -\frac{1-2\nu_n-\xi z}{4(1-\nu_n)} \\
b_{13} &= -\frac{3-4\nu_n-\xi z}{8(1-\nu_n)\xi G_n} \\
b_{14} &= -\frac{z}{8(1-\nu_n)G_n} \\
b_{21} &= -\frac{1-2\nu_n+\xi z}{4(1-\nu_n)} \\
b_{22} &= \frac{2(1-\nu_n)+\xi z}{4(1-\nu_n)} \\
b_{23} &= -b_{14} \\
b_{24} &= -\frac{3-4\nu_n+\xi z}{8(1-\nu_n)\xi G_n} \\
b_{31} &= -\frac{(1-\xi z)\xi G_n}{2(1-\nu_n)} \\
b_{32} &= -\frac{\xi^2 z G_n}{2(1-\nu_n)} \\
b_{33} &= b_{11} \\
b_{34} &= -b_{21} \\
b_{41} &= -b_{32} \\
b_{42} &= -\frac{(1+\xi z)\xi G_n}{2(1-\nu_n)} \\
b_{43} &= -b_{12} \\
b_{44} &= b_{22}
\end{aligned}
$$

4. $\sigma_r(r,z)$ & $\sigma_\theta(r,z)$ when Q is located in the i-th layer

   (a) When $i = 1, 2, \cdots, n-1$

$$
\begin{aligned}
\sigma_r &= 2G_i \int_0^\infty \xi e^{\xi z} \left[\Omega_i J_0(\xi r) - \frac{\Lambda_i}{r} J_1(\xi r) \right] d\xi \\
\sigma_\theta &= 2G_i \int_0^\infty \xi e^{\xi z} \left[\Theta_i J_0(\xi r) + \frac{\Lambda_i}{r} J_1(\xi r) \right] d\xi
\end{aligned}
$$

where

$$\begin{aligned}
\Lambda_i &= e^{\xi H_{i-1}}[G_{11}\ G_{12}\ G_{13}\ G_{14}]_i \cdot [F(\xi, h_{i-1})]\widetilde{\Phi}_1(\xi, 0) \\
\Omega_i &= e^{\xi H_{i-1}}[\psi_1\ \psi_2\ \psi_3\ \psi_4]_i \cdot [F(\xi, h_{i-1})]\widetilde{\Phi}_1(\xi, 0) \\
\Theta_i &= e^{\xi H_{i-1}}[\omega_1\ \omega_2\ \omega_3\ \omega_4]_i \cdot [F(\xi, h_{i-1})]\widetilde{\Phi}_1(\xi, 0)
\end{aligned}$$

The components in $[\psi_1\ \psi_2\ \psi_3\ \psi_4]_i$ are

$$\begin{aligned}
\psi_1 &= \frac{\xi}{4(1-\nu_i)}\left[2 + \xi z + (2 - \xi z)e^{-2\xi z}\right] \\
\psi_2 &= \frac{\xi}{4(1-\nu_i)}\left[1 + \xi z - (1 - \xi z)e^{-2\xi z}\right] \\
\psi_3 &= \frac{1}{8(1-\nu_i)G_i}\left[3 - 2\nu_i + \xi z - (3 - 2\nu_i - \xi z)e^{-2\xi z}\right] \\
\psi_4 &= \frac{1}{8(1-\nu_i)G_i}\left[2\nu_i + \xi z + (2\nu_i - \xi z)e^{-2\xi z}\right]
\end{aligned}$$

The components in $[\omega_1\ \omega_2\ \omega_3\ \omega_4]_i$ are

$$\begin{aligned}
\omega_1 &= \frac{\nu_i \xi}{2(1-\nu_i)}\left(1 + e^{-2\xi z}\right) \\
\omega_2 &= \frac{\nu_i \xi}{2(1-\nu_i)}\left(1 - e^{-2\xi z}\right) \\
\omega_3 &= \frac{\nu_i}{4(1-\nu_i)G_i}\left(1 - e^{-2\xi z}\right) \\
\omega_4 &= \frac{\nu_i}{4(1-\nu_i)G_i}\left(1 + e^{-2\xi z}\right)
\end{aligned}$$

(b) When $i = n$

$$\begin{aligned}
\sigma_r &= 2G_n \int_0^\infty \xi e^{\xi z}\left[\Omega_n J_0(\xi r) - \frac{\Lambda_n}{r} J_1(\xi r)\right] d\xi \\
\sigma_\theta &= 2G_n \int_0^\infty \xi e^{\xi z}\left[\Theta_n J_0(\xi r) + \frac{\Lambda_n}{r} J_1(\xi r)\right] d\xi
\end{aligned}$$

where

$$\begin{aligned}
\Lambda_n &= e^{\xi H_{n-1}}[G_{11}\ G_{12}\ G_{13}\ G_{14}]_n \cdot [F(\xi, h_{n-1})]\widetilde{\Phi}_1(\xi, 0) \\
\Omega_n &= e^{\xi H_{n-1}}[\psi_1\ \psi_2\ \psi_3\ \psi_4]_n \cdot [F(\xi, h_{n-1})]\widetilde{\Phi}_1(\xi, 0) \\
\Theta_n &= e^{\xi H_{n-1}}[\omega_1\ \omega_2\ \omega_3\ \omega_4]_n \cdot [F(\xi, h_{n-1})]\widetilde{\Phi}_1(\xi, 0)
\end{aligned}$$

The components in $[G_{11}\ G_{12}\ G_{13}\ G_{14}]_n$ are

$$\begin{aligned} G_{11} &= \frac{2(1-\nu_n)-\xi z}{4(1-\nu_n)} \\ G_{12} &= -\frac{1-2\nu_n-\xi z}{4(1-\nu_n)} \\ G_{13} &= -\frac{3-4\nu_n-\xi z}{8(1-\nu_n)\xi G_n} \\ G_{14} &= -\frac{z}{8(1-\nu_n)G_n} \end{aligned}$$

The components in $[\psi_1\ \psi_2\ \psi_3\ \psi_4]_n$ are

$$\begin{aligned} \psi_1 &= \frac{\xi(2-\xi z)}{4(1-\nu_n)} \\ \psi_2 &= -\frac{\xi(1-\xi z)}{4(1-\nu_n)} \\ \psi_3 &= -\frac{3-2\nu_n-\xi z}{8(1-\nu_n)G_n} \\ \psi_4 &= \frac{2\nu_n-\xi z}{8(1-\nu_n)G_n} \end{aligned}$$

The components in $[\omega_1\ \omega_2\ \omega_3\ \omega_4]_n$ are

$$\begin{aligned} \omega_1 &= \frac{\nu_n\xi}{2(1-\nu_n)} \\ \omega_2 &= -\omega_1 \\ \omega_3 &= -\frac{\nu_n}{4(1-\nu_n)G_n} \\ \omega_4 &= -\omega_3 \end{aligned}$$

References

[1] ARA, Inc. (2004) Guide for mechanistic-empirical design of new and rehabilitated pavement structures. Final Report. National Cooperative Highway Research Program Project 1-37A.

[2] ARA, Inc. (2007) Interim mechanistic-empirical pavement design guide manual of practice. Final Draft. National Cooperative Highway Research Program Project 1-37A.

[3] E.S. Barber. (1957) Calculation of maximum pavement temperatures from weather reports. *Highway Research Board Bulletin 168*, National Research Council, Washington, D.C., 1-8.

[4] S. Baltzer, H.J. Ertman-Larson, E.O. Lukanen and R.N. Stubstad. (1994) Prediction of AC temperature for routine load/deflection measurements. *Proceedings, The Fourth International conference on the Bearing Capacity of Roads and Airfields, Volume I.* Minnesota Department of Transportation, 401-412.

[5] R.L. Burden and J.D. Faires. (2001) *Numerical analysis*, seventh edition, Brooks/Cole.

[6] D.M. Burmister. (1945) The general theory of stresses and displacements in layered soil systems, I. *Journal of Applied Physics*, 16, 84-94.

[7] D.M. Burmister. (1945) The general theory of stresses and displacements in layered soil systems, II. *Journal of Applied Physics*, 16, 126-127.

[8] D.M. Burmister. (1945) The general theory of stresses and displacements in layered soil systems, III. *Journal of Applied Physics*, 16, 296-302.

[9] H.S. Carslaw and J.C. Jaeger. (1959) *Conduction of heat in solids*, Oxford University Press.

[10] W. Chong, R. Tramontini, and L. P. Specht. (2009) Application of the Laplace transform and its numerical inversion to temperature profile of a two-layer pavement under site condition. *Numerical Heat Transfer, Part A*, 55, 1004-1018.

[11] Churchill, R. V. (1972) *Operational mathematics*, third edition, McGraw-Hill Book Company.

[12] M.I. Darter and E.J. Barenberg. (1977) Design of zero-maintenance plain jointed concrete pavement. *Publication No. FHWA-RD-77-111*, Vol. 1, FHWA, U.S. Dept. of Transportation.

[13] E. Dave and W.G. Buttlar. (2010) Thermal reflective cracking of asphalt concrete overlays. *International Journal of Pavement Engineering*, January, 1-12.

[14] J. Davidovits. (1997) Geopolymers: inorganic polymeric new materials. *Journal of Thermal Analysis*, 37, 1633-1656.

[15] P.J. Davis and P.Rabinowitz. (1984) *Methods of numerical integration*, second edition, Academic Press, Inc.

[16] D.L. De Jong, M.G.F. Peutz, and A.R. Korswagen. (1979) Computer program BISAR, layered systems under normal and tangential surface loads. Koninklijke-Shell Laboratorium, Amsterdam, Netherlands.

[17] B.J. Dempsey and M.R. Thompson. (1970) A heat transfer model for evaluating frost action and temperature related effects in multi-layered pavement systems. *Highway Research Record No. 342*, National Research Council, Washington, D.C., 39-56.

[18] B.K. Diefenderfer, I.L. Al-Qadi and S.D. Diefenderfer. (2006) Model to predict pavement temperature profile: development and validation. *ASCE Journal of Transportation Engineering*, 132(2), 162-167.

[19] Y.H. Huang. (2004) *Pavement analysis and design*, second edition, Pearson Education, Inc. New York.

[20] C.K. Hsieh, C. Qin and E.E. Ryder. (1989) Development of computer modeling for prediction of temperature distribution inside concrete pavements. Report Number FL/DOT/SMO/90-374, Final Report to Florida Department of Transportation.

[21] M.C. Hironaka and L.J. Malvar. (2000) AV-8B aircraft exhaust blast resistant pavement systems. Technical Report TR-2121-SHR, Naval Facilities engineering Service Center, Port Hueneme, California, 56 pages.

[22] M.C. Hironaka and L.J. Malvar. (1998) Jet exhaust damaged concrete. *Concrete International*, 20(10), 32-35.

[23] M.C. Hironaka and L.J. Malvar. (1995) F/A-18 APU resistant pavement systems. Technical Report.

[24] G.F. Hayhoe. (2002) LEAF-A new layered elastic computational program for FAA pavement design and evaluation procedures. Presented at FAA Technology Transfer Conference, U.S. Department of Transportation, Atlantic City, N.J.

[25] A. Jones. (1962) Tables of stresses in three-layer elastic systems. *Highway Research Board Bulletin 342*, 176-214.

[26] J.W. Ju and Y. Zhang. (1998) Axisymmetric thermomechanical constitutive and damage modeling for airfield concrete pavement under transient high temperature. *Mechanics of Materials*, 29, 307-323.

[27] J.W. Ju and Y. Zhang. (1998) A thermomechanical model for airfield concrete pavement under transient high temperature loadings. *International Journal of Damage Mechanics*, 7, 24-46.

[28] L. Khazanovich and Q. Wang. (2007) MnLayer: high-performance layered elastic analysis program. *Journal of the Transportation Research Board*, No.2037, 63-75.

[29] L. Khazanovich and A.M. Ioannides. (1995) DIPLOMAT: an analysis program for both bituminous and concrete pavements. *Journal of the Transportation Research Board. 1482*, National Research Council, Washington, D.C., 52-60.

[30] E. Kohler, G. Long and J. Roesler. (2002) Construction of extended life continuously reinforced concrete pavement at ATREL. Transportation Engineering Series No. 126, Illinois Cooperative Highway and Transportation Series No. 282, UILU-ENG-2002-2009, University of Illinois, Urbana, IL, 54 pp.

[31] R.Y. Liang and Y-Z. Niu. (1998) Temperature and curling stress in concrete pavements: analytical solution. *ASCE Journal of Transportation Engineering*, 124(1), 91-100.

[32] C. Liu and D. Yuan. (2000) Temperature distribution in layered road structures. *Journal of Transportation Engineering*, 126(1), 93-95.

[33] A.E.H. Love. (1944) *A treatise on the mathematical theory of elasticity*, fourth edition, Dover Publications, Inc., New York.

[34] E.O. Lukanen, C. Han and E.L.Jr. Skokl (1998). Probabilistic method of asphalt binder selection based on pavement temperature. *Transportation Research Record No. 1609*, TRB, National Research Council, Washington, D.C., 12-20.

[35] E.O. Lukanen, R.N. Stubstad and R. Briggs. (2000) *Temperature predictions and adjustment factors for asphalt pavements*, Report No. FHWA-RD-98-085. Federal Highway Administration.

[36] J.W. Maina and K. Matsui. (2004) Developing software for elastic analysis of pavement structure responses to vertical and horizontal surface loadings. *Journal of the Transportation Research Board. 1896*, 107-118.

[37] K. Matsui, J.W. Maina, and T. Inoue. (2002) Axi-symmetric analysis of elastic multilayer system considering interface slips. *International Journal of Pavements*, 1(1), 55-66.

[38] D.L. Powers. (1999) *Boundary value problems,* fourth edition, Harcourt Academic Press.

[39] R.O. Rasmussen, J.M. Ruiz, D.K. Rozycki and B.F. McCullough. (2002) Constructing high-performance concrete pavements with FHWA HIPERPAV systems analysis software. *Transportation Research Record No. 1813*, Transportation Research Board, Washington, D.C., 11-20.

[40] J. Roesler. (2009) *Theoretical solution for temperature profile in multi-layered pavement systems subjected to transient thermal loads.*, University of Illinois, Technical Proposal.

[41] T.N. Rumney and R. A. Jimenez. (1969) Pavement temperatures in the southwest. *Highway Research Record No. 361*, National Research Council, Washington, D.C., pp. 1-13.

[42] A.K. Schindler, J.M. Ruiz, R.O. Rasmussen, G.K. Chang and L.G. Wathne. (2004) Concrete pavement temperature prediction and case studies with the FHWA HIPERPAV models. *Cement and Concrete Composites 26*, 463-471.

[43] I.N. Sneddon. (1972) *The use of integral transforms,* McGraw-Hill, New York.

[44] M. Solaimanian and T.W. Kennedy. (1993) Predicting maximum pavement surface temperature using maximum air temperature and hourly solar radiation. *Transportation Research Record 1417*, Transportation Research Board, Washington, D.C., 1-11.

[45] M.R. Spiegel. (1965) *Schaum's outline of theory and problems of Laplace transforms,* Schaum Publishing Co., 29-30.

[46] N.M. Steen, G.D. Byrne and E.M. Gelbard. (1969) Gaussian quadratures for the integrals $\int_0^\infty \exp(-x^2)f(x)dx$ and $\int_0^b \exp(-x^2)f(x)dx$. *Mathematics of Computation*, 23, July 1969, 661-671.

[47] W.A. Strauss. (1992) *Partial differential equations: an intriduction,* John Wiley & Sons, Inc.

[48] A.H. Stroud and D. Secrest. (1966) *Gaussian quadrature formulas,* Prentice-Hall, Inc.

[49] S.P. Timoshenko and J.N. Goodier. (1970) *Theory of elasticity,* third edition, McGraw-Hill, New York.

[50] N. W. Tschoegl. (1989) *The phenomenological theory of linear viscoelastic behavior: an introduction*, Springer, New York.

[51] J. Uzan. (1994) Advanced backcalculation techniques. *Proc., 2nd International Symposium on NDT of Pavements and Backcalculation of Moduli.* ASTM Special Technical Publications No. 1198, Philadelphia, Pa., 3-37.

[52] D. Wang. (1996) Analytical solutions of temperature field and thermal stresses in multi-layered asphalt pavement systems. M.S. thesis, School of Transportation Science and Engineering, Harbin Institute of Technology (in Chinese).

[53] D. Wang, J.R. Roesler and D.-Z. Guo. (2009) An analytical approach to predicting temperature fields in multi-layered pavement systems. *Journal of Engineering Mechanics*, 135(4), 334-344.

[54] G. N. Watson. (1966) *A Treatise on the theory of Bessel functions*, second edition, Cambridge University Press.

[55] H. M. Westergaard. (1926) Analysis of stresses in concrete pavement due to variations of temperature. *Highway Research oard, Proceedings of Annual Meeting*, 6, 201-215.

[56] W-G. Wong and Y. Zhong. (2000) Flexible pavement thermal stresses with variable temperature. *J. Transp. Eng.*, 126(1), 46-49.

[57] G.-C. Wu. (1997) The analytic theory of the temperature fields of bituminous pavement over semi-rigid roadbase. *J. Appl. Math. Mech.*, 18(2), 181-190.

[58] C. Yavuzturk, K. Ksaibati and A.D. Chiasson. (2005) Assessment of temperature fluctuations in asphalt pavements due to thermal environmental conditions using a two-dimensional, transient finite-difference approach. *Journal of Materials in Civil Engineering*, 17(4), 465-475.

[59] E.J. Yoder and M.W. Witczak. (1975) *Principles of pavement design,* second edition, John Wiley & Sons, Inc., New York.

[60] E. Zauderder. (2006) *Partial differential equations of applied mathematics,* third edition, John Wiley & Sons, Inc., New York.

[61] Y. Zhong, Z.-R. Wang, and D.-Z. Guo. (1992) The transfer matrix method for solving axisymmetrical problems in multi-layered elastic half space. *J. Civil Eng.*, 25(6), 37-43 (in Chinese).